# Surface Modification of Silica Particles and Upconverting Particles Using Click Chemistry

DISSERTATION ZUR ERLANGUNG DES DOKTORGRADES DER NATURWISSENSCHAFTEN (DR. RER. NAT.) DER FAKULTÄT CHEMIE UND PHARMAZIE DER UNIVERSITÄT REGENSBURG

vorgelegt von

Heike Sabine Mader

aus Bietigheim-Bissingen

(Landkreis Ludwigsburg)

im April 2010

# Surface Modification of Silica Particles

# and Upconverting Particles

# Using Click Chemistry

Doctoral Thesis

by

Heike Sabine Mader

Diese Doktorarbeit entstand in der Zeit von Dezember 2006 bis März 2010 am Institut für Analytische Chemie, Chemo- und Biosensorik an der Universität Regensburg.

Die Arbeit wurde angeleitet von Prof. Dr. Otto S. Wolfbeis.

# Acknowledgments

# Table of Contents

# 1 Introduction and Aim of Work

Fluorescence-based detection is still widely used in modern bioanalytical research and routine applications. Commonly, organic fluorophores are employed as labels and markers for trace amounts of analytes. Organic fluorophores are easily accessible, versatile and simple to use but they do have considerable drawbacks. Generally, only one or very few fluorophores can indicate one biomolecule recognition event. As a consequence, the brightness of the label dictates the detection limit of the analyte. Furthermore, organic fluorophores are susceptible to photobleaching or even degradation in certain environments. In addition, background fluorescence originating from the sample matrix may interfere with the measurement. Even though the dyes may be easily conjugated to biomolecules such as DNA and proteins, the determination of specific biomolecules of interest might lead to a complex and time consuming conjugation chemistry that is not suitable for routine analysis. These limitations have led to the increasing replacement of molecular tags by nanoparticles (NPs)[1,2]. These particles with diameters from approximately 1 – 150 nm do have several advantages compared to classic fluorophores. With optimized composition and surface modification, NPs grant an enhanced emission intensity signal, increased sensitivity and better reproducibility in target detection. Generally, they show a high surface to volume ratio, good biocompatibility and are stable against degradation and photobleaching. Several different types of NPs have been investigated for bioanalytical applications.

First of all, particles of the type quantum dot (QDs) are very small (1-10 nm in diameter), up to 20x brighter than common organic fluorophores and extremely photostable. Additionally, their emission color can be tuned by variation of their diameter. However, the employment of QDs does have its limitations. Usually, the QD's core consists of toxic heavy metals such as cadmium or lead, making cytotoxicity an issue for in vivo applications. Quantum dots are not dispersible in aqueous solutions and they need to be polymer coated to allow their use in biological applications. Furthermore, single QD crystals show discontinuous emission ("blinking") which is limiting their use for single particle tracking applications such as flow cytometry.[1,3,4]

Dye doped polymer particles represent a second type of fluorescent nanobeads. Micro- and nanoparticles composed of polystyrene, polyacrylonitrile (PAN), polymethylmethacrylate (PMMA), and polylactic acid have been commercialized. They are widely used in biological applications as cell tracers, immunofluorescent reagents and standardization reagents in microscopy and flow cytometry. However, polymer particles usually are hydrophobic and tend to swell in organic solvents thereby causing dye leakage.[1]

Another class of NPs is silica nanoparticles doped or labeled with fluorescent dyes. They represent a very robust group of particle markers. Silica NPs are easily prepared, even commercially available and the silicium dioxide ($SiO_2$) material enables a diversity of chemical and physical modifications. The NPs are highly hydrophilic, chemically and mechanically stable and their biocompatibility renders them a fairly benign material regarding *in vivo* applications. Nanobeads made from silica are not susceptible to microbial attack and they show no tendency to swelling or porosity changes with varying pH. Additionally, dye doped silica NPs possess high photostability and sensitivity.[1,3,4] Due to these advantages doped silica NPs are applied as labels in flow cytometry[5], protein purification[6], immuno[7] and gene[8,9] assays, or as biomarkers for scanning probe microscopy-based imaging[10,11] and sensing[12] techniques. Besides they are used for gene[13] or drug[14,15] delivery, as intracellular transporters[16] or for multiplexed encoding.[17]

Lanthanide complexes have been widely used as dopants in various kinds of NPs, in order to obtain biolabels with high photostability and long fluorescence lifetimes.[18,19] Lanthanide doped NPs possess unique luminescent properties such as a large Stokes' shift, distinct absorption and emission lines and a high quantum yield.[20] Nevertheless, lanthanide ions in complexes or chelates may still be prone to quenching by water or hydroxy groups.

In the last decade, inorganic rare earth (RE) nanomaterials have been proposed to be more suitable as optical biolabels, as the rigid crystal host lattice protects the emitting RE dopants from environmental influences.[21] Moreover, lanthanide ions are known to exhibit not only downconversion (conventional Stokes) luminescence but also efficient upconversion (anti-Stokes) fluorescence.[22] Upconversion (UC) describes the conversion of low energy near infrared (NIR) radiation to higher-energy (visible) light by multi-photon absorption and subsequent emission of dopant-

dependent luminescence. This concept has been known since the 1960s[23] but primarily been exploited for the development of optical devices such as infrared quantum counters, temperature sensors and solid-state lasers[24]. Thus, the use of the UC effect has been limited to bulk glass or crystalline materials for more than 30 years. Only in the late 1990s and early 2000s, when nanoparticle research became prevalent, the potential of UC materials for bioanalytical assays and imaging was recognized. It was discovered that upconversion nanoparticles (UCNP) inherit the unique optical properties of their bulk material. UCNPs have the advantage of being photoexcitable in the NIR (around 980 nm) where the auto-absorption of any biological matter is quite weak, thereby reducing background of both absorption and luminescence (which would occur, along with Raman scatter, at wavelengths of >980 nm anyway) to virtually zero. The large anti-Stokes shift allows easy separation of the discrete emission peaks from the excitation source. In addition, UCNPs are chemically stable and do not bleach or blink. The luminescence emission wavelength of the UCNPs is not size-dependent as it is for QDs and multicolor emission can easily be accomplished by varying host crystal and RE dopant. Applications of UCNPs (which are virtually invisible in low concentrations) include authentication in general, in security,[25,26] anti-counterfeit,[27,28] brand protection,[29] flow cytometry,[30,31] photodynamic therapy,[32] and point-of-care diagnostics[33]. In bioanalytical terms, they have been demonstrated to be useful in immuno[34,35,36] and gene[37,38] assays, as luminescent labels,[21] in sensing pH,[39] and in imaging of cells.[40,41,42]

Upconverting microparticles (UCµPs), as opposed to UCNPs, obviously are much larger but more efficient in terms of upconversion. They are commercially available and used, for example, in security inks or for visualization of IR radiation.[43] UCµPs also have been employed in homogeneous immunoassays[44,45,46] and enzyme activity assays[47] following bead-milling so to reduce the size to the sub-micron range. Low energy laser diodes are adequate for photo-excitation, and their (visible) emission is rather bright. Unlike UCNPs, they cannot be well suspended (as a kind of colloidal dispersion) in aqueous or organic solutions.

For application in affinity assays (such as in high-throughput screening) and in bioassays, the surface of UCNPs and UCµPs has to be functionalized in order to covalently immobilize biomolecules on their surfaces. Such surface chemistries are expected to be versatile so to enable immobilization of proteins, receptors, enzymes, or nucleic acid oligomers, to mention a few. Moreover, UCNPs whose surface is not

appropriately modified can be suspended fairly well in certain organic solvents, but not in water. This is crucial, however, with respect to many bioapplications.[21] Only if proper surface modification is accomplished, their bioanalytical potential can be fully exploited.

The most common method to improve dispersibility involves the coating of NPs with a thin layer of silica. The resulting silica coated NPs are chemically stable, fairly biocompatible, nontoxic, and can be prepared in narrow size distribution. Silica is well documented as a coating agent for quantum dots,[48,49] metal oxides,[50,51] lanthanide nanoparticles,[7] and even upconverting particles.[21,35,52,53] Yet another benefit of silica coated particles, as for pure silica NPs is based on the different types of functional groups that can be attached to the particle surface using appropriate silane reagents.[3,54,55]

The introduction of functional groups to the surface of almost any kind of micro- and nanoparticles also is required to enable bioconjugation. Various kinds of functionalized particles have been reported in the literature. Generally, linkers with terminal amino, thiol or carboxy groups are prefered.[1,21,56,57] However, the functional groups required for these kinds of conjugation are quite abundant in proteinic biomolecules, a fact that compromises selective conjugation. Moreover, amino groups and carboxy groups are charged in pH 6 - 8 solution and thus give rise to electrostatic (i.e. unspecific) interaction including adsorption and particle aggregation. The so-called "click-chemistry" is an attractive alternative because the functional groups involved (azido and alkyne) are hardly present in biomolecules including proteins and oligomers. It is therefore said to be "bioorthogonal".[58]

One of the so-called click reactions (see 2.3.1) involves the dipolar cycloaddition of an organic azido group to an alkyne group, also known as the Huisgen ligation.[59] The catalytic effect of $Cu^+$ on this cycloaddition was independently discovered by the groups of Meldal[60] and of Sharpless[61]. The reagents used often are available in a reasonable number of synthetic steps. Cycloaddition proceeds in high yields, occurs at room temperature in many organic solvents and – most notably in terms of biological applications – also in aqueous solution at near-neutral pH. Generally, simple purification steps are required only due to the almost complete and regioselective conversion into the 1,4-disubstituted 1,2,3-triazole.[62,63] Furthermore,

no protecting groups are required for the click reaction as it tolerates a variety of functional groups and shows high kinetic stability.

The use of the "click" concept has spread into a variety of fields, such as drug design,[64] peptide[65,66] or protein[67,68] functionalization and fluorescent biolabeling,[69] which is not surprising considering all its advantages. Yet, its main impact it may have had in materials and polymer science. Applications of the click reaction lie in the design of novel polymeric materials, macromolecular engineering, functionalization of nanomaterials and bioconjugation.[70] Its bioorthogonality and tolerance towards a wide range of functional groups and reaction conditions particularly makes it an ideal tool for the biofunctionalization of nanomaterials. So far, the click reaction has been used do functionalize silica NPs,[54,71] QDs,[72] gold,[73,74] and metal oxide[75,76] nanobeads and various polymeric[77,78] particles. Combined with the benefits of upconverting and silica NPs, click chemistry provides a versatile and powerful tool in the development of new functional nanomaterials.

The aim of this work was to develop a new method for surface modification of silica NPs, UCµPs and UCNPs based on the click chemistry concept. Commercially available silica NPs and upconverting µPs as well as synthesized upconverting NPs were to be functionalized with azido and alkyne groups using suitable silane reagents. The particles functionalized in that manner were to be clicked to biorecognition sites such as biotin and maleinimide as well as fluorescent dyes and applied as biolabels and in sensor systems.

## 1.1 References

[1]    Wang L, Wang K, Santra S, Zhao X, Hilliard LR, Smith JE, Wu Y, Tan W (2006) **Watching Silica Nanoparticles Glow in the Biological World**, Anal. Chem. 78: 646-654.

[2]    Knopp D, Tang D, Niessner R (2009) **Review: Bioanalytical Applications of Biomolecule-Functionalized Nanometer-Sized Doped Silica Particles**, Anal. Chim. Acta 647: 14-30.

[3]    Wang L, Zhao W, Tan W (2008) **Bioconjugated Silica Nanoparticles: Development and Applications**, Nano Res. 1: 99-115

[4]    Yao G, Wang L, Wu Y, Smith J, Xu J, Zhao W, Lee E, Tan W (2006) **FloDots: Luminescent Nanoparticles**, Anal. Bioanal. Chem. 385: 518-524.

[5]    Wang L, Zhao W, O'Donoghue M, Tan WH (2007) **Fluorescent Nanoparticles for Multiplexing Bacteria Monitoring**, Bioconjugate Chem. 18: 297-301.

6    Kim SH, Jeyakumar M, Katzenellenbogen JA (2007) **Dual-Mode Fluorophore-Doped Nickel Nitrilotriacetic Acid-Modified Silica Nanoparticles Combine Histidine-Tagged Protein Purification with Site-Specific Fluorophore Labeling**, J. Am. Chem. Soc. 129: 13254-13264.

7    Ye, Z, Tan M, Wang G, Yuan J (2004) Preparation, **Characterization, and Time-Resolved Fluorometric Application of Silica-Coated Terbium (III) Fluorescent Nanoparticles**, Anal. Chem. 76: 513-518.

8    Zhao X, Tapec-Dytioco R, Tan W (2003) **Ultrasensitive DNA Detection Using Highly Fluorescent Bioconjugated Nanoparticles**, J. Am. Chem. Soc. 125: 11474-11475.

9    Zhao W, Wang L, Tan W (2007) **Fluorescent Nanoparticle for Bacteria and DNA Detection, Bio-Applications of Nanoparticles**, Springer Science+Business Media LLC, Landes Bioscience, Volume 620 edited by Chan, WCW pp 129-136.

10   Ow H, Larson DR, Srivastava M, Baird BA, Webb WW, Wiesner U (2005) **Bright and Stable Core-Shell Fluorescent Silica Nanoparticles**, Nano Lett. 5: 113-117.

11   Rieter WJ, Kim JS, Taylor KML, An H, Weili L, Tarrant T, Lin W (2007) **Hybrid Silica Nanoparticles for Multimodal Imaging**, Angew. Chem. Int. Ed. 46: 3680-3682, Angew. Chem. 119: 3754-3756.

12   Burns A, Sengupta P, Zedayko T, Baird B, Wiesner U (2006) **Core/Shell Fluorescent Silica Nanoparticles for Chemical Sensing: Towards Single-Particle Laboratories**, Small 2: 723-726.

13   Roy I, Ohulchanskyy TY, Bharali DJ, Pudavar HE, Mistretta RA, Kaur N, Prasad PN (2005) **Optical Tracking of Organically Modified Silica Nanoparticles as DNA Carriers: A Nonviral, Nanomedicine Approach for Gene Delivery**, P. Natl. Acad. Sci. USA 102: 279-284.

14   Slowing II, Trewyn BG, Giri S, Lin VSY (2007) **Mesoporous Silica Nanoparticles for Drug Delivery and Biosensing Applications**, Adv. Funct. Mater. 17: 1225-1236.

15   Slowing II, Vivero-Escoto JL, Wu CW, Lin VSY (2008) **Mesoporous Silica Nanoparticles as Controlled Release Drug Delivery and Gene Transfection Carriers**, Adv. Drug. Deliver. Rev. 60: 1278-1288.

16   Bottini M, Cerignoli F, Mills DM, D'Annibla F, Leone M, Rosato N, Magrini A, Pelecchia M, Bergamaschi A, Mustelin T (2007) **Luminescent Silica Nanobeads: Characterization and Evaluation as Efficient Cytoplasmic Transporters for T-Lymphocytes**, J. Am. Chem. Soc. 129: 7814-7823.

17   Wang L, Tan W (2006) **Multicolor FRET Silica Nanoparticles by Single Wavelength Excitation**, Nano Lett. 6: 84-88.

18   Eliseeva SV, Bünzli J-CG (2010) **Lanthanide Luminescence for Functional Materials and Bio-Sciences**, Chem. Soc. Rev. 39: 189-227.

19   Bünzli J-CG, Piguet C (2005) **Taking Advantage of Luminescent Lanthanide Ions**, Chem. Soc. Rev. 34: 1048-1077.

20   Sivakumar S, Diamente PR, van Veggel FCJM (2006) **Silica-Coated $Ln^{3+}$-Doped $LaF_3$ Nanoparticles as Robust Down- and Upconverting Biolabels**, Chem. Eur. J 12: 5878-5884.

21   Shen J, Sun L-D, Yan X-H (2008) **Luminescent Rare Earth Nanomaterials for Bioprobe Applications**, Dalton Trans. 5687-5697.

22   Escribano P, Julián-López B, Planelles-Aragó J, Cordoncillo E, Viana B, Sanchez C (2008) **Photonic and Nanobiophotonic Properties of Luminescent Lanthanide-Doped Hybrid Organic-Inorganic Materials**, J. Mater. Chem. 18: 23-40.

23   Auzel F (2004) **Upconversion and Anti-Stokes Processes with f and d Ions in Solids**, Chem. Rev. 104: 139-173.

24   Wang F, Liu X (2009) **Recent Advances in the Chemistry of Lanthanide-Doped Upconversion Nanocrystals**, Chem. Soc. Rev. 38: 976-989.

[25]   Muth O, Brockmann H, Schmidt W, Bailleu A, Brauer G, Paeschke M, Ahlers B, Franz-Burgholz A, Zerbel H (inv.) (2002) **Eur. Pat. EP1241021**.

[26]   Kim WJ, Nyk M, Prasad PN (2009) **Color-Coded Multilayer Photopatterened Microstructures using Lanthanide (III) Ion Co-Doped NaYF₄ Nanoparticles with Upconversion Luminescence for Possible Applications in Security**, Nantechnology 20: 185301-185307.

[27]   Du H, Lan Y, Xia Z, Sun J (2009) **Synthesis and Upconversion Luminescence Properties of Yb$^{3+}$/Er$^{3+}$ Codoped BaGd$_2$(MoO$_4$)$_4$ Powder**, Mat. Res. Bull. 44: 1660-1662.

[28]   http://www.tradekey.com/ks-anti-counterfeit.

[29]   http://www.packagedesignmag.com/brandprotection/files/BPS-Solutions.pdf].

[30]   Corstjens PLAM, Chem Z, Zuiderwijk M, Bau HH; Abrams WR, Malamud D, Niedbala RS, Tanke HJ (2007) **Rapid Assay Format for Multiplex Detection of Humoral Immune Responses to Infectious Disease Pathogens (HIV, HCV and TB)**, Ann. N. Y. Acad Sci. 1098: 437-445.

[31]   Yan Z, Zhou L, Zhao Y, Wang J, Huang L, Hu K, Liu H (2006) **Rapid Quantitative Detection of Yersinia Pestis by Lateral-Flow Immunoassay and Up-Converting Phosphor Technology-Based Biosensor**, Sensor. Actuat. B-Chem. 119: 656-663.

[32]   Qian HS, Guo HC, Ho PC-L, Mahendran R, Zhang Y (2009) **Mesoporous-Silica-Coated Up-Conversion Fluorescent Nanoparticles for Photodynamic Therapy**, Small 5: 2285-2290.

[33]   Ouellette AL, Li JJ, Cooper DE, Ricco AJ, Kovacs GT (2009) **Evolving Point-of-Care Diagnostics Using Up-Converting Phosphor Bioanalytical Systems**, Anal. Chem. 81: 3216–3221.

[34]   Morgan CG, Dad S, Mitchell AC (2008) **Present Status of, and Future Prospects for, Upconverting Phosphors in Proximity-Based Bioassays**, J. Alloy. Compd. 451: 526-529.

[35]   Corstjens PLAM, Li S, Zuiderwijk M, Kardos K, Abrams WR, Niedbala RS, Tanke HJ (2005) **Infrared Up-Converting Phosphors for Bioassays**, IEE Proc.-Nanobiotechnol. 152: 64-72.

[36]   Wang M, Hou W, Mi C-C, Wang W-X, Xu Z-R, Teng H-H, Mao C-B, Xu S-K (2009) **Immunoassay of Goat Antihuman Immunoglobulin G Antibody Based on Luminescence Resonance Energy Transfer between Near-Infrared Responsive NaYF₄: Yb, Er Upconversion Fluorescent Nanoparticles and Gold Nanoparticles**, Anal. Chem. 81: 8783-8789.

[37]   Van der Rijke F, Zijlmans H, Li S, Vail T, Raap AK, Niedbala RS, Tanke HJ (2001) **Up-Converting Phosphor Reporters for Nucleic Acid Microarrays**, Nat. Biotechnol. 19: 273-276).

[38]   Zhang P, Rogelj S, Nguyen K, Wheeler D (2006) **Design of a Highly Sensitive and Specific Nucleotide Sensor Based on Photon Upconverting Particles**, J. Am. Chem. Soc. 128: 12410-12411.

[39]   Sun L, Peng H, Stich MIJ, Achatz D, Wolfbeis OS (2009) **pH Sensor Based on Upconverting Luminescent Lanthanide Nanorods**, Chem. Comm. 5000-5002.

[40]   Chatterjee DK, Rufaihah AJ, Zhang Y (2008) **Upconversion Fluorescence Imaging of Cells and Small Animals Using Lanthanide Doped Nanocrystals**, Biomaterials. 29: 237-943.

[41]   Hu H, Xiong L, Zhou J, Li F, Cao T, Huang C (2009) **Multimodal-Luminescence Core-Shell Nanocomposites for Targeted Imaging of Tumor Cells**, Chem. Eur. J. 15: 3577-3584.

[42]   Jalil RA, Zhang Y (2008) **Biocompatibility of Silica Coated NaYF₄ Upconversion Fluorescent Nanocrystals**, Biomaterials 29: 4122-4128.

[43]   www.sicpa.com

[44]   Kuningas K, Rantanen T, Karhunen U, Lövgren T, Soukka T (2005) **Simultaneous Use of Time-Resolved Fluorescence and Anti-Stokes Photoluminescence in a Bioaffinity Assay**, Anal. Chem. 77: 2826-2834.

45 Kuningas K, Ukonaho T, Päkkilä H, Rantanen T, Rosenberg J, Lövgren T, Soukka T (2006) **Upconversion Fluorescence Resonance Energy Transfer in a Homogeneous Immunoassay for Estradiol**, Anal. Chem. 78: 1-57.

46 Soukka T, Rantanen T, Kuningas K (2008) **Photon Upconversion in Homogeneous Fluorescence-based Bioanalytical Assays**, Ann. N. Y. Acad. Sci. 1130: 188-200.

47 Rantanen T, Järvenpää ML, Vuojola J, Kuningas K, Soukka T (2008) **Fluorescence-Quenching-Based Enzyme-Activity Assay by Using Photon Upconversion**, Angew. Chem. Int. Ed. 47: 3811-3813, Angew. Chem. 120: 3871-3873.

48 Nann T, Mulvaney P (2004) **Single Quantum Dots in Spherical Silica Particles**, Angew. Chem. Int. Ed. 43: 5393-5396, Angew. Chem. 116: 5511-5514.

49 Selvan ST, Patra PK, Ang CY, Ying JY (2007) **Synthesis of Silica-Coated Semiconductor and Magnetic Quantum Dots and Their Use in the Imaging of Live Cells**, Angew. Chem. Int. Ed. 46: 1-6, Angew. Chem. 119: 2500-2504.

50 Ohmori M, Matijevic E (1993) **Preparation and Properites of Uniform Coated Inorganic Colloidal Particles: 8. Silica on Iron**, J. Colloid. Interf. Sci. 160: 288-292.

51 Yu SY, Zhang HJ, Yu JB, Wang C, Sun LN, Shi WD (2007) **Bifunctional Magnetic-Optical Nanocomposites: Grafting Lanthanide Complex onto Core-Shell Magnetic Silica Nanoarchitecture**, Langmuir 23: 7836-7840.

52 Li Z, Zhang Y (2006) **Monodisperse Silica-Coated Polyvinylpyrrolidone/NaYF$_4$ Nanocrystals with Multicolor Upconversion Fluorescence Emission**, Angew. Chem. Int. Ed. 45: 7732-7735. Angew. Chem. 118: 7896-7899.

53 Li, Z, Zhang Y, Jiang S (2008) **Multicolor Core/Shell-Structured Upconversion Fluorescent Nanoparticles**, Adv. Mater. 20: 4765-4769.

54 Mader H, Li X, Saleh S, Link M, Kele P, Wolfbeis OS (2008) **Fluorescent Silica Nanoparticles**, Ann. N. Y. Acad. Sci. 1130: 213-223.

55 Liu S, Zhan HL, Liu TC, Liu B, Cao YC, Huang ZL, Zhao YD, Luo QM (2007) **Optimization of the Methods for Introduction of Amine Groups onto the Silica Nanoparticle Surface**, J. Biomed. Mater. Res. A. 80 A: 752-757.

56 Corstjens PLAM, Zuiderwijk M, Nilsson M, Feindt H, Niedbala RS, Tanke HJ (2003**) Lateral-flow and Up-converting Phosphor Reporters to Detect Single-stranded Nucleic Acids in a Sandwich-hybridization Assay**, Anal. Biochem. 312: 191-200.

57 Hermanson GT (2008) **Bioconjugate Techniques**, 2nd Edition, Elsevier Inc. London, Burlington, San Diego.

58 Kurpiers T, Mootz HD (2009) **Bioorthogonal Ligation in the Spotlight**, Angew. Chem. Int. Ed. 48: 1729-1731, Angew. Chem. 121: 1757-1760.

59 Wolfbeis OS (2007) **The Click Reaction: Fluorescent Probing of a Metal Ion Using a Catalytic Reaction, and its Implications to Biolabeling Techniques**, Angew. Chem. Int. Ed. 46: 2980-2982, Angew. Chem. 119: 3038-30470.

60 Tornøe CW, Christensen C, Meldal M (2002) **Peptidotriazoles on Solid Phase: [1,2,3]-Triazoles by Regiospecific Copper(I)-Catalyzed 1,3-Dipolar Cycloaddition of Terminal Alkynes to Azides**, J. Org. Chem. 67: 3057-3064.

61 Rostovtsev VV, Green LG, Fokin VV, Sharpless KB (2002) **A Stepwise Huisgen Cycloaddition Process: Copper(I)-Catalyzed Regioselective "Ligation" of Azides and Terminal Alkynes**, Angew. Chem. Int. Ed. 41: 2596-2599, Angew. Chem. 114: 2708-2711.

62 Himo F, Lovell T, Hilgraf R, Rostovtsev VV, Noodleman L, Sharpless KB, Fokin VV (2005) **Copper(I)-Catalyzed Synthesis of Azoles. DFT Study Predicts Unprecedented Reactivity and Intermediates**, J. Am. Chem. Soc. 127: 210-216.

63 Moses JE, Moorhouse AD (2007) **The Growing Applications of Click Chemistry**, Chem. Soc. Rev. 36: 1249-1262.

[64] Lutz J-F, Zarafshani Z (2008) **Efficient Construction of Therapeutics, Bioconjugates, Biomaterials and Bioactive Surfaces Using Azide-Alkyne "Click" Chemistry**, Adv. Drug Deliver. Rev. 60: 958-970.

[65] Gierlich J, Burley GA, Gramlich PME, Hammond DM, Carell T (2006) **Click Chemistry as a Reliable Method fort he High-Density Postsynthetic Functionalization of Alkyne-Modified DNA**, Org. Lett. 8: 3639-3642.

[66] Berndl S, Herzig N, Kele P, Lachmann D, Li X, Wolfbeis OS, Wagenknecht H-A (2009) **Comparison of a Nucleosidic vs Non-Nucleosidic Postsynthetic "Click" Modification of DNA with Base-Labile Fluorescent Probes**, Bioconjugate Chem. 20: 558-564.

[67] Lin P-C, Ueng S-H, Tseng M-C, Ko J-L, Huang K-T, Yu S-C, Adak AK, Chen Y-J, Lin C-C (2006) **Site-Specific Protein Modification trough Cu$^I$-Cataliyzed 1,2,3-Triazole Formationand Its Implementaion in Protein Microarray Fabrication**, Angew. Chem. Int. Ed. 45: 4286-4290, Angew. Chem. 118: 4392-4396.

[68] Hatzakis NS, Engelkamp H, Velonia K, Hofkens J, Christianen PCM, Svendsen A, Patkar SA, Vind J, Maan JC, Rowan AE, Nolte RJM (2006) **Synthesis and Single Enzyme Activity of a Clicked Lipase-BSA Hetero-Dimer**, Chem. Commun. 2012-2014

[69] Kele P, Mezö G, Achatz D, Wolfbeis OS (2009) **Dual Labeling of Biomolecules by Using Click Chemisty: A Sequential Approach**, Angew. Chem. Int. Ed. 48: 344-347, Angew. Chem. 121: 350-353.

[70] Lutz J-F (2007) **1,3-Dipolar Cycloadditions of Azides and Alkynes: A Universal Ligation Tool in Polymer and Materials Science**, Angew. Chem. Int. Ed. 46: 1018-1025, Angew. Chem. 119: 1652-1654.

[71] Zhan J, Wang X, Wu D, Liu L, Zhao H (2009) **Bioconjugated Janus Particles Prepared by in Situ Click Chemistry**, Chem. Mater. 21: 4012-4018.

[72] Binder WH, Sachsenhofer R, Straif CJ, Zirbs R (2007) **Surface-Modified Nanoparticles via Thermal and Cu(I)-mediated „Click" Chemistry: Generation of Luminescent CdSe nanoparticles with Polar Ligands Guiding Supramolecular Recognition**, J. Mater. Chem. 17: 2125-2132.

[73] Zhou Y, Wang S, Zhang K, Jiang X (2008) **Visual Detection of Copper(II) by Azide- and Alkyne-Functionalized Gold Nanoparticles Using Click Chemistry**, Angew. Chem. Int. Ed. 47: 7454-7456, Angew. Chem. 120: 7564-7566.

[74] Gole A, Murphy CJ (2008) **Azide-Derivatized Gold nanorods: Functional Materials for "Click" Chemistry**, Langmuir 24: 266-272.

[75] Lin P-C, Ueng S-H, Yu S-C, Jan M-D, Adak AK, Yu C-C, Lin C-C (2007) **Surface Modification of Magnetic Nanoparticle via Cu(I)-Catalyzed Alkyne-Azide [2+3] Cycloaddition**, Org. Lett. 9: 2131-2134.

[76] Von Maltzahn G, Ren Y, Park J-H, Min D-H, Kotamaraju VR, Jayakumar J, Fogal V, Sailor MJ, Ruoslahti E, Bhatia SN (2008) **In Vivo Tumor Cell Targeting with "Click" Nanoparticles**, Bioconjugate Chem. 19: 1570-1578.

[77] Evans CE, Lovell PA (2009) **Click Chemistry as a Route to Surface Functionalization of Polymer Particles Dispersed in Aqueous Media**, Chem. Commun. 2305-2307.

[78] Lu J, Shi M, Shoichet MS (2009) **Click Chemistry Functionalized Polymeric Nanoparticles Target Corneal Epithelial Cells through RGD-Cell Surface Receptors**, Bioconjugate Chem. 20: 87-94.

# 2 Fundamentals

## 2.1 Upconversion

### 2.1.1 Mechanisms of Upconversion

The occurrence of upconversion (UC) luminescence can be ascribed to three main processes: excited state absorption (ESA), energy transfer upconversion (ETU), and photon avalanche (PA). All these processes are based on sequential absorption of two or more photons, differentiating these from simultaneous multiphoton absorption.[1,2]

The ESA principle is based on successive absorption of two photons. The general energy diagram for a simple three-level system is presented in figure 2.1a. First, one electron is excited to the metastable level E1 in a ground state absorption (GSA) process if the excitation energy is resonant with the transition from the ground state G to the excited state E1. Subsequently, a second photon promotes the electron to the higher state E2 resulting in UC emission corresponding to the E2 → G transition. ESA is independent of the rare earth (RE) ion concentration of the upconverting material as it is a single ion process.[1,2]
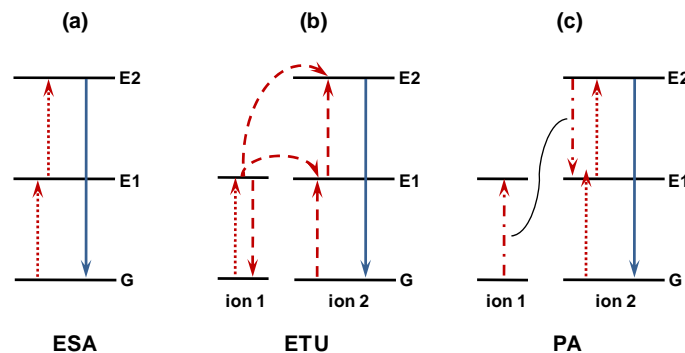


**Figure 2.1** General schemes for UC processes in RE doped material: (a) excited state absorption, (b) energy transfer upconversion (c) photon avalanche. The dotted, dashed, dashed/dotted and full arrows represent photon excitation, non-radiative energy transfer, cross relaxation and emission processes, respectively.

The concept of ETU is similar to the ESA principle as it is based on sequential absorption of two photons to populate the energy level E2, as well. However, in ETU the excitation is realized by an energy transfer between two neighboring RE ions. Ion

1 acts as sensitizer (or energy donor) and ion 2 as activator (energy acceptor). A number of different mechanisms are known, in figure 2.1b the successive energy transfer is depicted exemplarily. Hereby, only the sensitizer ion absorbs photons and is excited to level E1. The activator is promoted to its excited state E1 by a first non-radiative energy transfer while the sensitizer ion relaxes back to ground level G. A second excitation of the activator and subsequent energy transfer enables the population of the emitting state E2. The UC efficiency of an ETU process is influenced by the dopant concentration which determines the average distance between neighboring dopant ions.[1,3]

The third main UC luminescence process, the PA upconversion is based on an unconventional pumping mechanism as it can produce strong emission from level E2 without any resonant GSA. The excited state E1 is populated by a non-resonant weak GSA, followed by a resonant ESA to promote the ion to the emissive level E2 (figure 2.1c). Next, a cross relaxation energy transfer occurs between the excited ion and a neighboring ion that is still in ground state. This results in both ions populating the intermediary level E1. Subsequently, both ions can be promoted to level E2 by resonant ESA again. This initiates further cross relaxation and exponentially increases the population of E2 resulting in strong UC emission as an avalanche process. A characteristic of the PA process is that the excitation intensity has to be kept above a certain threshold value to enable efficient upconversion.[1,3]

The UC luminescence efficiency in these three processes differs substantially. ESA generates the weakest UC luminescence and is only of interest in singly doped crystals. In materials with metastable, intermediary energy levels that can function as storage reservoir for pump energy efficient UC based on PA is viable. Though, the PA process is disadvantageous because of its dependence on excitation power and its slow response to excitation due to the numerous looping cycles of ESA and cross relaxation processes. In contrast, ETU happens instantaneously, is independent of excitation power, and produces UC emission two orders of magnitude higher than ESA. Therefore, many UC materials with more than one dopant ion have been developed, based on the ETU process.[1]

### 2.1.2 Composition and Photoluminescent Properties of Upconverting Materials

Inorganic crystals in general do not display UC luminescence at room temperature. The UC phenomenon typically occurs in singly or multiply doped host systems. Hence, research concentrates on materials that consist of a crystalline host and RE dopants added to the host lattice in low concentrations. For the development of micro and nanoscale materials with distinct optical properties the exact composition is particularly crucial. Two different RE ions need to be used as dopants to put into effect a material emitting ETU-luminescence. [1,2]

The dopants must exhibit multiple metastable energy states in order to enable efficient UC. Thus, lanthanides (Ln) are perfectly suited for this purpose. They basically exist in their most stable oxidation state as trivalent ions ($Ln^{3+}$). The 4f electrons of lanthanides are well shielded by the completely filled $5s^2$ and $5p^6$ shells resulting in weak electron-phonon coupling. This effect is responsible for the sharp and narrow f-f transition bands. Additionally, f-f transitions are Laporte forbidden, resulting in low transition probabilities and long-lived excited states. Generally, lanthanide ions possess more than one excited 4f energy state, except for $La^{3+}$, $Ce^{3+}$, $Yb^{3+}$ and $Lu^{3+}$. Consequently, most Ln ions are able to exhibit UC luminescence. However, excited and intermediary states have to be in energetical proximity to enable photon absorption and energy transfer to produce efficient emission. Such a ladder-like configuration of the energy levels is particularly featured by $Er^{3+}$, $Tm^{3+}$, and $Ho^{3+}$. Thus, these ions are frequently used as activators. Moreover, $Er^{3+}$ and $Tm^{3+}$ possess relatively large energy gaps, resulting in low probabilities for non-radiative multiphoton relaxations. Therefore, erbium and thulium doped crystals have shown the most efficient UC luminescence to date.[1]

In singly doped UCNPs, the UC emission is mainly produced by ESA (figure 2.1a). Hence, the distance between two adjacent activator ions and the absorption cross-section of the ions are the key parameters for efficient upconversion. High concentrations of activator ions give rise to luminescence quenching due to annihilating cross-relaxations. Thus, the doping level should be kept low. Furthermore, most activator ions possess low absorption cross-sections resulting in low ESA efficiency. So, the UC efficiency of mono-doped NPS is rather low in general.[1]

An effective method to substantially increase UC efficiency is the so called co-doping with a second lanthanide ion, the sensitizer. By choosing a sensitizer with an adequate absorption cross-section in the NIR region, the ETU process between sensitizer and activator can be exploited. The energy level scheme of $Yb^{3+}$ is very simple with only one excited 4f state of $^2F_{5/2}$ (see figure 2.2). The transition between the ground state $^2F_{7/2}$ and the excited state $^2F_{5/2}$ of $Yb^{3+}$ is located around 980 nm and has a higher absorption cross-section than that of any other Ln ion. Moreover, this transition is well resonant with f-f transitions of common UC activators such as $Er^{3+}$, $Tm^{3+}$, and $Ho^{3+}$, enabling energy transfer to other ions.[1]
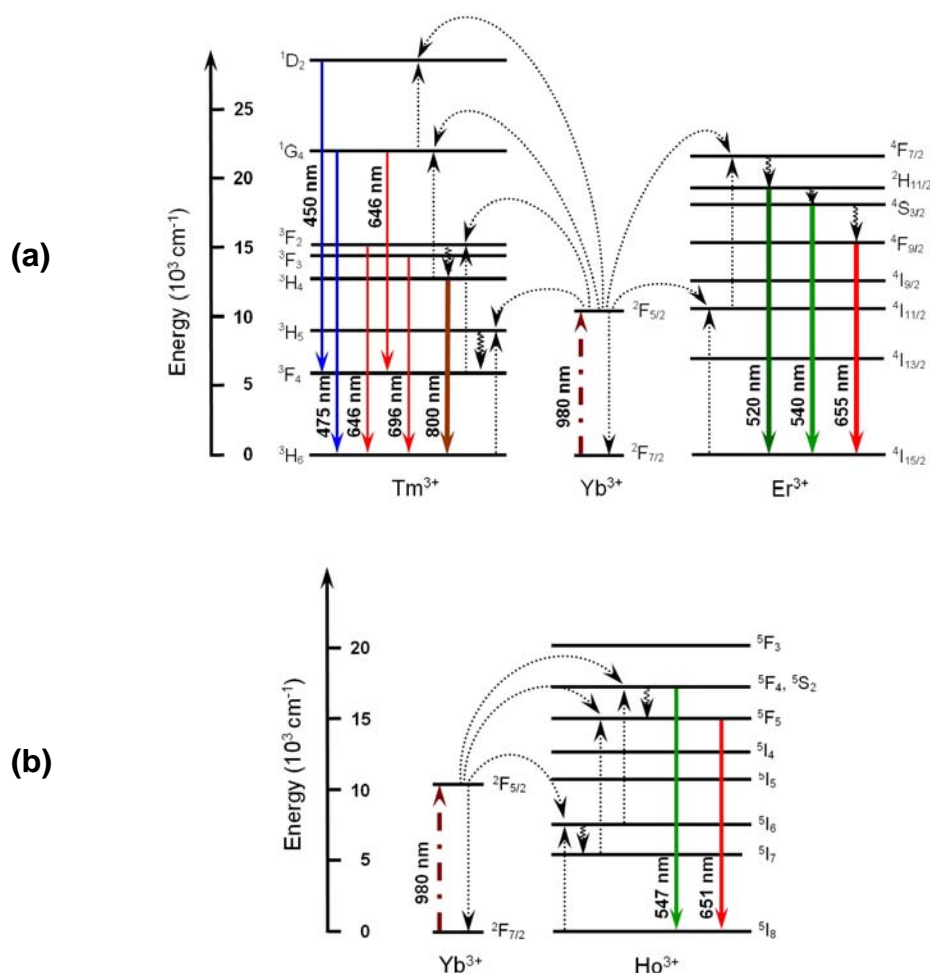


**Figure 2.2** Proposed energy transfer and UC emission mechanisms in $Yb^{3+}$, $Er^{3+}$, $Tm^{3+}$ and $Ho^{3+}$ doped $NaYF_4$ under 980 nm excitation. The dashed-dotted, dotted, curly, and full arrows refer to photon excitation, energy transfer, multiphoton relaxation, and emission processes. The $^{2S+1}L_J$ notation applied to label the f energy states represent the spin (S), orbital (L) and angular (J) momentum quantum numbers according to the Russel-Saunders notation.[1,4]

Trivalent ytterbium is an ideal UC sensitizer due to these characteristics. In doubly doped UC crystals the sensitizer concentration is to be chosen high (15 – 25 mol%) while the activator dopant should be present in concentrations lower than 3 mol% to diminish emission quenching due to cross-relaxation processes. The energy transfer mechanisms for $Yb^{3+}$ doped $NaYF_4$ co-doped with $Er^{3+}$, $Tm^{3+}$, or $Ho^{3+}$, respectively is shown in figure 2.2.[1]

The blue luminescence of thulium doped NPs at 450 nm and 475 nm can be assigned to the $^1D_2 \rightarrow {}^3F_4$ and the $^1G_4 \rightarrow {}^3H_6$ transitions, which are 4- and 3-photon processes, respectively. Weak emissions corresponding to $^3F_2/^3F_3 \rightarrow {}^3H_6$ and $^1G_4 \rightarrow {}^3F_4$ transitions can be observed at 646 nm and 696 nm. A strong emission located in the NIR at 800 nm can be attributed to the $^3H_4 \rightarrow {}^3H_6$ transition.[4,5] Erbium doped NPs commonly show three main peaks located at 520 nm, 540 nm, and 655 nm corresponding to the $^2H_{11/2} \rightarrow {}^4I_{15/2}$, $^4S_{3/2} \rightarrow {}^4I_{15/2}$ and $^4F_{9/2} \rightarrow {}^4I_{15/2}$ transitions, respectively. All of these transitions are 2-photon processes.[4,5] $Er^{3+}$ doped particles mainly appear green on excitation at 980 nm as the eye is more sensitive to green light. However, the ratio of the green to the red emission peaks is strongly dependent on the concentrations of the $Yb^{3+}$ sensitizer and the $Er^{3+}$ activator.[6] The two main emission peaks in $Ho^{3+}$ doped NPs are located at 547 nm and 651 nm corresponding to the $^5F_4/^5S_2 \rightarrow {}^5I_8$ and $^5F_5 \rightarrow {}^5I_8$ transitions. Both emissions are obtained by a 2-photon process.[4] Other lanthanide ions such as $Ce^{3+}$ [7] and $Gd^{3+}$ [8] have been used as activators to produce upconverting materials. Yet, the highest UC efficiency so far has been achieved by using $Er^{3+}$, $Tm^{3+}$, or $Ho^{3+}$ as emitters.

The choice of the host material is also crucial for the preparation of UCNPs with efficient UC emission. In general, host crystals should have close lattice matches to dopant ions and low phonon energies to minimize non-radiative relaxation processes and maximize radiative emission. Inorganic compounds based on RE elements form ideal host materials for Ln dopants as all trivalent RE ions show similar ionic size and chemical properties. Additionally, the ionic size of alkaline earth ions such as $Ca^{2+}$, $Sr^{2+}$, and $Ba^{2+}$ and some transition metal ions like $Zr^{4+}$ and $Ti^{4+}$ is similar to that of $Ln^{3+}$ ions. Consequently, these ions have been used[9,10,11] to prepare materials capable of upconversion. However, doping with $Ln^{3+}$ ions results in the formation of crystal defects such as interstitial anions and cation vacancies to maintain charge neutrality.[1,9] This can lead to optical properties that are difficult to control. Phosphates[12], oxides[13], oxysulfides[14] and fluorides[15] are mainly used as anions in

the crystal host. Phosphates and oxides are chemically stable but possess virtually high phonon energies[1,16], thus giving rise to non-radiative energy losses. In contrast, oxysulfides are not stable against acids. Fluorides show low phonon energies and high chemical stability. Therefore, they are widely used as host crystal for upconverting NPs.

Not only has the choice of the host material large influence on the efficiency of the UC emission but also the crystal structure. This is especially evident in sodium yttrium fluoride ($NaYF_4$). Hexagonal phase $\beta$-$NaYF_4$ crystals exhibit a UC emission an order of magnitude higher than $\alpha$-$NaYF_4$ particles.[17] This effect is due to the formation of different crystals fields around the dopant Ln ions in matrices with diverse symmetry. In a highly symmetric cubic host material f-f transitions are strongly parity forbidden and thus, the UC emission efficiency is rather weak. In a host with lower symmetry, such as the hexagonal crystal system, there are more uneven components surrounding the dopant ion, thus, enhancing f-f transition probabilities.

The luminescence efficiency depends aside from matrix effects also on particle size.[18] Generally, bigger particles exhibit UC with higher intensity. Therefore, much lower excitation energies are required when working with UCµPs. The effect of the particle size on UC efficiency is not yet fully understood, but there might be a correlation between the surface-volume-ratio and emission intensity.


### 2.1.3 Synthesis of Upconverting Nanoparticles


A variety of methods to prepare UCNPs in different sizes has been developed in recent years.[1] A very simple and convenient technique is the co-precipitation method, permitting NP preparation in tunable sizes and narrow size distributions. In a typical procedure, solutions of Ln salts are injected into a solution of the host material (such as sodium fluoride to form $NaYF_4$ or $YF_3$ NPs or phosphoric acid to form $LnPO_4$ NPs) with subsequent spontaneous precipitation of the nanocrystals.[12,19] The particle growth can be tuned and stabilized by using capping ligands (ammonium di-*n*-octadecyldithiophosphate)[20] or chelating agents (ethylenediaminetetraacetic acid, EDTA).[19] For the preparation of $NaYF_4$ in particular, a heat treatment or annealing

process is required to obtain efficient UCNPs. Co-precipitation generally gives cubic $\alpha$-NaYF$_4$. Calcination at high temperatures results in sharpening of the crystal structure or even in an at least partial phase transfer to the hexagonal $\beta$-NaYF$_4$, which shows higher UC efficiency.[19] The co-precipitation method does not demand any costly apparatus, complex procedures, or harsh reaction conditions and is not time consuming. Furthermore, the surface of the UCNPs prepared by this method is hydrophilic, possibly due to coordination of EDTA.

Another technique for the preparation of upconverting particles is the thermal decomposition method yielding highly monodisperse UCNPs.[21,22] Metal trifluoroacetate precursors are thermolyzed in the presence of oleic acid and 1-octadecene. Octadecene acts as high boiling solvent (315°C), whereas oleic acid serves as stabilizing agent to suppress particle agglomeration. In case of NaYF$_4$, the thermal decomposition method directly yields hexagonal $\beta$-NaYF$_4$, with no need for any annealing process. Drawbacks of this method are its expensive and air-sensitive metal precursors, and the toxic byproducts. Furthermore, the oleic acid coordinates to the particles surface rendering them hydrophobic as it is nearly impossible to remove.[23] Therefore, NPs synthesized with the thermal decomposition method are well dispersible in organic solvents but hardly in aqueous solution.

The hydro(solvo)thermal method uses a pressurized solvent and reaction temperatures above the critical point to improve the solubility of solids and to accelerate reactions between solid states.[24,25] This approach allows for the preparation of highly crystalline material at much lower temperatures and without the need for an annealing process. However, specialized reaction vessels, known as autoclaves, which resist the high pressures during the reaction, are required. Crystal size and morphology is tunable by polyol- or micelle-mediation.[26,27] Recently, ionic liquids have been used to prepare $\beta$-NaYF$_4$ under relatively mild conditions.[28]

The sol-gel process provides UCNPs for applications such as thin film coating or glass materials.[1] The method is based on the hydrolysis and polycondensation of metal alkoxide or acetate precursors.[29] Usually, a post heat-treatment step is required. NPs prepared with the sol-gel technique commonly are not suitable for biological application and can not be dispersed in aqueous solutions due to considerable particle aggregation.

Summarized, sol-gel and solvothermal methods generally require long reaction times. As opposed to this, UCNPs can be prepared within minutes with the combustion method.[1] Herein, oxidic nanoparticles are prepared in a highly exothermic reaction that spreads through the reaction material in a self-sustained manner without the need for additional heat after primarily initiated by a heat source. This makes the method time and energy saving. The substantial particle aggregation and the formation of amorphous material as side reaction are disadvantageous.[30] Flame synthesis represents another time saving method for the preparation of UCNPs.[1] Yttrium oxides can be prepared by this continuous and easily scalable method. Particle size and morphology as well as photoluminescent properties are strongly dependent on flame temperature.[31] In summary, choice of the appropriate synthesis method allows for the development of readily tailored UCNPs whose properties can be adjusted to the envisioned applications.

## 2.1.4 Surface Modification of Upconverting Nanoparticles

UCNPs need to be dispersible in aqueous solution and their non-toxicity has to be ensured in order to be of use for bioanalytical applications. Furthermore, the introduction of functional groups to the particle surface is vital for the covalent attachment of biomolecules. Various strategies to render the UCNPs water dispersible and biofunctional have been pursued.

Carboxy-functionalized UCNPs have been prepared by a ligand-exchange method.[32] The UCNPs were synthesized according to the thermal decomposition method in oleylamine. The oleylamine ligand present at the surface after particle preparation was then replaced by the bifunctional polyethylene glycol 600 diacid generating hydrophilicity and introducing carboxy functionalities. Water-dispersible UCNPs without functionalities were prepared by using a polyethylene glycol-phosphate ligand.[33]

Ligand oxidation provides another method for particle functionalization.[34] Hydrophilic carboxy-groups can be introduced to oleic acid stabilized $NaYF_4$ NPs by oxidation of the carbon-carbon double bonds in the oleic acid chain with the Lemieux-von Rudloff reagent. However, this method is limited to ligands containing unsaturated C-C bonds.[1]

Oleylamine stabilized NaYF$_4$ nanocrystals have also been modified by ligand attraction of an additional amphiphilic block copolymer[35] onto the particle surface. The amphiphilic copolymer polyacrylic acid (PAA) attaches to the stabilized NPs by hydrophobic van der Waals interactions. The carboxy groups of the PAA are directed outwards from the particle surface after coating rendering the NPs water dispersible and bioconjugatable.

Layer-by-layer assembly of oppositely-charged polyions[36,37] to the particles surface has also been used for biofunctionalization of UCNPs. Positively charged poly(allylamine hydrochloride) (PAH) and negatively charged poly(sodium 4-styrenesulfonate) (PSS) are subsequently adsorbed to the NPs forming a stable amino functionalized shell. This method provides versatile, highly stable, and biocompatible NPs with controllable shell thickness and charge. Drawbacks are the required washing steps and the limitation of this process to hydrophilic UCNPs.[1]

Electrostatic immobilization of negatively charged poly(ethylene glycol)-*b*-poly(acrylic acid)[38] was also used to generate water dispersible nanocrystals. Streptavidin could be coimmobilized to introduce biofunctionality to this type of particle. A derivative of poly(acrylic acid) (PAA) was used to introduce carboxy groups to bead-milled UCµPs and subsequently to attach streptavidin.[39]

All methods to coat UCNPs mentioned so far are based on non-covalent attachment of polymers by electrostatic or hydrophobic interactions. The only covalent coating method to date is the surface silanization technique.[40] In this approach the UCNPs are coated with a thin layer of silica (more precisely SiO$_2$) by the controlled hydrolysis and polycondensation of precursors such as tetraethyl orthosilicate (TEOS). Functional groups can easily be introduced by the use of organosilanes. Particularly aminosilanes have been used to modify the silica surface. The aminomodified UCNPs can be further biofunctionalized by covalent attachment of biomolecules such as biotin,[40] folic acid,[41] peptides,[42] proteins,[43] antibodies,[44,45] and DNA.[37,46] Silica coated UCNPs have also been directly linked to aminomodified DNA[47] without the use of organosilanes. Polymers such as poly(vinyl pyrrolidone) (PVP)[48] have been used to stabilize the silica shell and control its thickness. Benefits of the silica coating technique are the applicability to both hydrophilic and hydrophobic UCNPs and that entrapment of secondary reporters such as magnetic NPs (Fe$_3$O$_4$)[43,49] or organic dyes becomes possible.[50] In addition, the resulting coated

UCNPs are non-toxic,[51] monodisperse and can be easily dispersed in aqueous solution.

## 2.2 Silica Nanoparticles and Coatings

Silica nanoparticles have been commercialized and are available in various size distributions. As mentioned, silica is a rather benign and biocompatible material. Therefore, it represents an ideal construction tool for bioanalytical applicable fluorescent reporter particles. Furthermore, it is suitable for the coating of nanoparticles made from both organic and inorganic materials, UCNPs being only one example. Additionally, functional groups can be easily introduced to silica surfaces by using the appropriate silane reagents. The chemistry and properties of silica surfaces and particles have been extensively studied in the past.[52,53] Therefore, the following section concentrates on the coating of UCNPs and the biofunctionalization of the silica surface in general.

### 2.2.1 Coating Process

Two general synthetic routes are known to prepare silica coatings: The Stöber process and the microemulsion process. In 1968, Stöber et al.[54] introduced a method for preparing monodisperse silica nanoparticles with diameters ranging from 50 nm to 2 μm. This technique can also be used for the coating of UCNPs with $SiO_2$. In a typical procedure, the UCNPs are dispersed in alcohol (ethanol or 1-propanol). Subsequently, a silica alkoxide precursor (such as TEOS) is added, which hydrolyzes to monosilicic acid in presence of ammonium hydroxide. Monosilicic acid is very prone to intermolecular condensations as it is only stable in very low concentration in alcoholic solutions. The catalyst ammonium hydroxide ensures that the concentration of silicic acid is above its solubility and that the nucleation concentration is consequently exceeded.[55,56] Accordingly, the monosilicic acid undergoes a homogeneous condensation process. First, disilicic acid is formed, followed by a trimer et cetera, until a shell around the UCNP core is formed. A schematic representation of the hydrolysis of TEOS is shown in figure 2.3.
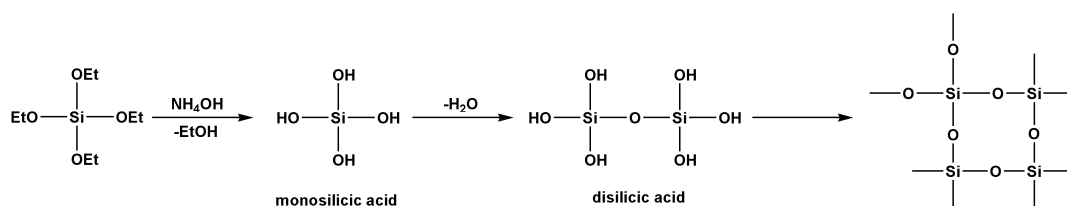
**Figure 2.3** Hydrolysis of TEOS in presence of ammonium hydroxide as catalyst.

Generally, the Stöber process yields monodispersely coated particles with an evenly distributed shell thickness. Nevertheless, the formation of pure silica particles besides the coating of the UCNPs is always a side effect in coating processes. Therefore, it is crucial to control the concentrations of both TEOS precursor and ammonia catalyst to suppress the development of secondary nuclei. Silica coated NPs obtained by the Stöber process can either be separated from the reaction solution via centrifugation or via size exclusion chromatography. Keeping the particles in their colloidal state should be preferred as silica coated NPs shows a tendency towards aggregation.

The second synthetic route to prepare silica shells is the reverse-micelle or water-in-oil (w/o) microemulsion process. Here, surfactant molecules are used to stabilize and disperse water droplets in an organic solvent or "oil".[56] A schematic representation of a microemulsion system is illustrated in figure 2.4. TEOS is used as precursor for particle coating and ammonium hydroxide as catalyst analogously to the Stöber method. The processes differ in the distribution of the reactants between the aqueous phase in the interior of the micelles and the surrounding organic solvent.
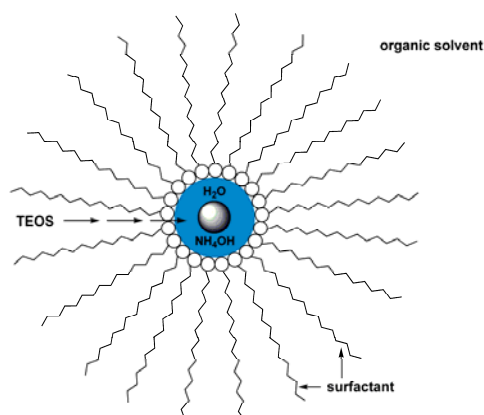


**Figure 2.4** Schematic representation of a water-in-oil microemulsion coating process.

The polar ammonium hydroxide is located in the water phase, whereas TEOS is partitioned between aqueous and organic phase. Diffusion of the TEOS into the micelles, which act as "nanoreactors", promotes the coating reaction. The coated UCNPs are separated from the reaction solution by breaking of the microemulsion via addition of acetone. The size of the developing particles generally is determined by the size of the water nanodroplets, which is controlled by the water-to-surfactant molar ratio.[55] However, the type of microemulsion system chosen also has an effect on particle size. Furthermore, the ideal reaction conditions have to be specifically adjusted to the type and size of the UCNPs that are to be coated. Another drawback of the microemulsion method is that the coated NPs have to be precipitated and centrifuged to isolate them. The particles cannot be kept in a colloidal state to minimize aggregation effects. Moreover, it is virtually impossible to completely remove the surfactant molecules by washing. Typically, the microemulsion process is applied to UCNPs with a hydrophobic surface,[51] whereas the Stöber method can be used for both hydrophilic and hydrophobic UCNPs.[43,57]

## 2.2.2 Surface Modification and Bioconjugation

Particles with a silica surface need to be linked to biorecognition elements, such as proteins, antibodies or DNA molecules, to be of use in bioanalysis or biotechnological applications.[56] Most of these molecules can be physically adsorbed onto the silica surface. However, covalent linkage is to be preferred as it allows controlling the number and orientation of the immobilized reporter molecules and avoids desorption of these. Suitable functional groups need to be introduced to the particle surface to enable covalent attachment. This is commonly done by applying organically modified silanes (with carboxy, thiol, or amino groups) in a secondary silica coating process. This process is usually referred to as "silanization". A typical silanization reagent used for introducing functional groups is illustrated in figure 2.5. One of the hydrolyzable sites (ethoxy in TEOS) is substituted by an alkyl chain with a functional group at its end. The other three groups are commonly ethoxy, methoxy or chlorine groups, which are easily hydrolyzable.
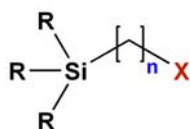
**Figure 2.5** Typical structure of a silanization reagent with X representing a functional group and R a hydrolyzable site.

The organically modified silanes react with the free hydroxy groups on the silica surface analog to the hydrolysis and polycondensation process of TEOS described before. Silanization can be performed in a post-coating step after the prior coating with TEOS.[56] However, it is much more practicable to use a mixture of TEOS and the desired organosilane to attain a silica coating and functionalization in a one-pot reaction as it requires only one separation step.[49,58]
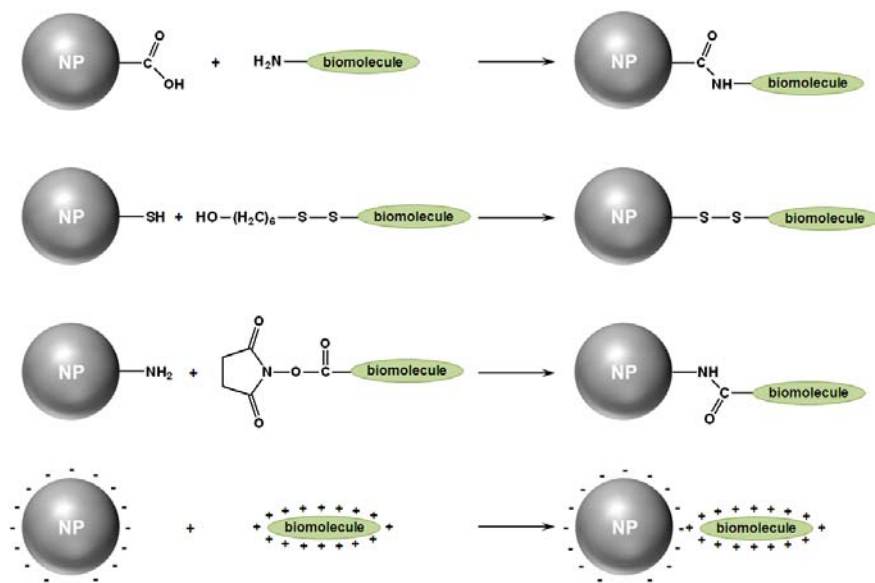


**Figure 2.6** Representative bioconjugation schemes for attaching biomolecules to particles with silica surface.

The most frequently used organosilanes to date contain carboxy, thiol, or amino moieties[59], respectively, as the reactive groups for covalent bioconjugation. Carboxy-modified NPs allow for the coupling to amine containing biomolecules via carbodiimide reagents. Disulfide-modified oligonucleotides can be linked to thiol-functionalized NPs by disulfide-coupling chemistry. NPs with amino moieties can be

attached to a large variety of amino reactive biological entities via succinimidyl esters and iso(thio)cyanates.[56,60] The most common bioconjugation schemes are illustrated in figure 2.6 in comparison to the electrostatic adsorption process.

All functional groups used for these conjugations are abundant in proteinic biomolecules giving rise to unspecific binding reactions. Furthermore, introduction of amino or carboxy groups alters the overall charge of the particles surface. This can lead to a decrease in the colloidal stability of the NPs and thus cause severe particle aggregation. Therefore, other functional groups have been taken into account for the modification of silica NPs. Among these, azido and alkyne have become very popular,[61,62,63] as they undergo a 1,3-dipolar cycloaddition also referred to as "click reaction".

## 2.3 Click Chemistry

### 2.3.1. Definition of Click Chemistry

In 2001, Sharpless et al,[64] defined the term "click chemistry" for the development of modular, easy-to-make building blocks in organic chemistry. A certain process must meet specific criteria to be termed "click reaction". The reaction must be modular, of wide scope, and give high yields. It has to be carried out under simple reaction conditions with readily available starting materials. The process must be insensitive towards water or oxygen and should not require hazardous solvents. Characteristics include stereospecifity and physiological stability of the product. Byproducts should be inoffensive and reaction work-up and purification must be simple, without chromatographic methods.[64,65]

A number of reactions have been found that meet this criteria. They usually rely on carbon-heteroatom bond-formation. In general, the click chemistry family includes cycloaddition reactions, particularly of the 1,3-dipolar type, and hetero-Diels-Alder reactions. Additionally, nucleophilic substitution reactions, especially ring-openings of strained heterocyclic electrophiles such as epoxides, or aziridines can be included to this class. Furthermore, carbonyl reactions of the "non-aldol" kind (formation of ureas, aromatic heterocycles) and additions to carbon-carbon multiple bonds (epoxidation, dihydroxylation, but also specific Michael additions) can be termed click reactions.[64]

However, the premier example of a click reaction, is the copper catalyzed azide-alkyne cycloaddition (CuAAC).

## 2.3.2 The 1,3-Dipolar Cycloaddition of Azides and Alkynes

The 1,3-dipolar cycloaddition of azides and alkynes to give 1,2,3-triazoles has been known for more than 100 years[66] and has been extensively studied in the 1960s by Rolf Huisgen.[67] The reaction scheme is shown in figure 2.7.
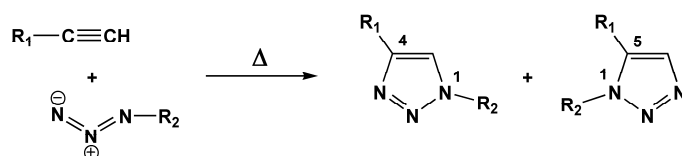


**Figure 2.7** The Huisgen 1,3-dipolar cycloaddition of alkynes and azides.

At first glance, the reaction does not seem to be suitable for click chemistry as it is not regioselective and usually gives the 1,4-disubstituted 1,2,3-triazole and its 1,5-regioisomer in equimolar mixtures. Additionally, the reaction only proceeds at elevated temperature and long reaction times are required. In 2002, the groups of Sharpless[68] and Meldal[69] independently discovered that this cycloaddition reaction is catalyzed by copper(I) ions giving only the 1,4-regioisomer. Furthermore, the reaction now proceeds at room temperature within hours and can be performed in aqueous solutions as well. A Cu(I) salt such as copper iodide (CuI) can be used as catalyst or the Cu(I) is generated *in situ* by using a Cu(II) salt like copper sulfate (CuSO$_4$) and a reducing agent such as sodium ascorbate. A 0.01 molar equivalent of the catalyst is sufficient to promote the reaction. A reaction scheme of the CuAAC is given in figure 2.8.
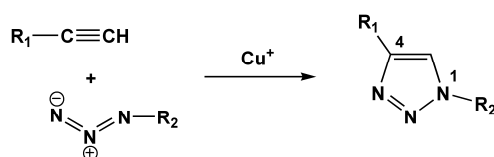


**Figure 2.8** The CuAAC reaction giving only the 1,4-disubstituted 1,2,3-triazole in presence of Cu(I).

The mechanism of the copper catalyzed cycloaddition of azides and terminal alkynes has been extensively studied.[68,70] The catalytic cycle proposed by the Sharpless group is shown in figure 2.9. The cycle starts with the coordination of the alkyne **1** to the Cu(I) species forming the acetylide **2** via the formation of a acetylene $\pi$-complex. In the second step (**B**), one of the copper ligands is replaced by the azide compound. The nitrogen proximal to the carbon forms the bond to the copper species giving intermediate **3**.
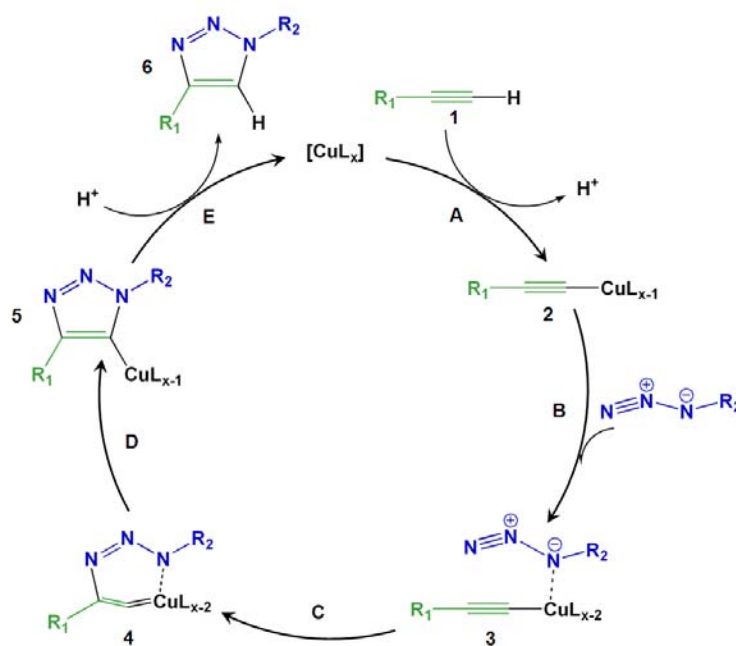


**Figure 2.9** Proposed catalytic cycle for the Cu(I) catalyzed cycloaddition, adapted from references 68 and 70. L stands for a random ligand, the most frequent one is water.

Subsequently, the C-2 carbon of the alkyne is attacked by the distal nitrogen of the azide in **3** giving a six-membered Cu(III) metallacycle (**4**). This step is endothermic. Yet, the energy barrier is much lower than the barrier for the uncatalyzed reaction explaining the accelerating effect of the Cu(I) catalysis. Species **5** is formed in step **D** via a ring contraction reaction. Finally, the product **6** is produced by a proton transfer reaction completing the catalytic cycle. The Cu(I) provides a reliable and powerful tool for the selective synthesis of 1,4 disubstituted 1,2,3-triazoles. Interestingly, it has been found that the 1,5 disubstituted 1,2,3-triazole can also be selectively obtained via ruthenium catalysis.[71,72] However, this reaction still needs elevated temperatures and hazardous solvents such as benzene. Therefore, it is completely inapplicable for bioconjugations.

Azides and alkynes are among the least reactive functional groups in organic chemistry even though they also belong to the most energetic species known. Their stability, being merely of kinetic origin, is the main reason for the slow nature of the cycloaddition reaction in the absence of a catalyst. Furthermore, it ensures inertness towards biological molecules and towards the reaction conditions inside living systems.[65] Therefore, the CuAAC is one of only few reactions considered bioorthogonal.[73] There are certain applications, though, where the use of Cu(I) is not desired. Even low concentrations of copper are cytotoxic, excluding the CuAAC from all kinds of living cell labeling applications. In response to this, the so called Cu-free click chemistry[74] has been developed. Hereby, a strained cyclooctyne ring is used instead of the terminal alkyne. The ring-strain promotes the cycloaddition reaction and the Cu catalyst becomes redundant. This makes the Cu-free azide-alkyne cycloaddition an ideal tool for bioorthogonal ligations *in vivo.*[75,76] Combining the Cu-free method with the Cu-mediated reaction enables specific double labeling in a so called "sequential approach".[77] This is of interest especially for FRET-based investigations.[62]

The Cu-catalyzed cycloaddition of azides and terminal alkynes is the only process relying on the click concept used in this work. Therefore, the CuAAC will be referred to as "the click reaction" in the following, which is in agreement with most literature related to this topic.

## 2.4 References

[1]     Wang F, Liu X (2009) **Recent Advances in the Chemistry of Lanthanide-Doped Upconversion Nanocrystals**, Chem. Soc. Rev. 38: 976-989.

[2]     Auzel F (2004) **Upconversion and Anti-Stokes Processes with f and d Ions in Solids**, Chem. Rev. 104: 139-173.

[3]     Joubert M-F (1999) **Photon Avalanche Upconversion in Rare Earth Laser Materials**, Opt. Mater. 11: 181-203.

[4]     Yang LW, Han HL, Zhang YY, Zhong JX (2009) **White Emission by Frequency Up-Conversion in Yb$^{3+}$-Ho$^{3+}$-Tm$^{3+}$ Triply Doped Hexagonal NaYF$_4$ Nanorods**, J. Phys. Chem. C 113: 18995-18999.

[5]     Wang J, Liu X (2008) **Upconversion Multicolor Fine-Tuning: Visible to Near-Infrared Emission from Lanthanide-Doped NaYF$_4$ Nanoparticles**, J. Am. Chem. Soc. 130: 5642-5643.

[6]     Mai H-X, Zhang Y-W, Sun L-D, Yan C-H (2007) **Highly Efficient Multicolor Up-Conversion Emissions and Their Mechanisms of Monodisperse NaYF$_4$: Yb, Er Core and Core/Shell Structured Nanocrystals**, J. Phys. Chem. C 111: 13721-13729.

7  Chen G, Liu H, Somesfalean G, Liang H, Zhang Z (2009) **Upconversion Emission Tuning from Green to Red in Yb$^{3+}$/Ho$^{3+}$-codoped NaYF$_4$ Nanocrystals by Tridoping with Ce$^{3+}$ Ions**, Nanotechnology 20: 385704-1 - 385704-6.

8  Mahalingam V, Naccache R, Vetrone F, Capobianco JA (2009) **Sensitized Ce$^{3+}$ and Gd$^{3+}$ Ultraviolet Emissions by Tm$^{3+}$ in Colloidal LiYF$_4$ Nanocrystals**, Chem. Eur. J. 15: 9660-9663

9  Wang G, Peng Q, Li Y (2009) **Upconversion Luminescence of Monodisperse CaF$_2$: Yb$^{3+}$/Er$^{3+}$ Nanocrystals**, J. Am. Chem. Soc. 131: 14200-14201.

10  Patra A, Friend CS, Kapoor R, Prasad PN (2003) **Fluorescence Upconversion Properties of Er$^{3+}$-Doped TiO$_2$ and BaTiO$_3$ Nanocrystallites**, Chem. Mater. 15: 3650-3655.

11  Hyppänen I, Hölsa J, Kankare J, Lastusaari M, Pihlgren L (2008) **Preparation and Characterization of Nanocrystalline ZrO$_2$: Yb$^{3+}$, Er$^{3+}$ Up-conversion Phosphors**, Ann. N. Y. Acad. Sci. 1130: 267-271.

12  Heer S, Lehmann O, Haase M, Güdel H-U (2003) **Blue, Green, and Red Upconversion Emission from Lanthanide-Doped LuPO$_4$ and YbPO$_4$ Nanocrystals in a Transparent Colloidal Solution**, Angew. Chem. Int. Ed. 42: 3179-3182, Angew. Chem. 115: 3288-3291.

13  Lü Q, Gu JY, Sun L, Li AH, Zhao LC (2008) **Silica-/Titania-coated Y$_2$O$_3$: Tm$^{3+}$, Yb$^{3+}$ Nanoparticles with Improvement in Upconversion Luminescence Induced by Different Thickness Shells**, J. Appl. Phys. 103: 123533.

14  Hyppänen I, Hölsä J, Jouko K, Lastusaari M, Pihlgren L (2009) **Up-conversion Luminescence Properties of Y$_2$O$_2$S: Yb$^{3+}$, Er$^{3+}$ Nanophosphors**, Opt. Mater. 31: 1787-1790.

15  Aebischer A, Hostettler M, Hauser J, Krämer K, Weber T, Güdel HU, Bürgi H-B (2006) **Structural and Spectroscopic Characterization of Active Sites in a Family of Light-Emitting Sodium Lanthanide Tetrafluorides**, Angew. Chem. Int. Ed. 45: 2802-2806, Angew. Chem. 118: 2869-2873..

16  Zhang L, Hu H, Qi C, Lin F (2001) **Spectroscopic Properties and Energy Transfer in Yb$^{3+}$/Er$^{3+}$-Doped Phosphate Glasses**, Opt. Mater. 17: 371-377.

17  Krämer KW, Biner D, Frei G, Güdel HU, Hehlen MP, Lüthi SR (2004) **Hexagonal Sodium Yttrium Fluoride Based Green and Blue Emitting Upconversion Phosphors**, Chem. Mater. 16: 1244-1251.

18  Shan J, Ju Y (2009) **A Single-Step Synthesis and the Kinetic Mechanism for Monodisperse and Hexagonal-Phase NaYF$_4$: Yb, Er Upconversion Nanophosphors**, Nanotechnology 20: 275603 (13 pp).

19  Yi G, Lu H, Zhao S, Ge Y, Yang W, Chen D, Guo L-H (2004) **Synthesis, Characterization, and Biological Application of Size-Controlled Nanocrystalline NaYF$_4$: Yb, Er Infrared-to-Visible Up-Conversion Phosphors**, Nano Lett. 4: 2191-9196.

20  Yi G-S. Chow G-M (2005) **Colloidal LaF$_3$: Yb, Er, LaF$_3$: Yb, Ho and LaF$_3$: Yb, Tm Nanocrystals with Multicolor Upconversion Fluorescence**, J. Mater. Chem. 15: 4460-4464.

21  Mai, H-X, Zhang Y-W, Sun L-D, Yan C-H (2007) **Highly Efficient Multicolor Up-Conversion Emissions and Their Mechanisms of Monodisperse NaYF$_4$: Yb, Er Core and Core/Shell-Structured Nanocrystals**, J. Phys. Chem. C 111: 13721-13729.

22  Qian H-S, Zhang Y (2008) **Synthesis of Hexagonal-Phase Core-Shell NaYF$_4$ Nanocrystals with Tunable Upconversion Fluorescence**, Langmuir 24: 12123-12125.

23  Boyer J-C, Vetrone F, Cuccia LA, Capobianco JA (2006) **Synthesis of Colloidal Upconverting NaYF$_4$ Nanocrystals Doped with Er$^{3+}$, Yb$^{3+}$ and Tm$^{3+}$, Yb$^{3+}$ via Thermal Decomposition of Lanthanide Trifluoroacetate Precursors**, J. Am. Chem. Soc. 128: 7444-7445.

24  Wang F, Chatterjee DK, Li Z, Zhang Y, Fan X, Wang m (2006) **Synthesis of Polyethylenimine/NaYF$_4$ Nanoparticles with Upconversion Fluorescence**, Nanotechnology 17: 5786-5791.

25    Liu C, Chen D (2007) **Controlled Synthesis of Hexagon Shaped Lanthanide-Doped LaF$_3$ Nanoplates with Multicolor Upconversion Fluorescence**, J. Mater. Chem. 17: 3875-3880.

26    Zhang F, Wang Y, Yu T, Zhang F, Shi Y, Xie S, Li Y, Xu L, Tu B, Zhao D (2007) **Uniform Nanostructured Arrays of Sodium Rare-Earth Fluorides for Highly Efficient Multicolor Upconversion Luminescence**, Angew. Chem. Int. Ed. 46: 7976-7979, Angew. Chem. 119: 8122-8125.

27    Zhang F, Li J, Shan J, Xu L, Zhao D (2009) **Shape, Size, and Phase-Controlled Rare-Earth Fluoride Nanocrystals with Optical Up-Conversion Properties**, Chem. Eur. J. 15: 11010-11019.

28    Liu X, Zhao J, Sun Y, Song K, Yu Y, Du C, Xianggui K, Zhang H (2009) **Ionothermal Synthesis of Hexagonal Phase NaYF$_4$: Yb$^{3+}$, Er$^{3+}$/Tm$^{3+}$ Upconversion Nanophosphors**, Chem. Commun. 6628-6630.

29    Patra A, Friend CS, Kapoor R, Prasad PN (2003) **Fluorescence Upconversion Properties of Er$^{3+}$-Doped TiO$_2$ and BaTiO$_3$ Nanocrystallites**, Chem. Mater. 15: 3650-3655.

30    Pires AM, Serra OA, Davolos MR (2005) **Morphological and Luminescent Studies on Nanosized Er, Yb-Yttrium Oxide Up-Converter Prepared from Different Precursors**, J. Lumin. 113: 174-182.

31    Qin X, Yokomori T, Ju Y (2007) **Flame Synthesis and Characterization of Rare-Earth (Er$^{3+}$, Ho$^{3+}$, and Tm$^{3+}$) Doped Upconversion Nanophosphors**, Appl. Phys. Lett. 90: 073104 (3pp)

32    Yi GS, Chow GM (2006) **Synthesis of Hexagonal-Phase NaYF$_4$: Yb, Er and NaYF$_4$: Yb, Tm Nanocrystals with Efficient Up-Conversion Fluorescence**, Adv. Funct. Mater. 16: 2324-2329.

33    Boyer JC, Manseau MP, Murray JI, van Veggel FCJM (2010) **Surface Modification of Upconverting NaYF$_4$ Nanoparticles with PEG-Phosphate Ligands for NIR (800 nm) Biolabeling within the Biological Window**, Langmuir 26: 1157-1164.

34    Chen Z, Chen H, Hu H, Yu M, Li F, Zhang Q, Zhou Z, Yi T, Huang C (2008) **Versatile Synthesis Strategy for Carboxylic Acid-Functionalized Upconverting Nanophosphors as Biological Labels**, J. Am. Chem. Soc. 130: 3023-3029.

35    Yi GS, Chow GM (2007) **Water-Soluble NaYF$_4$: Yb, Er (Tm)/NaYF$_4$/Polymer Core/Shell/Shell Nanoparticles with Significant Enhancement of Upconversion Fluorescence**, Chem. Mater. 19: 341-343.

36    Wang L, Yan R, Huo Z, Wang L, Zeng J, Bao J, Wang X, Peng Q, Li Y (2005) **Fluorescence Resonant Energy Transfer Biosensor Based on Upconversion-Luminescent Nanoparticles**, Angew. Chem. Int. Ed. 44: 6054-6057, Angew. Chem. 117: 6208-6211.

37    Wang L, Li Y (2006) **Green Upconversion Nanocrystals for DNA Detection**, Chem. Commun. 2557-2559.

38    Kamimura M, Miyamoto K, Saito Y, Soga K, Nagasaki Y (2008) **Design of Poly(ethylene glycol)/Streptavidin Coimmobilized Upconversion Nanophosphors and Their Application to Fluorescence Biolabeling**, Langmuir 24: 8864-8870.

39    Kuningas K, Rantanen T, Karhunen U, Lövgren T, Soukka T (2005) **Simultaneous Use of Time-Resolved Fluorescence and Anti-Stokes Photoluminescence in a Bioaffinity Assay**, Anal. Chem. 77: 2826-2834.

40    Sivakumar S, Diamente PR, van Veggel FCJM (2006) **Silica-Coated Ln$^{3+}$-Doped LaF$_3$ Nanoparticles as Robust Down- and Upconverting Biolabels**, Chem. Eur. J 12: 5878-5884.

41    Hu H, Xiong L, Zhou J, Li F, Cao T, Huang C (2009) **Multimodal-Luminescence Core-Shell Nanocomposites for Targeted Imaging of Tumor Cells**, Chem. Eur. J. 15: 3577-3584.

42    Zako T, Nagata H, Terada N, Utsumi A, Sakono M, Yohda M, Ueda H, Soga K, Maeda M (2009) **Cyclic RGD Peptide-Labeled Upconversion Nanophosphors for Tumor Cell-Targeted Imaging**, Biochem. Biophys. Res. Commun. 381: 54-58.

43   Lu H, Yi G, Zhao S, Chem D, Guo L-H, Cheng J (2004) **Synthesis and Characterization of Multi-Functional Nanoparticles Possessing Magnetic. Up-Conversion Fluorescence and Bio-Affinity Properties**, J. Mater. Chem. 14: 1336-1341.

44   Wang M, Hou W, Mi C-C, Wang W-X, Xu Z-R, Teng H-H, Mao C-B, Xu S-K (2009) **Immunoassay of Goat Antihuman Immunoglobulin G Antibody Based on Luminescence Resonance Energy Transfer between Near-Infrared Responsive NaYF$_4$: Yb, Er Upconversion Fluorescent Nanoparticles and Gold Nanoparticles**, Anal. Chem. 81: 8783-8789.

45   Wang M, Mi C-C, Wang W-X, Liu C-H, Wu Y-F, Xu Z-R, Mao C-B, Xu S-K (2009) **Immunolabeling and NIR-Excited Fluorescent Imaging of HeLa Cells by Using NaYF$_4$: Yb, Er Upconversion Nanoparticles**, ACS Nano 3: 1580-1586.

46   Jiang S, Zhang Y (2010) **Upconversion Nanoparticles-Based FRET System for Study of siRNA in Live Cells**, Langmuir published online DOI: 10.1021/la904011q

47   Zhang P, Rogelj S, Nguyen K, Wheeler D (2006) **Design of a Highly Sensitive and Specific Nucleotide Sensor Based on Photon Upconverting Particles**, J. Am. Chem. Soc. 128: 12410-12411.

48   Li Z, Zhang Y (2006) **Monodisperse Silica-Coated Polyvinylpyrrolidone/NaYF$_4$ Nanocrystals with Multicolor Upconversion Fluorescence Emission**, Angew. Chem. Int. Ed. 45: 7732-7735, Angew. Chem. 118: 7896-7899.

49   Liu Z, Yi G, Zhang H, Ding J, Zhang Y, Xue J (2008) **Monodisperse Silica Nanoparticles Encapsulating Upconversion Fluorescent and Superparamagnetic Nanocrystals**, Chem. Commun. 694-696.

50   Li Z, Zhang Y, Jiang S (2008) **Multicolor Core/Shell-Structured Upconversion Fluorescent Nanoparticles**, Adv. Mater. 20: 4765-4769.

51   Jalil RA, Zhang Y (2008) **Biocompatibility of Silica Coated NaYF$_4$ Upconversion Fluorescent Nanocrystals**, Biomat. 29: 4122-4128.

52   Iler RK (1979)**The Chemistry of Silica: Solubility, Polymerization, Colloid and Surface Properties, and Biochemistry**, John Wiley & Sons, New York

53   Bergna HE, Roberts WO (2005) **Colloidal Silica: Fundamentals and Applications**, Taylor & Francis Group, Boca Raton, FL

54   Stöber W, Fink A (1968) **Controlled Growth of Monodisperse Silica Spheres in the Micron Size Range**, J. Colloid. Interf. Sci. 26: 62-69.

55   Yao G, Wang L, Wu Y, Smith J, Xu J, Zhao W, Lee E, Tan W (2006) **FloDots: Luminescent Nanoparticles**, Anal. Bioanal. Chem. 385: 518-524.

56   Wang L, Wang K, Santra S, Zhao X, Hilliard LR, Smith JE, Wu Y, Tan W (2006) **Watching Silica Nanoparticles Glow in the Biological World**, Anal. Chem. 78: 646-654.

57   Wang M, Mi C, Zhang Y, Liu J, Li F, Mao C, Xu S (2009) **NIR-Responsive Silica-Coated NaYbF$_4$:/Er/Tm/Ho Upconversion Fluorescent Nanoparticles with Tunable Emission Colors and Their Applications in Immunolabeling and Fluorescent Imaging of Cancer Cells**, J. Phys. Chem. C 113: 19021-19027.

58   Deng G, Markowitz MA, Kust PR, Gaber BP (2000) **Control of Surface Expression of Functional Groups on Silica Particles**, Mat. Sci. Eng. C-Bio. S 11: 165-172.

59   Petushkov A, Intra J, Graham JB, Larsen SC, Salem AK (2009) **Effect of Crystal Size and Surface Functionalization on the Cytotoxicity of Silicalite-1 Nanoparticles,** Chem. Res. Toxicol. 22: 1359–1368.

60   Knopp D, Tang D, Niessner R (2009) **Review: Bioanalytical Applications of Biomolecule-Functionalized Nanometer-Sized Doped Silica Particles**, Anal. Chim. Acta 647: 14-30.

61   Mader H, Li X, Saleh S, Link M, Kele P, Wolfbeis OS (2008) **Fluorescent Silica Nanoparticles**, Ann. N. Y. Acad. Sci. 1130: 213-223.

62 Achatz DE, Mező G, Kele P, Wolfbeis OS (2009) **Probing the Activity of Matrix Metallopreteinase II with a Sequentially Click-Labeled Silica Nanoparticle FRET Probe**, ChemBioChem 10: 2316-2320.

63 Lin P-C, Ueng S-H, Yu S-C, Jan M-D, Adak AK, Yu C-C, Lien C-C (2007) **Surface Modification of Magnetic Nanoparticle via Cu(I)-Catalyzed Alkyne-azide [2+3] Cycloaddition**, Org. Lett. 9: 2131-2134.

64 Kolb HC, Finn MG, Sharpless KB (2001) **Click Chemistry: Diverse Chemical Function from a Few Good Reactions**, Angew. Chem. Int. Ed. 40: 2004-2021, Angew. Chem. 113: 1198-1220.

65 Kolb HC, Sharpless KB (2003) **The Growing Impact of Click Chemistry on Drug Discovery**, Drug Discov. Today 8: 1128-1137.

66 Michael A (1893) **Über die Einwirkung von Diazobenzolimid auf Acetylendicarbonsäuremethylester**, J. Prakt. Chem. 48: 94-95

67 Huisgen R (1963) **1,3-Dipolar Cycloadditions – Past and Future**, Angew. Chem. Int. Ed. 2: 565-632, Angew. Chem. 75: 604-637.

68 Rostovtsev VV, Green LG, Fokin VV, Sharpless KB (2002) **A Stepwise Huisgen Cycloaddition Process: Copper(I)-Catalyzed Regioselective "Ligation" of Azides and Terminal Alkynes**, Angew. Chem. Int. Ed. 41: 2596-2599, Angew. Chem. 114: 2708-2711.

69 Tornøe CW, Christensen C, Meldal M (2002) **Peptidotriazoles on Solid Phase: [1,2,3]-Triazoles by Regiospecific Copper(I)-Catalyzed 1,3-Dipolar Cycloaddition of Terminal Alkynes to Azides**, J. Org. Chem. 67: 3057-3064.

70 Himo F, Lovell T, Hilgraf R, Rostovtsev VV, Noodleman L, Sharpless KB, Fokin VV (2005) **Copper(I)-Catalyzed Synthesis of Azoles. DFT Study Predicts Unprecedented Reactivity and Intermediates**, J. Am. Chem. Soc. 127: 210-216.

71 Zhang L, Chen X, Xue P, Sun HHY, Williams ID, Sharpless KB, Fokin VV, Jia G (2005) **Ruthenium-Catalyzed Cycloaddition of Alkynes and Organic Azides**, J. Am. Chem. Soc. 127: 15998-15999.

72 Boren BC, Narayan S, Rasmussen LK, Zhang L, Zhao H, Lin Z, Jia G, Fokin VV (2008) **Ruthenium-Catalyzed Azide-Alkyne Cycloaddition: Scope and Mechanism**, J. Am. Chem. Soc. 130: 8923-8930.

73 Kurpiers T, Mootz HD (2009) **Bioorthogonal Ligation in the Spotlight**, Angew. Chem. Int. Ed. 48: 1729-1731, Angew. Chem. 121: 1757-1760.

74 Agard NJ, Prescher JA, Bertozzi CR (2004) **A Strain-Promoted [3+2] Azide-Alkyne Cycloaddition for Covalent Modification of Biomolecules in Living Systems**, J. Am. Chem. Soc. 126: 15046-15047.

75 Baskin JM, Prescher JA, Laughlin ST, Agard NJ, Chang PV, Miller IA, Lo A, Codelli JA, Bertozzi CR (2007) **Copper-free Click Chemistry for Dynamic in Vivo Imaging**, P. Natl. Acad. Sci. 104: 16793-16797.

76 Chang PV, Prescher JA, Sletten EM; Baskin JM, Miller IA, Agard NJ, Lo A, Bertozzi CR (2010) **Copper-free Click Chemisty in Living Animals**, P. Natl. Acad. Sci, published online, DOI: 10.1073/pnas.0911116107.

77 Kele P, Mezö G, Achatz D, Wolfbeis OS (2009) **Dual Labeling of Biomolecules by Using Click Chemisty: A Sequential Approach**, Angew. Chem. Int. Ed. 48: 344-347, Angew. Chem. 121: 350-353.

# 3 Particle Synthesis and Characterization

## 3.1 Silica Nanoparticles (SiNPs)

Silica nanoparticles (SiNPs) were used as model system to become acquainted with the silanization technique and click functionalization of silica surfaces. Therefore, the SiNPs were not self-synthesized but commercially available silica particles were used. The spherical and porous SiNPs are said to have a diameter of about 10 nm. Nevertheless, they show considerable aggregation as can be observed from the Transmission Electron Microscope (TEM) image in figure 3.1.
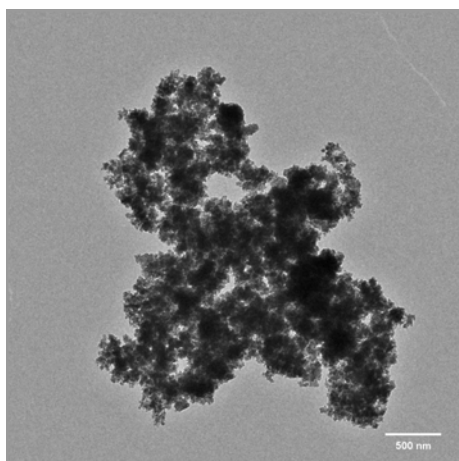


**Figure 3.1** TEM image of aggregated SiNPs (3000x magnification).

The SiNPs were used for silanization reactions without further modification. The aggregated nature of the particles did not cause any problems as the particles were not intended to be used in any bioanalytical applications.

## 3.2 Upconverting Microparticles (UCµPs)

Upconverting microparticles (UCµPs) only require low energy laser diodes (~10 mW) as excitation sources. Therefore, commercially available UCµPs with the compositions $La_2O_2S$: Yb, Er, referred to as **µP-1**, and $Y_2O_2S$: Yb, Tm referred to as **µP-2** were used to study their upconversion properties. The morphology of the

particles was investigated via scanning electron microscopy (SEM). Both kinds of particles are irregular in shape and size, with diameters ranging from approximately 5 to 15 µm (see figure 3.2).
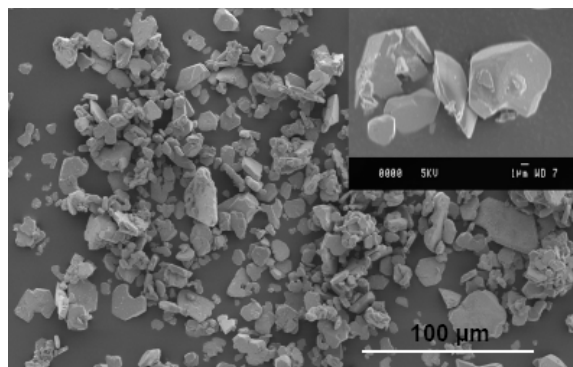


**Figure 3.2** SEM picture of UCµPs of type µP-1 in 400x magnification. The insert on the upper right shows the particles in a further 10-fold magnification.

The emission spectra of the µPs were acquired using a 10 mW, 980 nm continuous wave diode laser as the excitation source. The strong green and red intrinsic luminescence of **µP-1**, peaking at 540 nm and 660 nm, is clearly visible to the eye (see figure 3.3, green solid line).
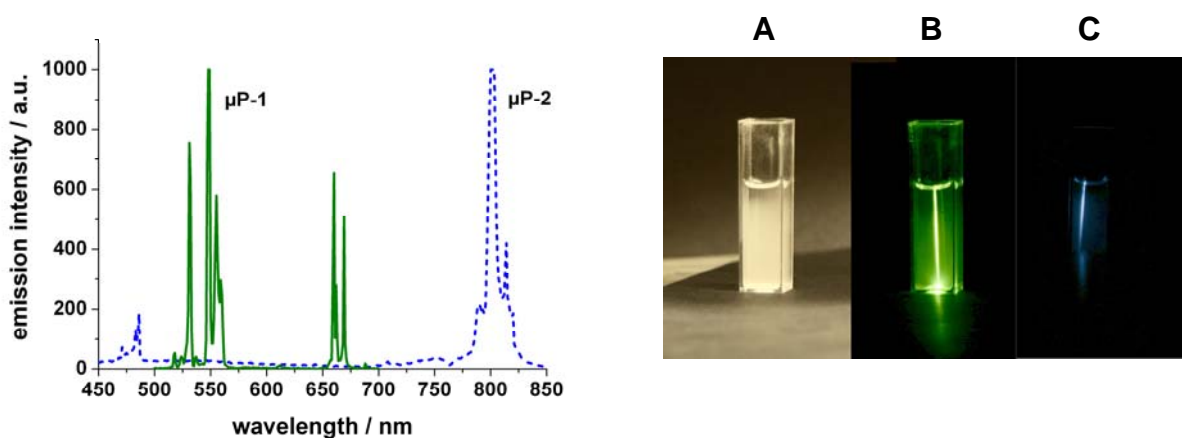


**Figure 3.3** (*Left*) Emission spectra of UCµPs of type **µP-1** (solid line) and **µP-2** (dashed line) following excitation with a 10-mW 980-nm diode laser. (*Right*) Photographs of µPs in aqueous dispersions (3 mg/mL): **A**: **µP-1** in daylight. **B**: green emission of **µP-1** under 980 nm excitation, **C**: blue emission of **µP-2** under 980 nm excitation

Strong blue (along with considerable near-infrared emission) is observed for microparticles of type **µP-2**, with rather sharp and discrete peaks located at 475 nm and 800 nm, respectively (figure 3.3, blue dotted line). These rather sharp lines of the upconverters represent an attractive feature that has a large potential in terms of multiplex signaling and sensing.

UCµPs are not dispersible in aqueous solution due to their large size. Therefore, they are not well suitable for bioanalytical purposes. They may be bead-milled to obtain sub-micron particles. However, grinding generates particles with even larger variation of shape and size. Furthermore, UC emission is decreased due to the reduced size as well as imperfections in the crystal structure caused by mechanical shearing.[1] There was a need for particles with smaller size, to address these problems and limitations. Therefore, upconverting nanoparticles (UCNPs) were synthesized as they are not commercially available.

## 3.3 Upconverting Nanoparticles (UCNPs)

### 3.3.1 Synthetic Procedure

The highest upconversion efficiencies to date have been observed in doped hexagonal phase $\beta$-NaYF$_4$.[2] Therefore, NaYF$_4$ was chosen as host material. The strongest emission can be obtained by using Er$^{3+}$, Tm$^{3+}$ and Ho$^{3+}$ as activator ions, which were therefore selected as dopant ions (see chapter 2.1.1). The preparation method of choice was the co-precipitation technique as it is reliable, fast, and does not require any special laboratory equipment. Furthermore, the surface of the resulting UCNPs is hydrophilic, facilitating their application in aqueous solutions.

The UCNPs were synthesized according to a method described by Yi et al.[3] Solutions of the trichlorides of the ions Y$^{3+}$ and Yb$^{3+}$, along with either Er$^{3+}$, Tm$^{3+}$ or Ho$^{3+}$ were combined with an ethylenediaminetetraacetic acid (EDTA) solution to form the respective EDTA complexes. This solution was injected quickly into a aqueous solution of sodium fluoride. The resulting mixture was stirred for 1 h at room temperature to give a colorless precipitate that was separated by centrifugation, washed with water and finally with ethanol. The precipitate was dried in a drying furnace and under vacuum. The colorless powder was annealed at 400 °C for 4.5 h under argon atmosphere.

## 3.3.2 NaYF$_4$ Doped with Yb$^{3+}$ and Er$^{3+}$

NaYF$_4$ nanoparticles with different dopant concentrations of Yb$^{3+}$ and Er$^{3+}$ were prepared. The percentages given refer to the composition of the initial mixture of the lanthanide-EDTA complexes. All types of particles were characterized using transmission electron microscopy (TEM), X-Ray diffraction (XRD) and fluorescence spectroscopy. A content of 17% Yb and 3% Er was chosen for the first type of upconverting nanoparticles (**NP-1**) according to the details given by Yi et al.[3] TEM pictures show particles which are crystalline and kind of spherical in shape (see figure 3.4, left) with diameters ranging from 60 to 90 nm. The XRD pattern (figure 3.4, right) of **NP-1** can be assigned to the cubic phase $\alpha$-NaYF$_4$ (International Centre for Diffraction Data (ICDD) No. 77-2042). Tempering of the particles at 400 °C did not result in a phase transfer to the hexagonal phase $\beta$-NaYF$_4$. The XRD data of the annealed particles only showed sharper peaks and a lower background signal indicating a better crystallinity of the material. The morphology of the particles did not change by the annealing process as could be verified via TEM.
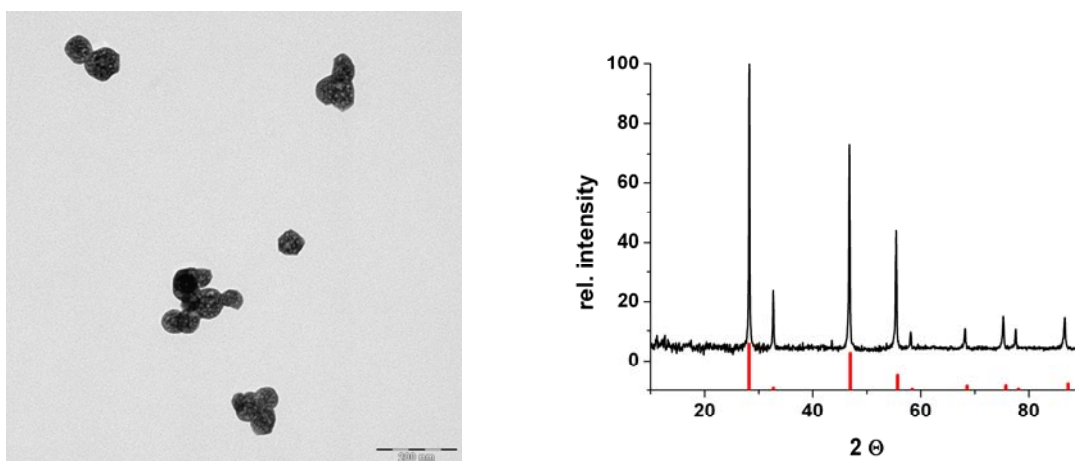


**Figure 3.4** (*Left*) TEM image of annealed $\alpha$-NaYF$_4$ of type **NP-1** (40000x magnification). (*Right*) XRD pattern of annealed $\alpha$-NaYF$_4$ of type **NP-1** in agreement to the cubic structure [77-2042] (red lines).

The composition of the particles of type **NP-1** was also analyzed via inductively coupled plasma optical emission spectrometry (ICP-OES). The results indicated that the ratio of Y:Yb:Er in the actual particles is 81.5:15.8:2.7. There is a discrepancy to

the molar ratios in the reaction solution (80:17:3). This difference results from the varying chelating constants of EDTA for the three lanthanide ions. The $Yb^{3+}$-EDTA complex possesses the highest binding constant which is why the ytterbium content in the final particles is lower than in the initial reaction solution.[3] In the following, the composition of the reaction solution will be equalized to the composition of the final nanoparticle as this is customary in the literature.[4,5]

The particles of the type **NP-1** were non-luminescent prior to the annealing process. After the heat treatment they showed the moderate luminescence intensity typical for $\alpha$-NaYF$_4$. In order to find nanoparticles with higher luminescence intensity or alternatively, higher phase transition efficiency, two more dopant concentrations were investigated. **NP-2** was prepared with 20 % $Yb^{3+}$ and 2 % $Er^{3+}$ as prior studies indicated that ytterbium concentrations between 20 and 25 % and erbium concentrations around 2 % are beneficial for upconversion efficiency.[4] However, TEM and XRD results were analog to the particles of type **NP-1** and no improvement in luminescence intensity could be determined. The concentration of the sensitizer $Yb^{3+}$ was raised to 25 % for the particles of type **NP-3** whereas the concentration of $Er^{3+}$ was left unchanged at 2%.
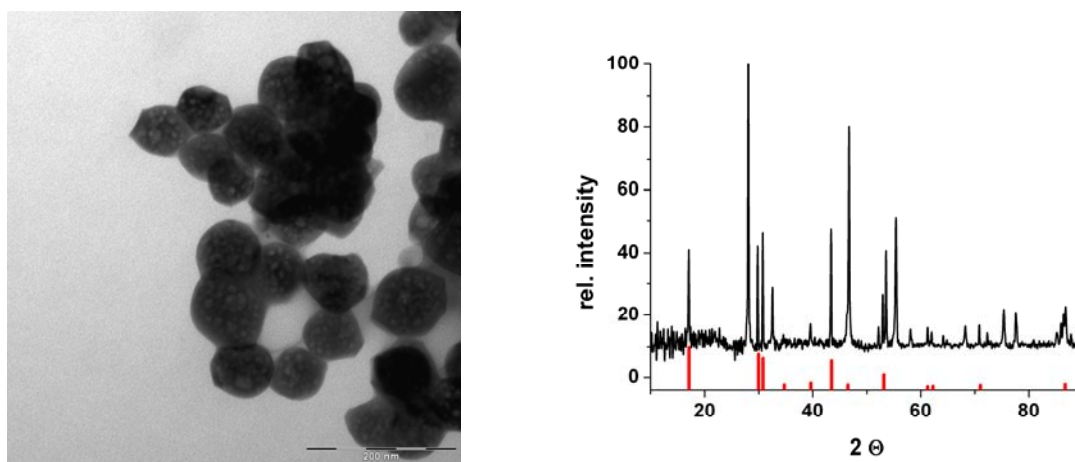


**Figure 3.5** (*Left*) TEM image of NaYF$_4$ nanoparticles of type **NP-3** (80000x magnification). (*Right*) XRD pattern of NaYF$_4$ nanoparticles of type **NP-3**, indicating a mixture of the cubic structure [77-2042] (see figure 3.4) and the hexagonal phase [28-1192] (red lines).

TEM pictures of **NP-3** show crystalline particles with diameters ranging from 60 to 90 nm (see figure 3.5). The NPs seem to have a higher tendency towards aggregation after the annealing process compared to the particles of type **NP-1**. The XRD of non

tempered particles only showed the pattern related to the cubic phase $\alpha$-NaYF$_4$ (ICDD No. 77-2042). After annealing at 400 °C a second pattern emerged in addition to the existing cubic phase, which can be assigned to the hexagonal phase $\beta$-NaYF$_4$ (ICDD No. 28-1192). This indicates a partial phase transfer of the particles of type **NP-3** from the cubic to the hexagonal phase by annealing. It was not considered to use higher temperatures, so to achieve a more complete conversion from the cubic to the hexagonal phase because this is compromised by a substantial increase in the size of the particles,[3] thereby reducing the dispersibility of the particles. There is also no indication that longer annealing times facilitate the phase transfer.

The emission spectra of the erbium doped nanoparticles were acquired using a 5-W, 980-nm continuous wave diode laser as the excitation light source. Upconversion nanoparticles require a stronger excitation power as the luminescence intensity is size dependent. Generally, smaller particles exhibit lower emission intensities. An emission spectrum of particles of type **NP-3** is shown in figure 3.6. The peak maxima are located at 520, 540, and 655 nm, as is typical for all particles doped with Er$^{3+}$. The luminescence of the UCNPs appears purely green to the naked eye (see figure 3.6) as the green peak at 540 nm is more than twice as high as the red peak at 655 nm and the eye is more sensitive to green light.
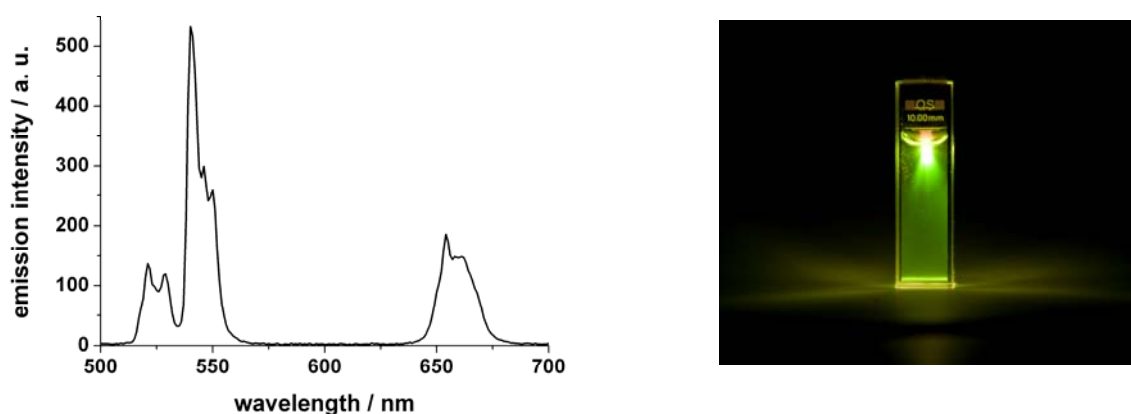


**Figure 3.6** (*Left*) Emission spectrum of UCNPs of type **NP-3** (Yb, Er). (*Right*) Photograph of an aqueous solution of **NP-3** (5 mg/mL) under 980 nm excitation.

The locations of the emission peaks are the same for all particles of the types **NP-1**, **NP-2** and **NP-3**. The emission intensities were compared to each other. **NP-1** exhibits a luminescence three times higher than **NP-2** (see figure 3.7). The emission intensity

of **NP-3** is more than 10 times higher than the one obtained for **NP-2**. This considerable difference in luminescence intensities can be assigned to the varying dopant concentrations. In case of **NP-3**, the presence of the hexagonal phase is causing a disproportionally strong increase in luminescence intensity. The particles of the type **NP-1** were used for surface modification experiments and assay development. They were later substituted by the brighter particles of the type **NP-3**.
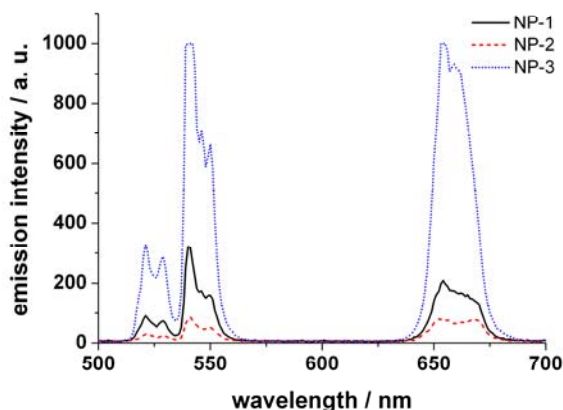


**Figure 3.7** Emission spectra of UCNPs of types **NP-1** (17 % Yb, 3 % Er, solid line), **NP-2** (20 % Yb, 2 % Er, dashed line) and **NP-3** (25 % Yb, 2 % Er, dotted line). Composition of the UCNPs has a large influence on upconversion properties.

Remarkably, it was found that the luminescence intensity of the UCNPs after tempering also depends on the kind of oven used for the heat treatment. Generally, annealing in a muffle furnace gave better results than tempering in a tube furnace. However, two samples of the same batch, tempered at two different days never exhibited the identical emission intensity. Even the ratio of the green to red peak varied to a certain degree (see figure 3.8). Most likely, this is due to irreproducible variations of the oven temperature during heat treatment.
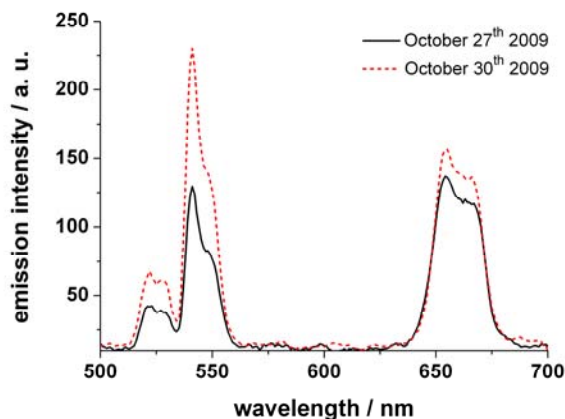
**Figure 3.8** Emission spectra of UCNPs of the type **NP-1** synthesized in the same batch but tempered at 400 °C at different dates (October 27th, 2009, solid line, and October 30th, 2009, dashed line)

## 3.3.3 NaYF$_4$ Doped with Yb$^{3+}$ and Tm$^{3+}$

NaYF$_4$ particles doped with Yb$^{3+}$ and Tm$^{3+}$ were prepared to obtain particles with blue emission. The synthetic procedure was analog to the method used for the preparation of **NP-1**. The UCNPs of the type **NP-4** contained 17 % Yb and 1.5 % Tm according to a literature example.[5] TEM images showed crystalline particles with roughly spherical shape (see figure 3.9).
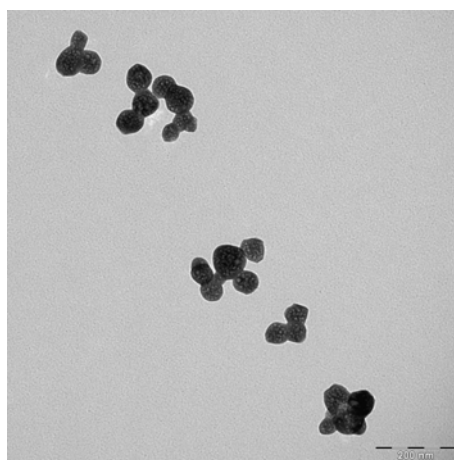


**Figure 3.9** TEM image of annealed NaYF$_4$ nanoparticles of type **NP-4** (40000x magnification)

The results are identical to those obtained for erbium doped **NP-1**. Therefore, it can be stated that the appearance of the particles is not affected by the activator dopant. XRD data indicated that the particles are of the cubic phase $\alpha$-NaYF$_4$ (ICDD No. 77-2042). This is true for non-tempered as well as for tempered NPs.

The nanoparticles of the type **NP-4** showed moderate blue luminescence at 475 nm and a strong emission at 800 nm, which is typical for UCNPs doped with thulium. In order to obtain particles with better upconversion efficiency, different dopant concentrations were investigated. **NP-5** contains 24.5 % Yb and 0.5 % Tm and was prepared by Daniela Achatz using the same co-precipitation method.[6] They show bright blue emission at 475 nm, and a very strong NIR emission at 800 nm (see figure 3.10). Additionally, small peaks at 646 nm and 696 can be observed. The nanoparticles of the type **NP-4** were used for surface modification experiments and later substituted by the brighter **NP-5** particles.
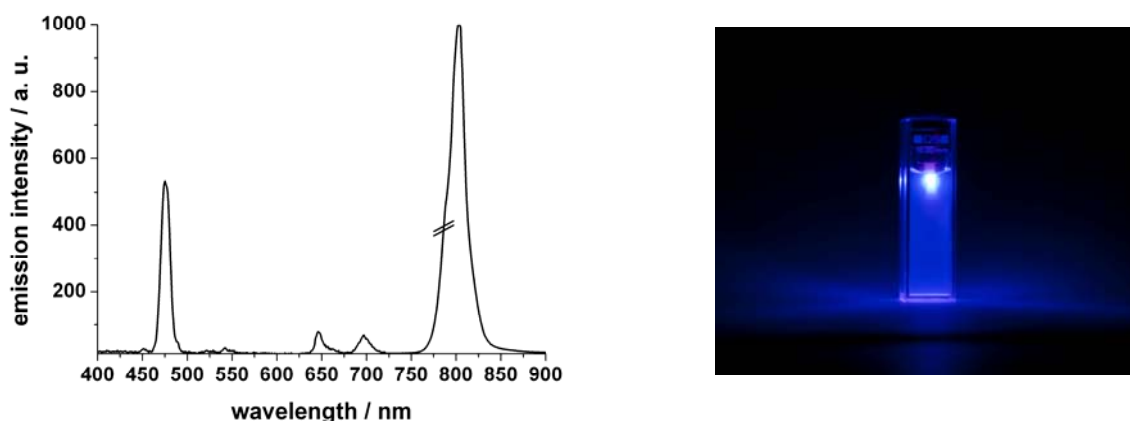


**Figure 3.10** (*Left*) Emission spectrum of UCNPs of type **NP-5** (Yb, Tm). The peak at 800 nm is reduced by factor 10 in the graph. (*Right*) Photograph of an aqueous solution of **NP-5** (5 mg/mL) under 980 nm excitation.

## 3.3.4 NaYF$_4$ Doped with Yb$^{3+}$ and Ho$^{3+}$

In another type of particles, holmium was used as dopant for NaYF$_4$ UCNPs. **NP-6** was doped with 25 % Yb and 2 % Ho. TEM pictures gave the same results as for erbium- or thulium-doped particles. XRD data of non-tempered and tempered **NP-6** particles indicated that a phase transfer of the cubic to the hexagonal phase had failed. The particles were 100 % cubic with diameters ranging from 60 – 90 nm.

The luminescence intensity of the particles of the type **NP-6** was considerably weaker compared to erbium doped UCNPs. The particles exhibit green and red emission peaks at 547 nm and 651 nm, respectively, which is typical for UCNPs doped with holmium. The intensity of the green peak is two times higher than the intensity of the red peak. Therefore, the particle emission under 980 nm excitation appears green to the naked eye.



**Figure 3.11** (*Left*) Emission spectrum of UCNPs of type **NP-6** (Yb, Ho). (*Right*) Photograph of an aqueous solution of **NP-6** (5 mg/mL) under 980 nm excitation.

In order to study the effect of different holmium concentrations, **NP-7** containing 25 % Yb and 0.5 % Ho was prepared. TEM and XRD results were the same as for **NP-6**, confirming cubic particles with diameters from 60 – 90 nm. The luminescence intensity was in the same range as for **NP-6** and was not affected by the reduction of the Ho$^{3+}$ content. However, the ratio of the green to red peak did change.
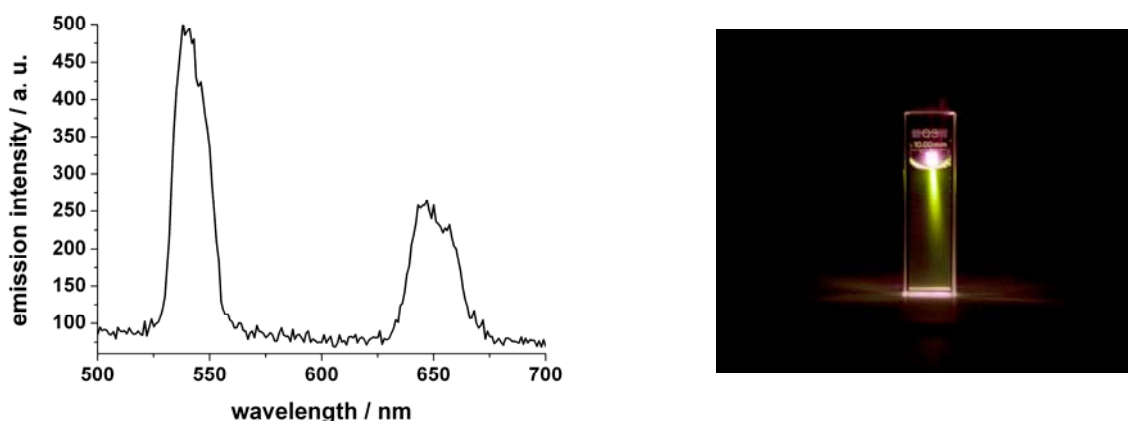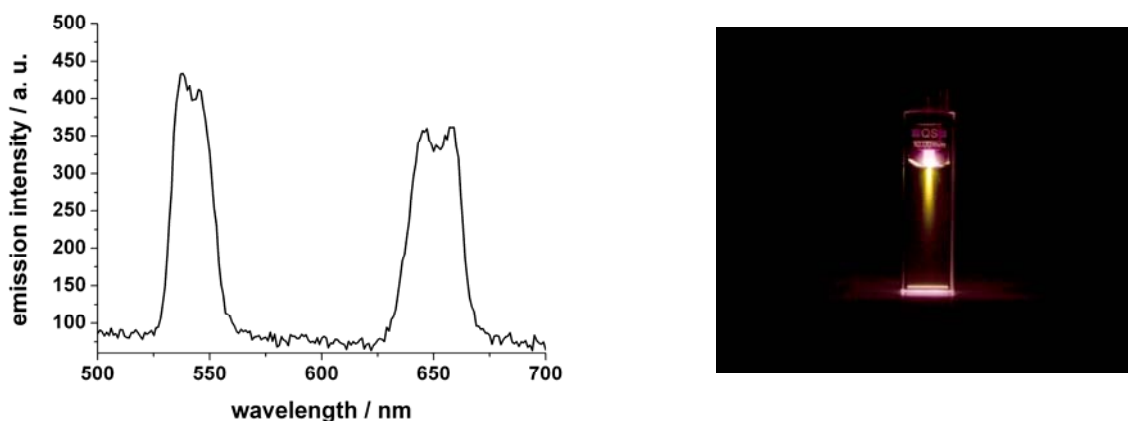


**Figure 3.12** (*Left*) Emission spectrum of UCNPs of type **NP-7** (Yb, Ho). (*Right*) Photograph of an aqueous solution of **NP-7** (5 mg/mL) under 980 nm excitation.

In particles of the type **NP-7** the green peak at 547 nm and the red peak at 651 nm have approximately the same intensity. As a result, the emission of the UCNPs under 980 nm appears yellow (mixture of green and red). Due to the limited brightness of the $Ho^{3+}$ doped particles, they were not used for further surface modification experiments.

## 3.3.5 NaYF$_4$ Doped with Yb$^{3+}$ and Er$^{3+}$ Synthesized in Ionic Liquids

Ionic liquids (ILs) were considered as solvents for particle synthesis with the aim of preparing bright upconversion nanoparticles without the need for an annealing step. In general, an ionic liquid can be defined as a liquid that consists only of ions, exhibits a melting point below 100 °C, and shows low viscosity.[7] Conventional ILs usually contain bulky organic cations with a low degree of symmetry (e. g. imidazolium, pyrrolidinium, tetraalkylphosphonium, trialkylsulfonium or quaternary ammonium). These cations impede the regular packing in a crystal lattice. As a consequence, the solid crystalline state becomes energetically less favorable, resulting in low melting points. The application of an anion with a delocalized charge is able to further increase this effect because interionic interactions are reduced.[7] Ionic liquids have been used for the preparation of $\beta$-NaYF$_4$ in an ionothermal method.[8]

The common ionic liquid ethylammonium nitrate (EAN) has a melting point of 11 °C and decomposes at ~250 °C. It is hydrophilic and displays solvent properties similar to water.[7,9] Additionally, EAN can be used in combination with surfactants to form reverse-microemulsions in oil with EAN as the polar phase. The application of EAN as a solvent in the co-precipitation method allows for the synthesis of the UCNPs at temperatures above 100 °C comparable to the solvothermal process. It was envisioned that precipitation the UCNPs at elevated temperature would facilitate the direct formation of hexagonal $\beta$-NaYF$_4$.

The synthesis of the UCNPs in ionic liquids was performed in collaboration with Oliver Zech[7] from the Institute of Physical Chemistry. **NP-8** was prepared directly in a solution of EAN. YCl$_3$, YbCl$_3$ and ErCl$_3$ were dissolved in EAN corresponding to a ratio of Y:Yb:Er of 80:17:3. The solution was heated to 160 °C and subsequently

injected into a 1 M sodium fluoride solution in EAN. The resulting mixture was stirred for 1 h and the colorless precipitate separated by centrifugation, and washed with water and finally with ethanol.

The particles of type **NP-8** show a morphology which is significantly different from the particles obtained with the conventional method (**NP-1** – **NP-7**) as can be observed from the TEM image in figure 3.13. The particles are of cubic shape with diameters ranging from 20 – 40 nm. XRD data showed a single pattern assigned to the cubic $\alpha$-NaYF$_4$ phase. The high background signal and the non-sharp peaks indicated a poorer crystallinity as obtained for **NP-1** – **NP-7**. A direct formation of hexagonal particles could not be observed. The exact composition of the NPs was determined with ICP-OES. Data indicated a content of 16.2 % of Yb and 2.5 % of Er. Both amounts are a little lower than in the initial reaction mixture (17 % and 3 %, respectively). It is not known whether this is due to the ionic liquid or just to the absence of the chelator EDTA in this method.
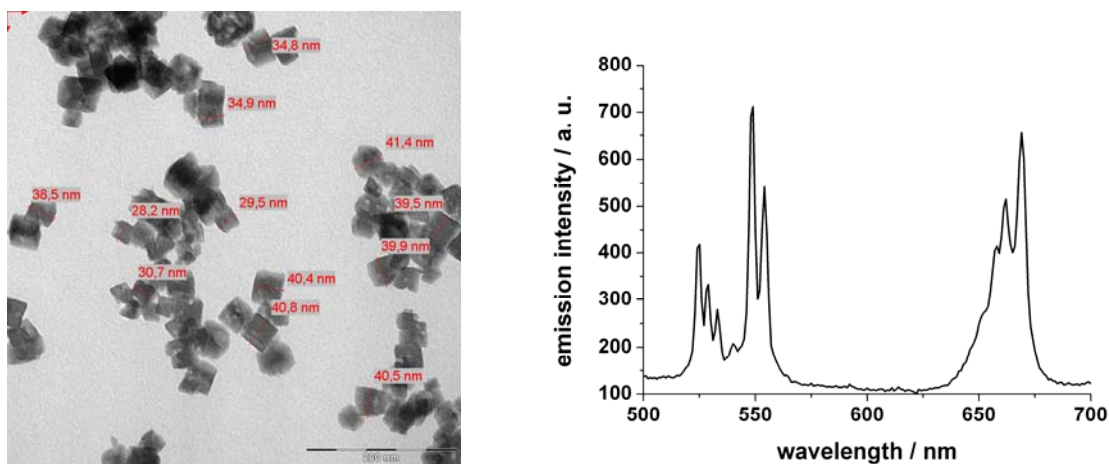


**Figure 3.13** *(Left)* TEM image of UCNPs of type **NP-8**, synthesized in the ionic liquid EAN (80000x magnification). *(Right)* Emission spectrum of UCNPs of type **NP-8** (bulk material).

In contrast to the particles synthesized in aqueous solution, the particles of type **NP-8** are luminescent without an additional annealing process. Unfortunately, this luminescence is very weak and could not be measured in solution. The emission spectrum was obtained from the powder material (figure 3.13). The green and red peaks typical for erbium doped particles can be observed. The overall appearance of the emission color is yellow.

The preparation of nanoparticles in micromulsions with small droplets inside the micelles usually guarantees the formation of very small particles. Therefore, **NP-9** was synthesized in a microemulsion of EAN in dodecane with 1-hexadecyl-3-methylimidazolium chloride as the surfactant. The microemulsion solution contained 50 w% dodecane, 40 w% surfactant and 10 w% EAN (resulting in droplet diameters of ~10 nm). $YCl_3$, $YbCl_3$, and $ErCl_3$ were dissolved in 5 mL of this solution corresponding to a ratio of Y:Yb:Er of 80:17:3. Then, the solution was heated to 160 °C and combined with 5 mL of the microemulsion solution containing 1 M NaF. The resulting mixture was stirred for 1 h. The nanoparticles were separated by centrifugation, and washed with water and finally with ethanol.
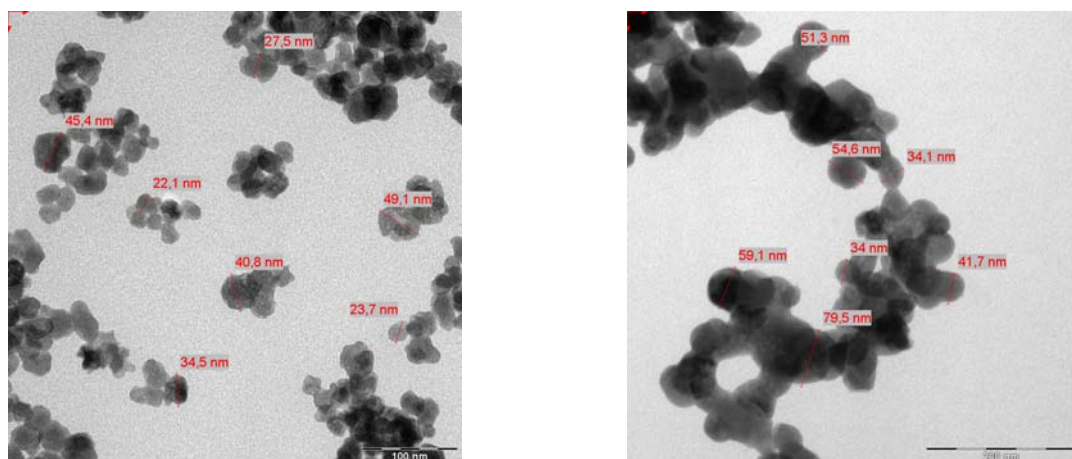


**Figure 3.14** (*Left*) TEM image of UCNPs of type **NP-9**, synthesized in ionic liquid microemulsion (100000x magnification). (*Right*) TEM image of UCNPs of type **NP-9** after annealing at 400°C (80000x magnification).

TEM pictures show particles with diameters from 20 – 50 nm and potato like shapes (see figure 3.14). The particles seem to have aggregated or formed outside the microemulsion droplets as their sizes exceed the nanodroplet dimensions. According to XRD data the nanoparticles of type **NP-9** were 100 % cubic. The NPs were directly luminescent but their luminescence was very weak so that it could hardly be detected in solution (see figure 3.15, left). Therefore, the particles were annealed at 400 °C for 4.5 h in a muffle furnace to enhance their luminescent properties. TEM images (see figure 3.14, right) show that the size of the particles was slightly increased by that process to 30 – 60 nm and that bigger aggregates had formed. As indicated by XRD data the NPs were still 100 % cubic. However, the emission intensity of the green

peak increased to the 9fold and the intensity of the red peak to the more than 15fold (see figure 3.15). It appears that the probability of the $^4F_{9/2} \rightarrow {}^4I_{15/2}$ transition assigned to the red emission at 655 nm increased to a higher degree compared to the $^2H_{11/2} \rightarrow {}^4I_{15/2}$, $^4S_{3/2} \rightarrow {}^4I_{15/2}$ transitions responsible for the green emission. The emission intensity of **NP-9** after annealing is still distinctly lower than the intensity of the particles of the types **NP-1** or **NP-3**. This could be at least partly due to their smaller size. The overall emission color of the UCNPs of the type **NP-9** therefore ranges between yellow and red.
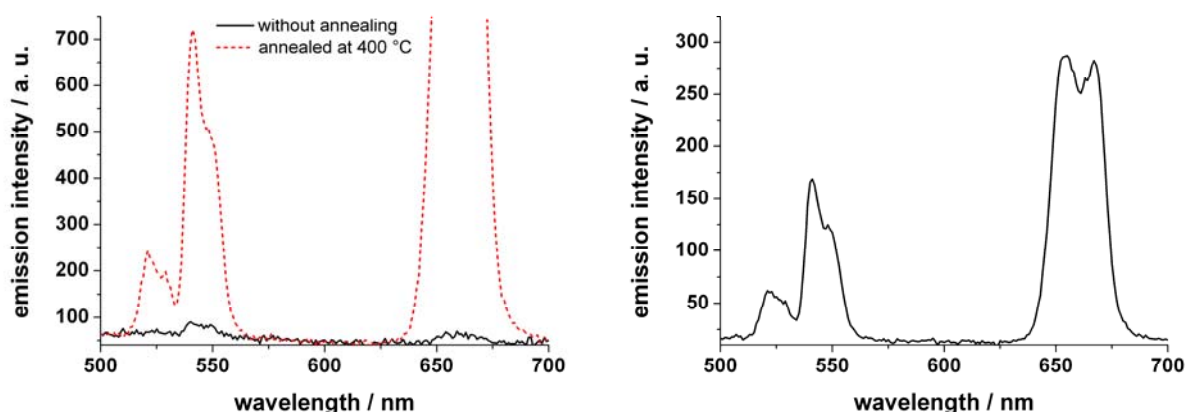


**Figure 3.15** *(Left)* Emission spectra of UCNPs of type **NP-9** prior to and after annealing at 400 °C. *(Right)* Full emission spectra of **NP-9** after annealing.

The particles of the types **NP-8** and **NP-9** were not used for further experiments as the direct preparation of hexagonal NaYF$_4$ NPs had failed and the emission intensity is not comparable to particles obtained by the conventional co-precipitation method. Furthermore, large amounts of the ionic liquid are required to prepare the UCNPs in a reasonable scale. In case of the microemulsion, numerous washing steps are required to remove the surfactant and the oil phase.

Nine different types of upconverting nanoparticles have been synthesized. **NP-1**, **NP-3**, **NP-4** and **NP-5** were selected for further experiments. Table 1 summarizes all particles used in this work.

**Table 3.1** Micro- and nanoparticles used in this work

| Code | Net formula | Size | Emission color | Dispersible? |
|------|-------------|------|----------------|--------------|
| SiNP | $SiO_2$ | ~ 10 nm | not fluorescent | moderately |
| µP-1 | $La_2O_2S$: Yb,Er | 5 - 15 µm | green and red | not dispersible |
| µP-2 | $Y_2O_2S$: Yb,Tm | 5 - 15 µm | blue and NIR | not dispersible |
| NP-1 | $NaYF_4$: 17 % Yb, 3 % Er | 60 – 90 nm | green and red | fairly well |
| NP-2 | $NaYF_4$: 20 % Yb, 2 % Er | 60 – 90 nm | green and red | fairly well |
| NP-3 | $NaYF_4$: 25 % Yb, 2 % Er | 60 – 90 nm | green and red | fairly well |
| NP-4 | $NaYF_4$: 17 % Yb, 1.5 % Tm | 60 - 90 nm | blue and NIR | fairly well |
| NP-5 | $NaYF_4$: 24.5 % Yb, 0.5 % Tm | 60 - 90 nm | blue and NIR | fairly well |
| NP-6 | $NaYF_4$: 25 % Yb, 2 % Ho | 60 – 90 nm | green and red | fairly well |
| NP-7 | $NaYF_4$: 25 % Yb, 0.5 % Ho | 60 – 90 nm | green and red | fairly well |
| NP-8 | $NaYF_4$: 17 % Yb, 3 % Er | 20 – 40 nm | green and red | fairly well |
| NP-9 | $NaYF_4$: 17 % Yb, 3 % Er | 30 – 60 nm | green and red | fairly well |

## 3.4 Discussion

Commercially available silica nanoparticles were characterized to serve as model system for particle silanization experiments. The morphology and the luminescent properties of upconversion microparticles were investigated. These UCµPs only require low excitation powers but they can not be used in bioanalytical applications due to their large size. Therefore, upconverting nanoparticles of the type $NaYF_4$ were synthesized using the co-precipitation method. Ytterbium was used as sensitzer dopant. Three different activator dopants, Er, Tm, and Ho were applied in varying concentrations. The best upconversion efficiencies generally were obtained when

using $Er^{3+}$ as dopant. Holmium doped cubic $NaYF_4$ only gave moderate luminescence at 547 nm and 651 nm. A phase transfer to the higher luminescent hexagonal $NaYF_4$, failed. The ratio of the green to red emission appears to depend strongly on the $Ho^{3+}$ concentration. UCNPs doped with thulium gave the strongest blue emission at 475 nm with contents of 24.5 % of $Yb^{3+}$, and 0.5 % of $Tm^{3+}$. For erbium doped NPs, a content of 25 % of $Yb^{3+}$ and 2% of $Er^{3+}$ was found to give the highest upconversion luminescence (**NP-3**). The ratio of the green to red peak was similar for all tested particles and did not appear to strongly relate to the dopant concentrations. Emission intensities of all particles depended strongly on the oven used for annealing and to some extent on the date of the annealing, indicating that the temperature in the ovens is not stable at all times. This problem has not been addressed in the literature so far. **NP-3** was the only composition for all tested UCNPs were a partial phase transfer from the cubic $\alpha$-$NaYF_4$ to the hexagonal $\beta$-$NaYF_4$ via annealing succeeded. As a consequence, the luminescence of **NP-3** was much brighter than for all other particles tested. It is not known whether the exact particle composition has an influence on the phase transfer probability. An effect of the inconsistent oven conditions can not be completely ruled out. Nevertheless, when samples of **NP-1**, **NP-2** and **NP-3** were tempered in the same oven at the same date, a phase transfer could only be determined for **NP-3** suggesting that an actual influence of the dopant concentrations is more likely. A further study on the fine-tuning of the dopant concentrations or annealing temperatures and times was not performed as the purpose of this work was to provide UCNPs of the type $NaYF_4$ with sufficient luminescence to be surface modified for further use in bioassays and sensors.

It can be stated that a careful control of the oven temperature is crucial for reproducible results regarding the luminescent intensity of the particles. However, the tube furnace and the muffle furnace used in this work did not meet this necessity. An oven fine-tuned for this purpose should be used in future works to ensure a constant quality of the UCNPs.

Furthermore, it was shown, that $NaYF_4$ UCNPs can also be synthesized via a co-precipitation method in the ionic liquid EAN at elevated temperatures. This method resulted in particles considerably smaller compared to the conventional co-precipitation method which were already luminescent without the need for an annealing step. However, the luminescence was very weak and not sufficient for the

application of the particles in assays or sensors. The envisioned direct synthesis of hexagonal NaYF$_4$ failed. It is assumed that higher temperatures or pressures (as in the ionothermal method) are required to favor the generation of $\beta$-NaYF$_4$. The luminescence intensity could be highly enhanced by tempering even though no phase transfer could be detected. In contrast to the particles of type **NP-1** with nearly the same composition the intensity of the red peak was much higher for the particles of the types **NP-8** and **NP-9**. This may be due to morphological differences in the crystal host lattice or the volume-to-surface ratio. Ionic liquids represent an attractive tool for the preparation of small hydrophilic UCNPs if higher temperatures can be used to facilitate the formation of $\beta$-NaYF$_4$.

Concluding, hydrophilic NaYF$_4$ UCNPs with Yb and Er, Tm, or Ho, respectively as dopants with narrow size distribution were synthesized with the aim to use them for surface modification with click chemistry. **NP-3** with a composition of 25 % of Yb$^{3+}$ and 2% of Er$^{3+}$ proved to have the best emission intensity. It was also shown that the ionic liquid EAN is suitable for the preparation of small UCNPs but at the expense of luminescence intensity.

## 3.5 References

[1]    Soukka T, Rantanen T, Kuningas K (2008) **Photon Upconversion in Homogeneous Fluorescence-based Bioanalytical Assays**, Ann. N. Y. Acad. Sci. 1130: 188-200.

[2]    Zhang F, Li J, Shan J, Xu L, Zhao D (2009) **Shape, Size, and Phase-Controlled Rare-Earth Fluoride Nanocrystals with Optical Up-Conversion Properties**, Chem. Eur. J. 15: 11010-11019.

[3]    Yi G, Lu H, Zhao S, Ge Y, Yang W, Chen D, Guo L-H (2004) **Synthesis, Characterization, and Biological Application of Size-Controlled Nanocrystalline NaYF$_4$: Yb, Er Infrared-to-Visible Up-Conversion Phosphors**, Nano Lett. 4: 2191-9196.

[4]    Mai H-X, Zhang Y-W, Sun L-D, Yan C-H (2007) **Highly Efficient Multicolor Up-Conversion Emissions and Their Mechanisms of Monodisperse NaYF$_4$: Yb, Er Core and Core/Shell Structured Nanocrystals**, J. Phys. Chem. C 111: 13721-13729.

[5]    Wei Y, Lu J, Zhang X, Chen D (2007) **Synthesis and Characterization of Efficient Near-Infrared Upconversion Yb and Tm codoped NaYF$_4$ Nanocrystal Reporter**, J. Alloy. Compd. 427: 333-340.

[6]    Achatz DE, Meier RJ, Fischer LH, Wolfbeis OS (2010) **Oxygen Sensor based on NaYF$_4$:Yb, Tm Upconverting Nanoparticles**, submitted

[7]    Zech O (2010) **Ionic Liquids in Microemulsions – a Concept to Extend the Conventional Thermal Stability Range of Microemulsions**, Dissertation, University of Regensburg

8    Liu X, Zhao J, Sun Y, Song K, Yu Y, Du C, Kong X, Zhang H (2009) **Ionothermal Synthesis of Hexagonal-Phase NaYF$_4$: Yb$^{3+}$, Er$^{3+}$/Tm$^{3+}$ Upconversion Nanophosphors**, Chem. Commun. 6628-6630.

9    Zech O, Thomaier S, Bauduin P, Rück T, Touraud D, Kunz W (2009) **Microemulsions with an Ionic Liquid Surfactant and Room Temperature Ionic Liquids As Polar Pseudo-Phase**, J. Phys. Chem. B 113: 465-473.

# 4 Surface Modification and Click Functionalization

## 4.1 Silanization and Coating of Particles

The reagents shown in figure 4.1 were used to introduce an azido group or a terminal alkyne group onto the surface of silica nanoparticles (SiNP) as well as upconverting micro- and nanoparticles (UCµPs and UCNPs) to make them applicable for click chemistry. Similar (but more complex) reagents have been used in the past[1,2] to modify the surface of silica nanoparticles. In being trimethoxy of triethoxysilanes, they are capable of reacting with surface hydroxy groups of numerous solid materials.
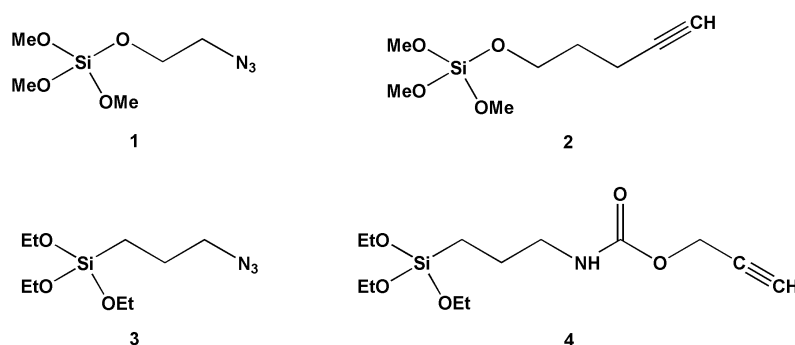


**Figure 4.1** Clickable silanes used in this work

### 4.1.1 Click Functionalized SiNPs

The silanes **1** and **2** were used for the modification of the silica particles (SiNPs). The SiNPs were suspended in dry toluene in a Schlenk flask and flushed with dry nitrogen. Subsequently, the respective silane (**1** or **2**) was added and the mixture was stirred for 48 h at 90°C. The mixture was allowed to cool and the particles were separated by centrifugation. The particles were washed several times with ethanol and acetone, and finally dried in a drying furnace at 60 °C. A schematic representation of the modification process is given in figure 4.2. The resulting azido or alkyne modified SiNPs were characterized using TEM and IR-spectroscopy.
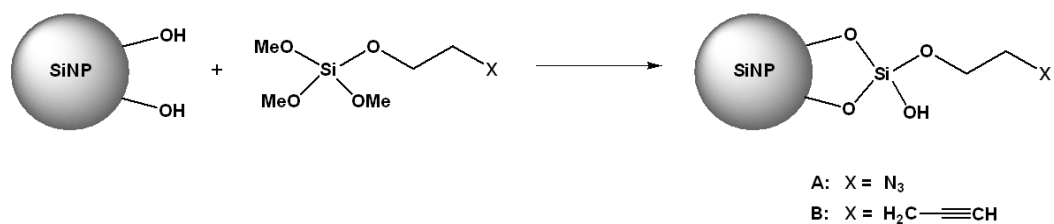
**Figure 4.2** Synthetic route to azido and alkyne modified SiNPs, respectively

Silanization of the SiNPs did not change their morphology. The particles are still highly aggregated and show no sign of a visible coating (see figure 4.3). Therefore, it is assumed that the functionalization took place via attachment of a monolayer of the respective silane (**1** or **2**). The azido modified silica nanoparticles are referred to as **SiNP-A**, the alkyne modified particles as **SiNP-B**.
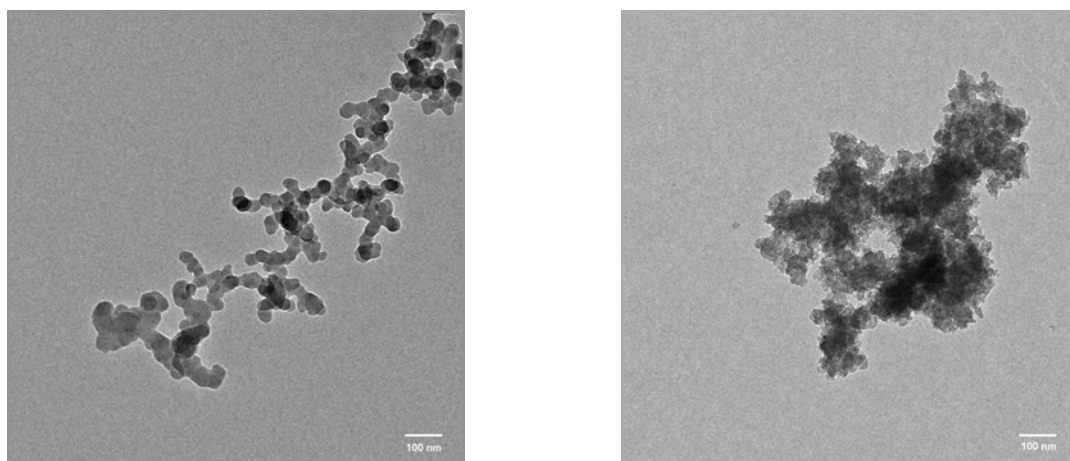


**Figure 4.3** *(Left)* TEM image of azido modified silica nanoparticles of type **SiNP-A** (10000x). *(Right)* TEM image of alkyne modified silica nanoparticles of type **SiNP-B** (10000x)

The presence of the functional groups was verified via IR spectroscopy. Unmodified SiNPs were used as reference in these differential spectra. The spectrum of the azido-NPs (**SiNP-A**), shown in figure 4.4a, displays a strong peak at 2124 cm$^{-1}$, characteristic of the anti-symmetric stretch vibration of the azido group[3], and peaks at 2945, 2887 and 2860 cm$^{-1}$ for the asymmetric vibration of the C-H bond. The IR spectrum of the alkyne-NPs (**SiNP-B**) shows a sharp peak at 2113 cm$^{-1}$ assigned to the C≡C stretching vibrations and the peaks at 2949, 2890 and 2852 cm$^{-1}$ are characteristic for the C-H stretch (see figure 4.4b).
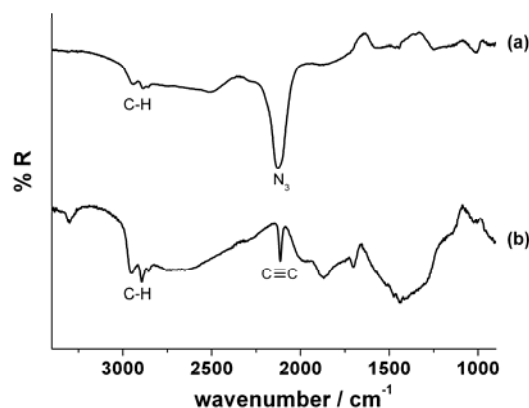
**Figure 4.4** IR reflectance spectra of surface modified silica nanoparticles. (a) type **SiNP-A** . (b) type **SiNP-B**. Note that reflectance rather than absorbance is given on the y axis due to the use of a reflectance spectrometer.

Both types of particles (**SiNP-A** and **SiNP-B**) were further used for click labeling with biotin and fluorescent dyes. The azido and alkyne modified SiNPs were stable as powder or in aqueous dispersions for several months. However, the oxygen bridge present in the silanes **1** and **2** might be susceptible to cleavage reactions. Therefore, they were substituted by silanes **3** and **4** for the modification of the UCµPs and UCNPs to guarantee even better stability.

## 4.1.2 Click Functionalized UCµPs

The UCµPs of the types **µP-1** and **µP-2** (see table 3.1) were functionalized using silanes **3** and **4** for the reasons given in the above paragraph. This is possible because of the (partially) oxidic nature of practically all microparticles. Oxides are present in hydrated form (i.e. hydroxides) on surfaces in a way comparable to silicium dioxide. This is even true for metal surfaces, graphite, or carbon nanotubes, all of which can react with alkoxy silanes in the manner illustrated in figure 4.5. Silane reagents such as aminopropyl triethoxysilane (APTS) previously[4,5,6,7] have been reacted with numerous surfaces including such uncommon ones as titanium, graphite, iron, or materials used for medical implants to render them reactive (via the amino groups introduced) towards biomolecules. This is a quite direct way of functionalization and also does not cause any aggregation of particles.
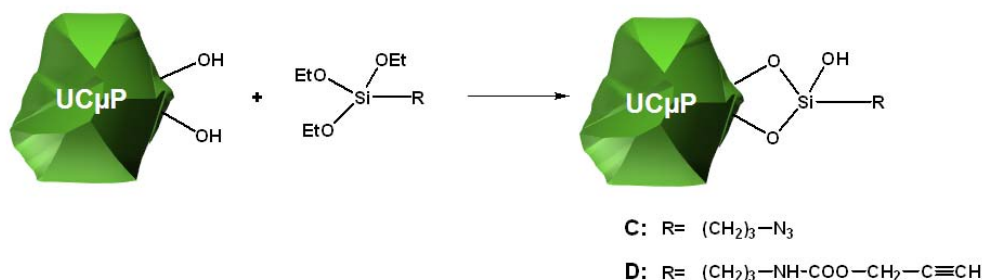
**Figure 4.5** Synthetic route to azido and alkyne modified μPs, respectively

**μP-1** was reacted with **3** to give azido modified **μP-1-C** and **μP-2** was reacted with **4** to give alkyne modified **μP-2-D**. For this, the UCμPs were suspended in dry toluene in a Schlenk flask and flushed with dry nitrogen. The respective silane (**3** or **4**) was added and the mixture stirred for 48 h at 90 °C. The mixture was allowed to cool and the particles were separated by centrifugation. The particles were washed several times with ethanol and acetone, and finally dried in a drying furnace at 60 °C. The resulting modified UCμPs were characterized by SEM, and IR spectroscopy. As can be seen from the SEM image in figure 4.6, surface modification virtually had no effect on the size or morphology of the particles. It is therefore concluded, that no silica shell developed around the microparticles but rather a monolayer of the functional silane was formed.
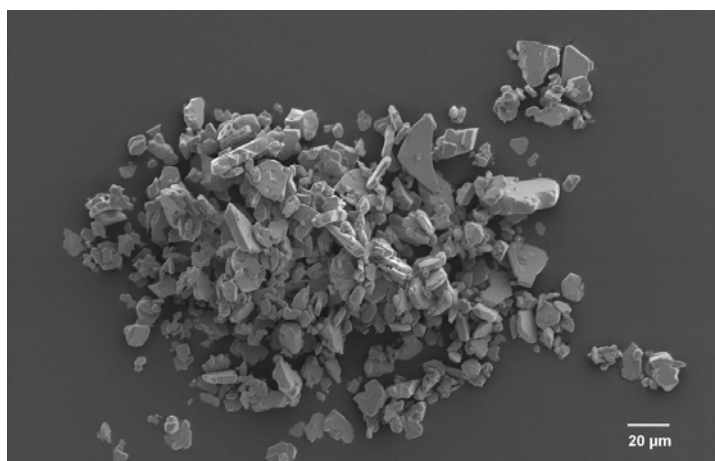


**Figure 4.6** SEM image of azido modified upconverting microparticles of type **μP-1-C** (400x magnification)

Infrared spectra were acquired next in order to verify the presence of azido or alkyne groups on the modified UCµPs. Those of the azido modified **µP-1-C** (see figure 4.7a) showed a strong peak at 2098 cm$^{-1}$ which is characteristic of the asymmetric stretch vibration of the azido group. Further peaks are found at 2965 and 2879 cm$^{-1}$ for the asymmetric stretching vibrations of the C-H bonds. The IR spectrum of the alkyne modified **µP-2-D** (see figure 4.7b) reveals a strong peak at 1710 cm$^{-1}$ owing to the C=O bond vibration of the urethane carbonyl group, and a peak at 1538 cm$^{-1}$ characteristic of the amide. The weak peak at 2126 cm$^{-1}$ is assigned to the C≡C stretching vibrations, and peaks at 2977, 2944 and 2887 cm$^{-1}$ to C-H stretches.
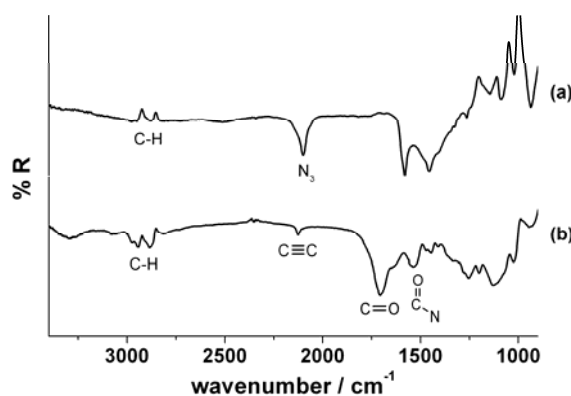


**Figure 4.7** IR reflectance spectra of surface modified upconverting microparticles. (a) type **µP-1-C**. (b) type **µP-2-D**. Note that reflectance rather than absorbance is given on the y axis due to the use of a reflectance spectrometer.

The modified UCµPs are stable as powder or in aqueous dispersion for several months and were used for click labeling with biotin and fluorescent dyes. The luminescent properties remained unchanged.

### 4.1.3 Silica Coated and Click Functionalized UCNPs

UCNPs may also be directly functionalized as described for the UCµPs due to the presence of hydroxy functions on the surface of an otherwise non-oxidic material. However, UCNPs coated with a (hydrophilic) silica coating are more stable in dispersion. Therefore, the UCNPs were simultaneously coated with silica and click-functionalized by employing a mixture of tetraethoxyorthosilicate (TEOS) and the

respective triethoxysilane (**3** or **4**) using a modified Stöber method[8] which was chosen because it is facile, fast, and provides highly reproducible results in terms of the thickness of the silica coating. A schematic of this one-step procedure for simultaneous coating and functionalization of UCNPs with either azide or alkyne is given in figure 4.8.
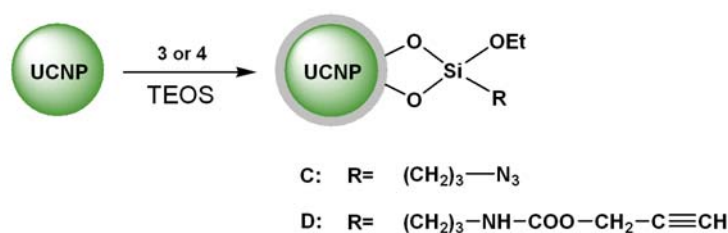


**Figure 4.8** Synthetic route to azido- and alkyne modified nanoparticles possessing a silica shell

In a general coating procedure, the UCNPs were dispersed in ethanol via ultrasonication. Subsequently, the mixture was heated to 40 °C, and water and 25 w% ammonia were added, followed by tetraethoxysilane (TEOS). The solution was stirred before the respective functionalized silane (**3** or **4**; µL) was added and the mixture was stirred again. The different amounts of reagents used in the different approaches are summarized in table 4.1. The functionalized silane is always added after the TEOS to ensure that the functional groups are incorporated at the surface and not inside the silica shell.

The silica coated UCNPs need to be separated from the reaction solution. Commonly, this is accomplished by several centrifugation and washing steps. However, silica NPs show a considerable dependency towards aggregation in solution, which is amplified by centrifugation. Redispersion is time consuming and it is impossible to fully restore the previous, separate state. Drying of the silica NPs even leads to irreversible agglomeration. As a consequence, it is vital to keep the silica coated UCNPs in a colloidal form. Therefore, the coated particles were purified by size exclusion chromatography (SEC) on Sephadex LH-60 and then kept in dispersion for use in further surface chemistry, thereby minimizing aggregation.

**Table 4.1** Exact amounts of the reagents used in the coating methods

| Method | $m_{NP}$ | $V_{EtOH}$ | $V_{H2O}$ | $V_{NH4OH}$ | $V_{TEOS}$ | $V_{Silane}$ |
|--------|----------|------------|-----------|-------------|------------|--------------|
| | in mg | | in mL | | | in µL |
| $C_1$ | 75 | 10 | 0.5 | 0.5 | 500 | 25 |
| $C_2$ | 75 | 10 | 0.5 | 0.5 | 400 | 25 |
| $D_2$ | 75 | 10 | 0.5 | 0.5 | 400 | 25 |
| $C_3$ | 30 | 80 | 7.5 | 8.5 | 100 | 25 |
| $D_3$ | 30 | 80 | 7.5 | 8.5 | 100 | 25 |
| $C_4$ | 30 | 80 | 7.5 | 8.5 | 50 | 25 |

In the first method ($C_1$), low amounts of water (0.5 mL) and ammonia (0.5 mL) were used combined with a high concentration of UCNPs in solution (7.5 mg/mL). 500 µL of TEOS were added and the azidosilane **3** (25 µL) was used as the respective functionalized silane. The coating process resulted in highly monodisperse particles of type **NP-1-C₁** with a shell thickness of ~10 nm (see figure 4.9, left). Aside from coated UCNPs also very small silica particles are visible on the TEM insert picture in figure 4.9, left. This indicates secondary nucleation in the reaction solution. Apparently, the smaller silica nanoparticles were not removed completely by SEC.
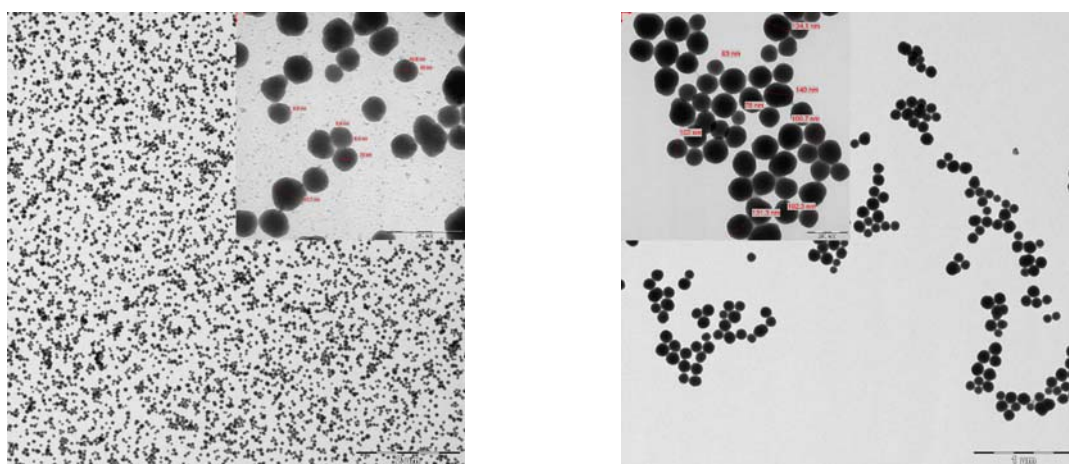


**Figure 4.9** *(Left)* TEM images of UCNPs of the type **NP-1-C₁** (5000x magnification, insert 80000x, scale bar 200 nm). *(Right)* TEM images of UCNPs of the type **NP-4-C₂** (10000x magnification, insert 40000x, scale bar 200 nm).

Therefore, the amount of TEOS in the reaction mixture was reduced in method $C_2$ to avert this secondary nucleation. The resulting coated UCNPS of type **NP-4-C$_2$** possessed a shell thickness of ~15 nm (see figure 4.9 right) and no trace of pure silica NPs could be found.

The equivalent amounts of TEOS and the functionalized silane were used to prepare alkyne modified UCNPs of type **NP-1-D$_2$**. The particles showed a shell thickness of ~15 nm and no pure silica NPs could be detected on TEM images (see figure 4.10). Experiments with using even lower amounts of TEOS or ammonia in order to reduce the shell size failed in that they resulted in irreproducible coatings or the appearance of a large amount of uncoated UCNPs accompanied by pure silica particles.
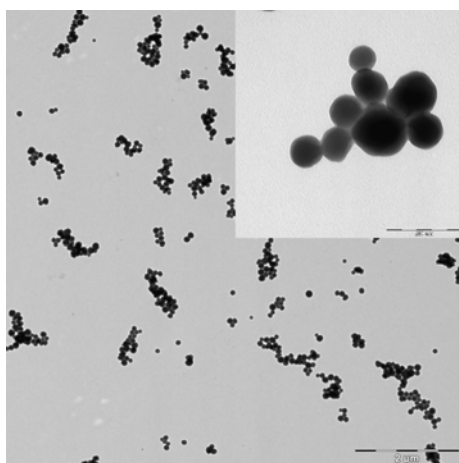


**Figure 4.10** TEM images of UCNPs of the type **NP-1-D$_2$** (5000x magnification, insert: 80000x, scale bar 200 nm).

The high concentration of the UCNPs in solution used in this method sometimes led to precipitates of aggregated uncoated particles and resulting unsatisfying coating results. Therefore, the coating process was changed to a method described by Lu et al.[9] using lower UCNPs concentrations and higher amounts of the catalysts ammonia and water. In method $C_3$ (see table 4.1), a UCNP concentration of 0.375 mg/mL was applied and 7.5 mL of water, and 8.5 mL of 25 w% ammonia were added. 100 μL of TEOS were used together with 25 μL of the azidosilane **3**. The coating resulted in spherical particles with a very defined and homogeneous silica shell with a thickness of ~25 nm (see figure 4.11). Furthermore, this method could be easily reproduced

with other types of particles and also with the alkynesilane with analog results. Reduction of the amount of TEOS by half ($C_4$ in table 4.1) did not lead to a noticeable decrease in the shell thickness, but gave rise to formation of pure silica particles. A study on the effect of the ammonia concentration on shell thickness was not performed due to time reasons. All further coating experiments were performed using method $C_3/D_3$. All particles coated with the Stöber method can be well dispersed in water and – unlike the uncoated particles – show little tendency towards aggregation in solution. The particles are stable for several months in aqueous or ethanolic dispersions.
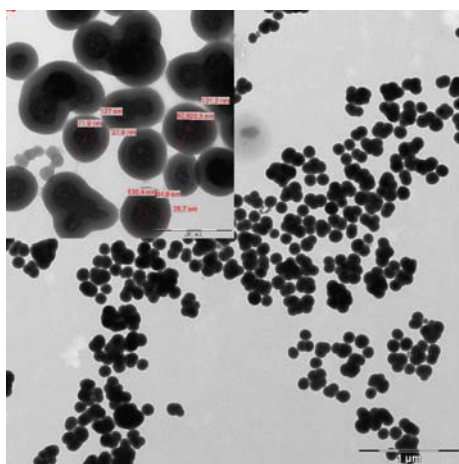


**Figure 4.11** TEM images of UCNPs of the type **NP-4-C$_3$** 10000x magnification, insert 80000x, scale bar 200 nm).

The microemulsion method was also investigated for coating UCNPs for comparison studies. A reverse microemulsion of water in cyclohexane using Triton X-100 and n-hexanol as surfactants was applied. The resulting coated particles of type **NP-1-C$_5$** showed a thin but inhomogeneous silica shell (~10 nm) (see figure 4.12). Additionally, the particles were highly aggregated as it is not possible to purify the particles via SEC. Numerous centrifugation and washing steps are required to remove the oil and surfactants from the particle surface. A complete removal of the surfactant molecules can never be ensured as some TEM pictures indicated the presence of residues. Due to these drawbacks, this method was not further investigated.
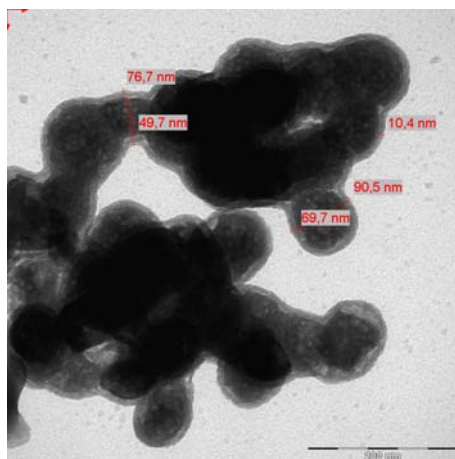
**Figure 4.12** TEM images of UCNPs of the type **NP-1-C$_5$**.

The particles coated via the Stöber method were further investigated via elementary analysis, IR spectroscopy and fluorescence spectroscopy. The IR spectrum of the azido-NPs (**NP-1-C**), shown in figure 4.13, display a strong peak at 2109 cm$^{-1}$, assigned to the anti-symmetric stretch vibration of the azido group, and peaks at 2942 and 2879 cm$^{-1}$ for the asymmetric vibration of the C-H bond. The IR spectrum of the alkyne-NPs (**NP-1-D**) show a strong peak at 1716 cm$^{-1}$ (owing to the C=O bond of the urethane carboxamide) and a peak at 1541 cm$^{-1}$ characteristic for the amide. The weak peak at 2133 cm$^{-1}$ is assigned to the C≡C stretch vibration, and the peaks at 2942 and 2889 cm$^{-1}$ to the C-H stretch.
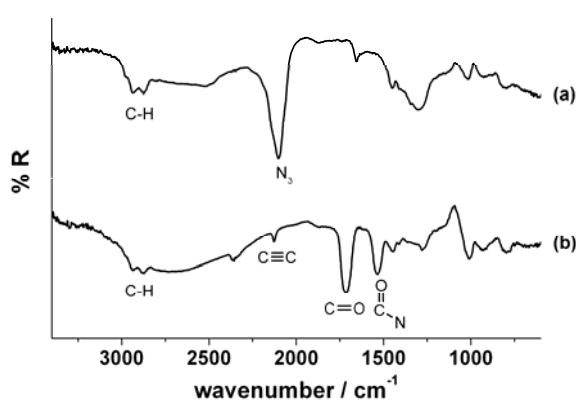


**Figure 4.13** IR reflectance spectra of surface modified upconverting nanoparticles. (a) type **NP-1-C**. (b) type **NP-1-D**. Note that reflectance rather than absorbance is given on the y axis due to the use of a reflectance spectrometer.

The amount of the azido or alkyne groups on the coated particles was determined by elementary analysis. The fractions of C, H, and N, respectively, are 3.1, 1.2, and 2.4 % for **NP-1-C**, and 3.5, 1.3, and 0.7 % for **NP-1-D**. The high nitrogen content of **NP-1-C** clearly indicates the presence of azido groups. The presence of nitrogen in **NP-1-D** results from the presence of the urethane group in the linker. This is equivalent to around 0.57 mmol of azido groups, and to around 0.50 mmol of alkyne groups, respectively, per gram of particles.

The luminescent properties of the coated UCNPs remained unchanged compared to the unmodified particles. Furthermore, the emission intensities of the unmodified, as well as the azido and alkyne modified particles are independent of the pH in the range from 3 to 10 (see figure 4.14).
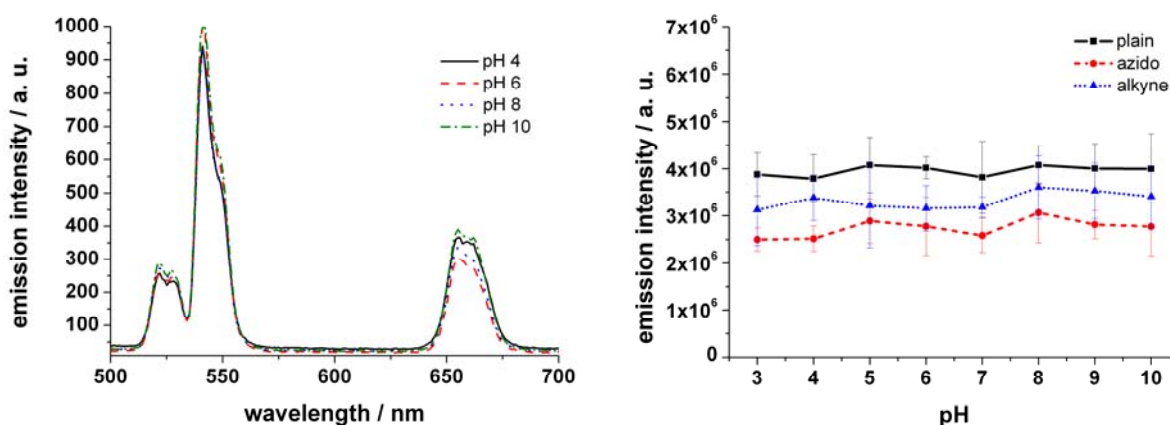


**Figure 4.14** Effect of pH on upconversion luminescence of coated particles. *(Left)* Selected luminescent spectra of azido modified particles at different pH values. *(Right)* Emission intensities of unmodified (plain), azido and alkyne modified UCNPs at 550 nm as a function of pH.

Additionally, it was found that the ionic strength of buffers in the usual concentration range does virtually not affect the luminescent properties of unmodified UCNPs, nor the silica coated azido or alkyne modified particles.
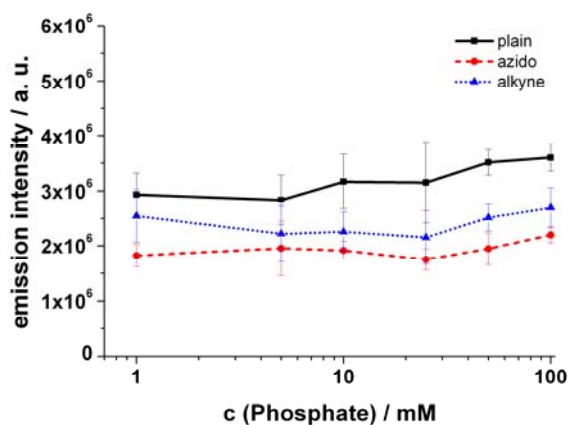
**Figure 4.15** Emission intensities of unmodified (plain), azido and alkyne modified UCNPs at 550 nm as a function of ionic strength.

All azido- or alkyne modified particles described in this section are summarized in table 4.2.

**Table 4.2** Figures of merit of the surface-modified particles described in this work

| Code | Functionality | Shell [nm] | Preparation |
|------|---------------|------------|-------------|
| SiNP-A | azido | - | SiNP + **1** |
| SiNP-B | alkyne | - | SiNP + **2** |
| µP-1-C | azido | - | µP-1 + **3** |
| µP-2-D | alkyne | - | µP-2 + **4** |
| NP-1-C$_1$ | azido | 10 | NP-1 coated with TEOS and **3** |
| NP-4-C$_2$ | azido | 15 | NP-4 coated with TEOS and **3** |
| NP-1-D$_2$ | alkyne | 15 | NP-1 coated with TEOS and **4** |
| NP-4-C$_3$ | azido | 25 | NP-4 coated with TEOS and **3** |
| NP-1-D$_3$ | alkyne | 25 - 30 | NP-1 coated with TEOS and **4** |
| NP-1-C$_5$ | azido | 10 | NP-1 coated with TEOS and **3** (ME) |

## 4.2 Click Labeling of the Particles with Biotin and Maleimide

Next, the nanoparticles were functionalized with groups so to make them conjugatable to biomolecules. Such "particle labels" are highly attractive alternatives to the widely used but toxic quantum dots of the CdSe type.[10] Two versatile functions were chosen. The first is the biotin group[11,12] (**5** and **6**) which is the "work horse" in numerous labeling protocols because of its very strong interaction (with a $K_D$ of ~$10^{-14}$ M) with (strept)avidins. The second is the maleinimide group (**7**) which undergoes addition to thiol groups at room temperature and in aqueous solution. It is widely used[13,14] to label proteins.



5: R = (CH₂)₂—N₃

6: R = (CH₂)₂—C≡CH

7
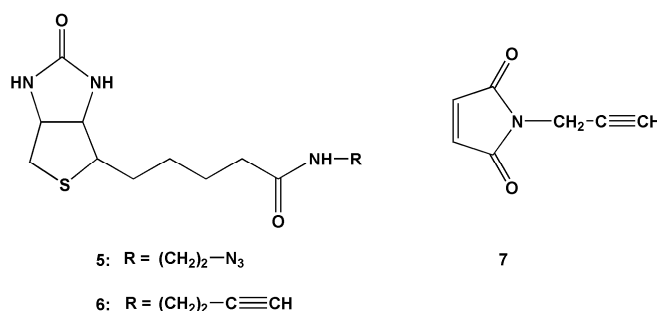
**Figure 4.16** Clickable biotins and maleinimide

The bioreactive particles were obtained by clicking the azido or alkyne modified particles listed in table 4.2 to the click reagents **5 – 7** of figure 4.16. Reactions proceed smoothly in ethanol/water solution in the presence of catalytic quantities of Cu(I) which can be generated in-situ from Cu(II) ion and ascorbate.

### 4.2.1 Bioreactive SiNPs

The azido-modified biotin **5** was clicked to azido-modified silica nanoparticles (**SiNP-B**) to give **SiNP-5**. Its differential IR spectrum (see figure 4.17), using alkyne-modified **SiNP-B** as a reference sample, reveals that the band for the alkyne group at 2113 cm$^{-1}$ is now negative indicating the disappearance of this functional group. The C-H stretches of biotin are found at 2923, and 2865 cm$^{-1}$. The peaks at 2359, 2334, 1697, and 1594 cm$^{-1}$ can be assigned to the N-H, C=O, and amide stretches of biotin.
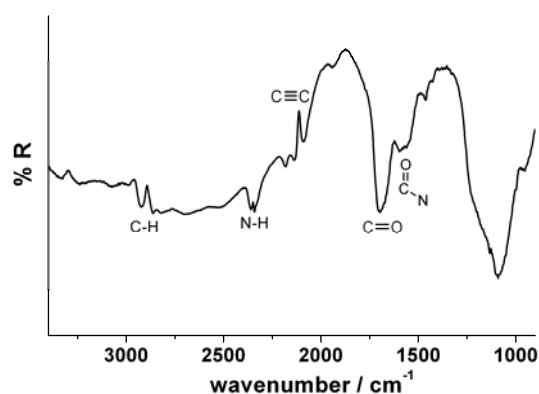
**Figure 4.17** IR difference reflectance spectra of **SiNP-B-5**. Negative peaks indicate the disappearance of bands (i.e., chemical functions).

## 4.2.2 Bioreactive UCμPs

The alkyne-modified biotin **6** was clicked to azido-modified microparticles (**μP-1-C**) to give **μP-1-C-6**. Its differential IR spectrum (see figure 4.18) using azido-modified **μP-1-A** as a reference sample reveals that the band for the azido group at ~2100 cm$^{-1}$ is virtually absent, while strong peaks have appeared at 2971, 2884, 1665 and 1491 cm$^{-1}$ which can be assigned to the C-H, C=O, and amide stretches of biotin.
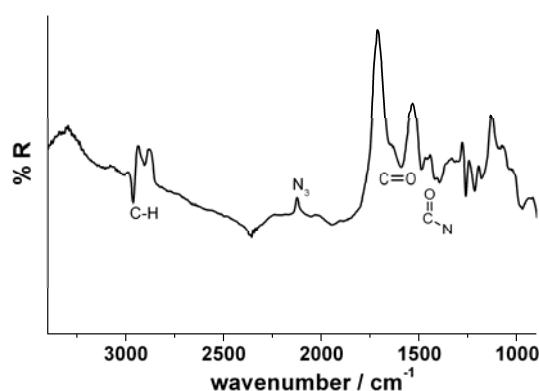


**Figure 4.18** IR difference reflectance spectra of **μP-1-C-6**. Negative peaks indicate the disappearance of bands (i.e., chemical functions).

### 4.2.3 Bioreactive UCNPs

The azido-modified biotin (**5**) was clicked to alkyne modified **NP-1-D** to give **NP-1-D-5**. The presence of the functional groups was verified via diffuse reflectance FT-IR spectroscopy as shown in figure 4.19. The spectra were acquired using the respective alkyne- or azido modified **NP-1** as a reference material. The negative peak at 2131 $cm^{-1}$ in the difference spectrum (figure 4.19a) indicates that the alkyne functionality has disappeared. The C-H stretch vibration is visible at 2983 and 2908 $cm^{-1}$. The peaks at 1665 and 1598 $cm^{-1}$ are assigned to the C=O and C-N amide stretches.
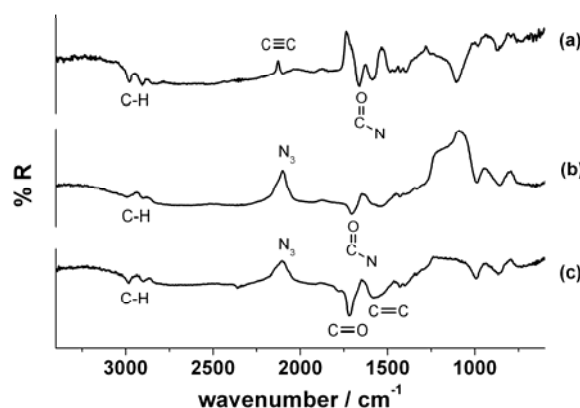


**Figure 4.19** IR difference reflectance spectra of (a), **NP-1-D-5**; (b), **NP-1-C-6**; (c), **NP-1-C-7**. Negative peaks indicate the disappearance of bands (i.e., chemical functions).

Alkyne-modified biotin (**6**), in turn, was clicked to azido-modified **NP-1-C** to give **NP-1-C-6**. The disappearance of the azido group is indicated by the negative peak at 2108 $cm^{-1}$.The C-H stretches are found at 3003 and 2906 $cm^{-1}$. The C=O stretch vibration is located 1709 $cm^{-1}$, and the C-N amide stretch at 1542 $cm^{-1}$ (figure 4.19b).

Finally, the alkyne-modified maleinimide (**7**) was clicked to azido-modified **NP-1-C** to give **NP-1-C-7**. The absence of the azido functionality is indicated by the negative peak at 2114 $cm^{-1}$. The C-H stretches are located at 3998 and 2906 $cm^{-1}$. The maleinimidic C=O stretches are found at 1788 and 1724 $cm^{-1}$. The C=C stretching peak is located at 1582 $cm^{-1}$ (figure 4.19c). All particles described in this section functionalized with either biotin or maleinimide are summarized in table 4.3.

**Table 4.3** Figures of merit of the bioreactive particles

| Code | Functionality | Reaction |
|------|---------------|----------|
| SiNP-B-5 | biotin | SiNP-B clicked to **5** |
| µP-1-C-6 | biotin | µP-1-C clicked to **6** |
| NP-1-D-5 | biotin | NP-1-D clicked to **5** |
| NP-1-C-6 | biotin | NP-1-C clicked to **6** |
| NP-1-C-7 | maleinimide | NP-1-C clicked to **7** |

## 4.3 Click Labeling of the Particles with Fluorescent Dyes

Azido- and alkyne-modified particles offer another attractive possibility in that they may be click-labeled with organic fluorophores[15] so to obtain particles with a variety of emission colors. In case of the intrinsically non-fluorescent silica nanoparticles this is necessary in order to make them accessible to fluorescence detection. Regarding UCµPs and UCNPs, dually emitting particles with various colors can be obtained depending on whether the upconverting (inorganic) core is photoexcited, or the (organic) fluorophores of the shell. Dually excitable particles with dual emissions are likely to have even more sophisticated applications than those outlined in the Introduction for conventional upconverters (such as color multiplexing or encoding). In order to investigate this, eight clickable fluorescent labels (see figure 4.20) were chosen for click-labeling of the particles. Reactions proceed smoothly in ethanol/water solution in the presence of catalytic quantities of Cu(I) which can be generated in-situ from Cu(II) ion and ascorbate.
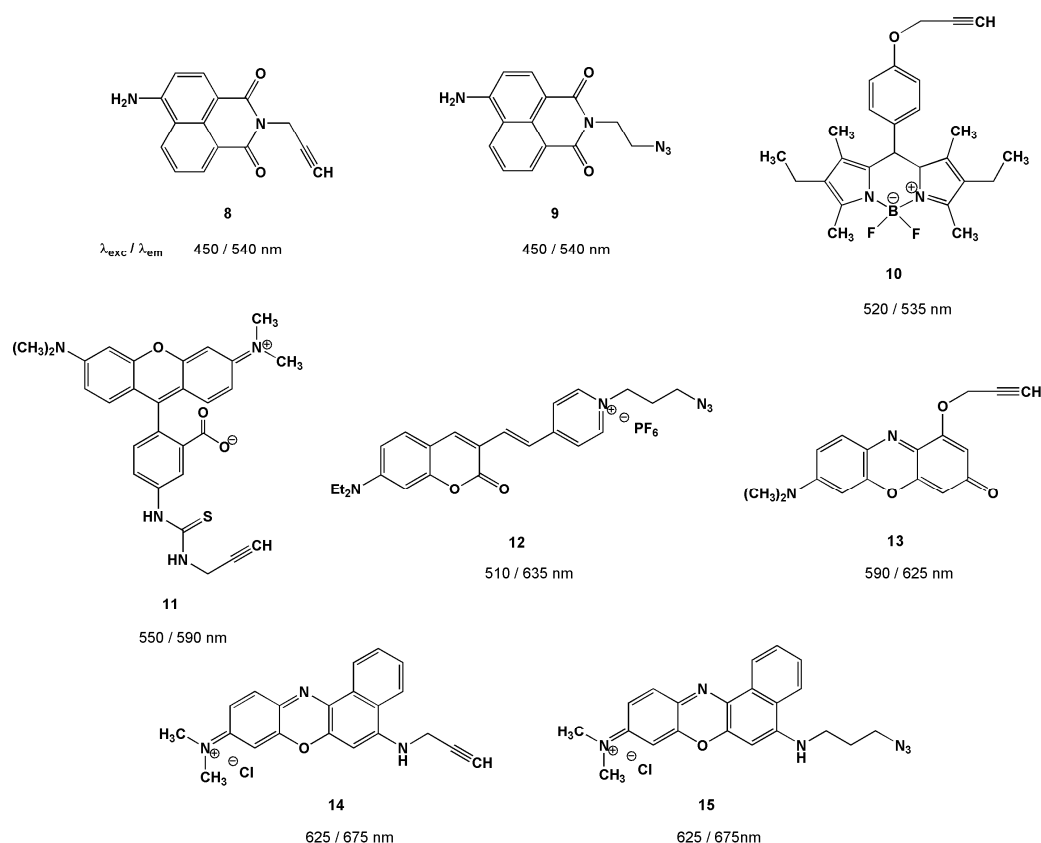
**Figure 4.20** Clickable fluorescent dyes used in this work

## 4.3.1 Fluorescently Labeled SiNPs

First of all, fluorescent silica nanoparticles were prepared by clicking the azido- or alkyne functionalized dyes to the respectively modified SiNPs. The alkyne modified naphthalimide **8** was clicked to **SiNP-A** to give **SiNP-A-8** with an emission peak at 540 nm. SiNPs labeled with the azido naphthalimide derivative **9** show identical luminescent properties. The bodipy dye **10** was clicked to **SiNP-A** to give **SiNP-A-10** with an emission wavelength of 535 nm. Dye **12** possesses a very large Stokes-shift and is therefore referred to as "Mega-Stokes"-label. The click product **SiNP-B-12** displays a fluorescence peaking at 635 nm. The absorption and emission of fluorophore **13** (like that of all oxazines of the Nile Red type) is strongly solvatochromic, but if covalently bound to the surface of particles of type **SiNP-A,** the excitation and emission maxima are rather invariable and found at 590 nm and 625 nm, respectively, both in water and ethanol suspension, indicating stronger interaction with the surface than with the solvent. The emission of particles clicked to the Nile Blue derivatives **14** and **15** is found at 675 nm. The fluorescence spectra for

all labelled SiNPs are given in figure 4.21. The emission colors range from green to red.
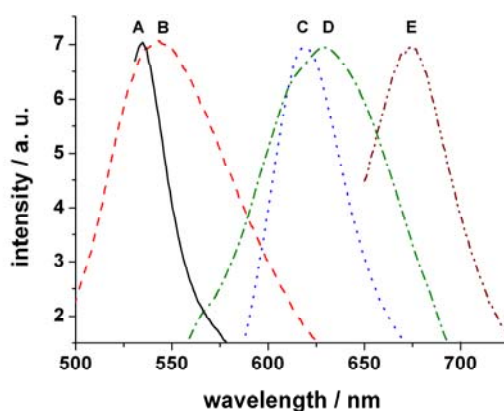


**Figure 4.21** Emission spectra of dye-labeled SiNPs. A: **SiNP-A-10**, B: **SiNP-A-8 / SiNP-B-9**, C: **SiNP-A-13**, D: **SiNP-B-12**, E: **SiNP-A-14 / SiNP-B-15**.

Reference samples obtained without the Cu(I) catalyst showed no signs of adsorbed dye for labels **8**, **9**, **10** and **13**. In case of the positively charged dyes **12**, **14** and **15** a low amount of electrostatically bound dye was detected. The particles were washed several times to remove excess dye. The supernatant of all click labeled particles remained clear after ~5 washing steps and no further dye leaching was observed. In contrast, the adsorbed dyes continued to wash out even after more than 10 washing steps. This suggests that the fluorescent labels are indeed covalently bound by the click reaction.



fluorophore     **8**      **9**      **10**         **14**

**Figure 4.22** Dye-labeled SiNPs as powder. From left to right: **SiNP-A-8**, **SiNP-B-9**, **SiNP-A-10**, **SiNP-A-14** (3 different dye loads).

Figure 4.22 shows a photograph of click labeled SiNPs in various colors. All three blue colored particles were obtained by using the Nile Blue derivative **14** as fluorescent label. It was found empirically that the amount of dye used for click

labeling and the reaction time strongly influence the luminescent properties of the particles. A high dye load resulting from long reaction time or high dye amounts gives rise to internal quenching of the dye fluorescence. Therefore, the particles should not be overlabeled to obtain best results for fluorescence intensities.

## 4.3.2 Fluorescently Labeled UCμPS

The alkyne-modified purple fluorescent dye **13** was clicked to azido-modified UCμPs of type **μP-1-C** to give **μP-1-C-13** which was investigated by fluorescence microscopy and fluorescence spectroscopy. A reference sample, obtained without using the copper(I) catalyst, showed no trace of the dye after washing the particles. The UCμPs clicked to the fluorophore **13**, in contrast, display the typical orange fluorescence of the oxazine label. A fluorescence microscopy image of the labeled microparticles under visible light excitation (550 nm) is given in figure 4.23. The orange-colored emission of the fluorophore covalently attached to the surface of the particles is clearly visible.
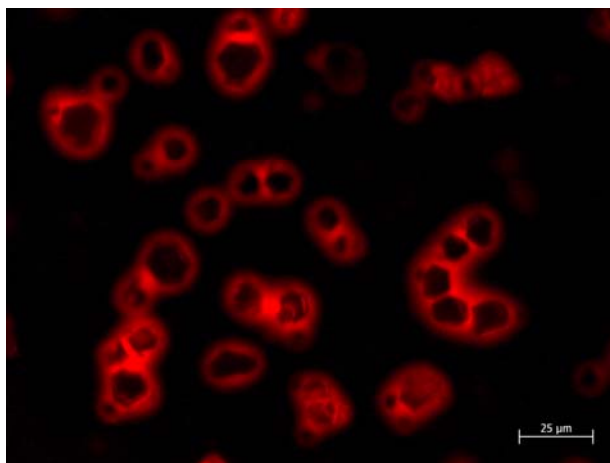


**Figure 4.23** Fluorescence microscopy image of the labeled microparticles of type **μP-1-C-13** under visible light excitation (515-560 nm).

### 4.3.3 Fluorescently Labeled UCNPs

Similarly, the azido-modified nanoparticles of type **NP-1-C** or were clicked to **10** and **13** to give **NP-1-C-10** and **NP-1-C-13**, respectively. Reference samples, obtained without the Cu(I) catalyst showed no sign of adsorbed dye indicating that the dyes are indeed covalently bound. The upconversion emission spectrum (under 980-nm excitation) and the conventional emission spectrum of the organic label (under 520-nm and 590-nm excitation, respectively) are given in figure 4.24. The absorption and emission of fluorophore **13** remained stable at 590 nm and 625 nm in all solvents showing the same effect as observed for the SiNPs.
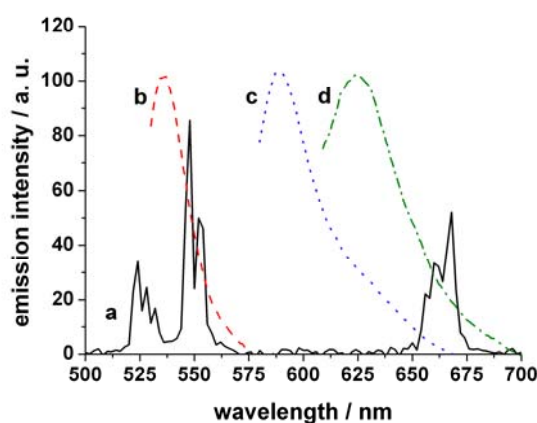


**Figure 4.24** Dual emission of nanoparticles of type **NP-1-C-10, NP-3-C-11** and **NP-1-C-13**. (a), upconversion emission (at 980-nm excitation); (b) emission of label **10** (photoexcitation at 520 nm); (c) emission of label **11** (photoexcitation at 550 nm) (d) emission of label **13** (photoexcitation at 590 nm).

The absorption band of the rhodamine dye **11** matches the green emission band of the UCNPs at 541 nm. Therefore, it was investigated whether the dye could be photo excited by the upconverting core so to create a kind of luminescence resonance energy transfer (LRET) system as have been reported in the literature.[16,17,18] For that purpose, **11** was clicked to UCNPs of the type **NP-3-C** to give **NP-3-C-11** and its luminescent properties were investigated. The emission peak of **NP-3-C-11** is found at 590 nm when photoexciting the dye at 550 nm (see figure 4.24c). Unfortunately, photoexcitation at 980 nm caused the normal emission of the UCNPs only, whilst no luminescence originating from the fluorophore on the UCNPs was observed. It was

deduced that the size of the silica shell (~25 nm) possibly prevents efficient resonance energy transfer.

Therefore, the silica coated UCNPs were added to solutions of the rhodamine dye **11** at different concentration to verify this assumption. A strong quenching of the green emission bands of the UCNPs was observed caused by the inner filter effect of the dye solution (see figure 4.25, left). A very weak emission originating from the fluorescent dye **11** could be detected at dye concentrations ranging from 10 µM to 100 µM (see figure 4.25, right).
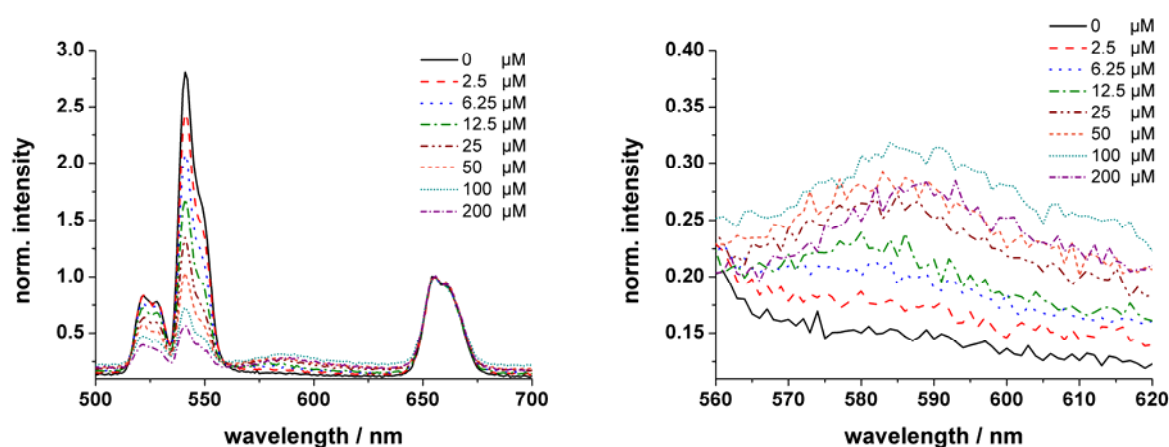


**Figure 4.25** *(Left)* Luminescence spectra of UCNPs of type **NP-3-C** (50 µg/mL) in a solution of the rhodamine dye **11** at different concentrations. Spectra are normalized to the peak at 655 nm. *(Right)* Detail of the emission of **11** at 590 nm, photo-exited by the UCNPs.

The thickness of the silica shell of the particles **NP-3-C** is about 25 nm. Therefore, the occurrence of an actual non-radiative resonance energy transfer as described by Förster (FRET) is not likely as this can usually only be observed at distances of 10 nm between donor and acceptor.[19] Consequently, it is assumed that in this case the UCNPs act as some kind of "nano-lamps" that are photo-exciting the dye in solution.[20] Experiments with uncoated microparticles and **11** gave similar results, supporting this hypothesis.

These findings indicate that a successful photoexcitation strongly depends on the dye concentration applied and possibly on the ratio of UCNP to dye concentration. The green emission band is significantly screened away by the inner filter effect of the dye solution but only a very small portion of the energy is converted

into a fluorescence emission of **11**. It appears that a very strict control of the dye load needs to be performed when click labeling the UCNPs with the intension to induce photoexcitation of the dye by the UCNP emission.

Table 4.4 summarizes all fluorescently labeled particles described in this section.

**Table 4.4** Figures of merit of the fluorescently labeled particles described in this section

| Code | Functionality | $\lambda_{exc}/\lambda_{em}$ | Preparation |
|------|---------------|---------------|-------------|
| SiNP-A-8 | fluorophore **8** | 450 / 540 | SiNP-A clicked with **8** |
| SiNP-B-9 | fluorophore **9** | 450 / 540 | SiNP-B clicked with **9** |
| SiNP-A-10 | fluorophore **10** | 520 / 535 | SiNP-A clicked with **10** |
| SiNP-B-12 | fluorophore **12** | 510 / 635 | SiNP-B clicked with **12** |
| SiNP-A-13 | fluorophore **13** | 590 / 625 | SiNP-A clicked with **13** |
| SiNP-A-14 | fluorophore **14** | 625 / 675 | SiNP-A clicked with **14** |
| SiNP-B-15 | fluorophore **15** | 625 / 675 | SiNP-B clicked with **15** |
| µP-1-C-13 | fluorophore **13** | 590 / 625 | µP-1-C clicked with **13** |
| NP-1-C-10 | fluorophore **10** | 520 / 535 | NP-1-C clicked with **10** |
| NP-3-C-11 | fluorophore **11** | 550 / 590 | NP-3-C clicked with **11** |
| NP-1-C-13 | fluorophore **13** | 590 / 625 | NP-1-C clicked with **13** |

## 4.4 Discussion

The method described here for chemically modifying the surface of SiNPs, UCµPs and UCNPs is straightforward and versatile. It is likely to be applicable to various other materials possessing oxidic (and thus hydroxylic) surfaces. It makes surfaces compatible with click chemistry which again is highly versatile, particularly with respect to bioconjugation because it is bioorthogonal and thus not troubled by functional groups often present in biological samples. In fact, click chemistry has

been applied to NPs made from silica,[21] gold,[22,23] iron oxide,[24,25] and various polymers.[26,27] The silica coating renders the UCNPs water dispersible and biocompatible.[28] The one-step method applied here is primarily intended for uses in context with bioassays. It is much simpler than two-step methods[29] such as those used for modifying UCNPs with amino groups. The Stöber method gives coating results considerably better reproducible and with a more homogeneous shell compared to the microemulsion technique. Purification of the UCNPs by size exclusion chromatography (SEC) is another attractive feature of the work presented here. When applying SEC, the NPs can be kept in solution at any time and aggregation is minimized. The thickness of the shell most likely can be reduced by adjusting the TEOS to ammonia ratio. The luminescent properties of the surface modified UCµPs and UCNPs were not altered. Moreover, varying pH values or buffer concentrations do not influence the emission intensities.

Click reaction of the reactive SiNPs as well as upconverting micro- and nanoparticles gave particles that can be conjugated to (a) (strept)avidin (via the biotin[30,31,32] group), and (b) thiols[33] (via the maleinimide groups). Thiol labeling is clearly to be favored in bioconjugation over amine labeling simply because most proteins possess numerous free amino groups (this leading to random labeling and to varying dye-to-protein ratios), but often only one to three thiol groups. Human serum albumin (HSA), for example, has one free thiol group only, but more than 50 amino groups that may be labeled.

In a further version, the click reaction leads to particles carrying organic fluorescent labels. Fluorescent SiNPs can be prepared with emission colors ranging from green to red. Longwave labels generally are to be favored as working at longer wavelengths reduces the occurrence of background luminescence. The intensity of the particles can be tuned by adjusting dye load and click reaction times. The fluorescently labeled UCµPs and UCNPs in turn, have attractive spectral features in giving dual emissions depending on the wavelength of excitation. If excited with near infrared (NIR) light, dual emission of the inorganic core is observed (green and bright red, or blue and NIR). If excited in the visible, the (single) emission of the organic fluorophore (green, yellow or orange) is being seen. Moreover, by varying the quantity of organic label, a wide range of intensities can be adjusted for both the "inorganic" and "organic" emission, thus giving a 2-dimensional matrix of two (or three) intensities (and possibly also lifetimes) that enables unambiguous encoding of

particles. It is assumed that if organic dyes are used that absorb at one of the two emission bands of the upconverters, various ratios of intensities of the dual emission may be adjusted. Furthermore, by choosing a dye with a spectral overlap, high molar absorptivity and a high quantum yield, a photoexcitation of the dye by the UCNPs emission is possible. This paves the way for photoexciting organic fluorophores with NIR laser light which otherwise is only accomplished by 2-photon absorption (with its need for strong lasers and the associated risk of photodamage). However, the dye load has to be strictly controlled for a successful photoexcitation of an organic dye via IR.

Generally, click reactions with the alkyne derivative in solution and the azido group on the particle surface worked faster and gave better results. This is in agreement with the catalytic mechanism given in section 2.3.2. The coordination of the copper ion is favored when the alkyne species is present in solution.[34]

## 4.5 References

[1]   Ortega-Muñoz M, Lopez-Jaramillo J, Hernandez-Mateo F, Santoyo-Gonzalez F (2006) **Synthesis of Glyco-Silicas by Cu(I) Catalyzed Click-Chemistry, and their Applications in Affinity Chromatography**, Adv. Synth. Catal. 348: 2410-2420.

[2]   Evans CE, Lovell PA (2009) **Click Chemistry as a Route to Surface Functionalization of Polymer Particles Dispersed in Aqueous Media**, Chem. Commun. 2305-2307.

[3]   Nakazawa J, Stack TDP (2008) **Controlled Loadings in a Mesoporous Material: Click-on Silica**, J. Am. Chem. Soc., 130, 14360-14361.

[4]   Puleo DA (1996) **Retention of Enzymatic Activity Immobilized on Silanized Co-Cr-Mo and Ti-6Al-4V**, J Biomed. Mater. Res. A. 37: 222-228.

[5]   Rezania A, Johnson R, Lefkow AR, Healy KE (1999) **Bioactivation of Metal Oxide Surfaces. 1. Surface Characterization and Cell Response**, Langmuir 15: 6931-6939.

[6]   Müller R, Abke J, Schnell E, Scharnweber D, Kujat R, Englert C, Taheri D, Nerlich M, Angele P (2006) **Influence of Suface Pretreatment of Titanium- and Cobalt-based Biomaterials on Covalent Immobilization of Fibrillar Collagen**, Biomaterials 27: 4059-4068.

[7]   Kim M, Hong J, Lee J, Hong CK, Shim SE (2008) **Fabrication of Silica Nanotubes Using Silica Coated Multi-Walled Carbon Nanotubes as the Template**, J Colloid Interf. Sci. 322: 321-326.

[8]   Stöber W, Fink A (1968) **Controlled Growth of Monodisperse Silica Spheres in the Micron Size Range**, J. Colloid. Interf. Sci. 26: 62-69.

[9]   Lu H, Yi G, Zhao S, Chen D, Guo L-H, Cheng J (2004) **Synthesis and Characterization of multi-functional Nanoparticles possessing Magnetic, Up-conversion Fluorescence and Bio-affinity Properties**, J. Mater. Chem. 14: 1336-1341.

[10] Hilderbrand SA, Shao F, Salthouse C, Mahmood U, Weissleder R (2009) **Upconversion Luminescent Nanomaterials: Application to in vivo Bioimaging**, Chem. Commun. 2009, 4188-4190.

[11] Wang L, Zhao W, O'Donoghue MB, Tan W (2007) **Fluorescent Nanoparticles for Multiplexed Bacteria Monitoring**, Bioconjugate Chem. 18: 297-301.

[12] Meier JL, Mercer AC, Rivera H, Burkart MD (2006) **Synthesis and Evaluation of Bioorthogonal Pantetheine Analogues for in Vivo Protein Modification**, J. Am. Chem. Soc. 128: 12474-12184.

[13] Brinkley M (1992) **A Brief Survey of Methods for Preparing Protein Conjugates with Dyes, Haptens, and Cross-Linking Reagents**, Bioconjugate Chem. 3: 2-13.

[14] Matsumoto T, Urano Y, Shoda T, Kojima H, Nagano T (2007) **A Thiol-Reactive Fluorescence Probe Based on Donor-Excited Photoinduced Electron Transfer: Key Role of Ortho Substitution**, Org. Lett. 9: 3375-3377.

[15] Kele P, Li X, Link M, Nagy K, Herner A, Lőrincz, Béni S, Wolfbeis OS (2009) **Clickable Fluorophores for Biological Labeling-With or Without Copper**, Org. Biomol. Chem. 7: 3486-3490.

[16] Sun LD, Gu JQ, Zhang SZ, Zhang YW, Yan CH (2009) **Lminescence Resonance Energy Transfer Baseod on β-NaYF$_4$: Yb, Er Nanoparticles and TRITC Dye**, Sci. China Ser. B-Chem. 52: 1590-1595.

[17] Li Z, Zhang Y, Jiang S (2008) **Multicolor Core/Shell-Structured Upconversion Fluorescent Nanoparticles**, Adv. Mater. 20: 4765-4769.

[18] Soukka T, Rantanen T, Kuningas K (2008) **Photon Upconversion in Homogeneous Fluorescence-based Bioanalytical Assays**, Ann. N. Y. Acad. Sci. 1130: 188-200.

[19] Miller JN (2005**) Fluorescence Energy Transfer Methods in Bioanalysis**, Analyst 130: 265-270.

[20] Morgan CG, Dad S, Mitchell AC (2008) **Present Status of, and Future Prospects for, Upconverting Phosphors in Proximity-Based Bioassays**, J. Alloy. Compd. 451: 526-529.

[21] Kele P, Mezö G, Achatz D, Wolfbeis OS (2009) **Dual Labeling of Biomolecules by Using Click Chemistry: A Sequential Approach**, Angew. Chem. Int. Ed. Engl. 48: 344-347, Angew. Chem. 121: 350-353.

[22] Boisselier E, Salmon L, Ruiz J, Astruc D (2008) **How to very Efficiently Functionalize Gold Nanoparticles by "Click" Chemistry**, Chem. Commun. 5788-5790.

[23] Zhou Y, Wang S, Zhang K, Jiang X (2008) **Visual Detection of Copper(II) by Azide- and Alkyne-Functionalized Gold Nanoparticles Using Click Chemistry**, Angew. Chem. Int. Ed. 47: 7454-7456, Angew. Chem. 120: 7564-7566.

[24] V. Maltzahn G, Ren Y, Park J-H, Min D-H, Kotamraju VR, Jayakumar J, Fogal V, Sailor MJ, Ruoslahti E, Bhatia SN (2008) **In Vivo Tumor Cell Targeting with "Click" Nanoparticles**, Bioconjugate Chem. 19: 1570-1578.

[25] He H, Zhang Y, Gao C, Wu J (2009) **Clicked Magnetic Nanohybrids with a Soft Polymer Interlayer**, Chem. Commun. 1655-1657.

[26] Nicolas J, Bansaid F, Desmaële D, Grogna M, Detrembleur C, Andrieux K, Couvreur P (2008) **Synthesis of Highly Functionalized Poly(alkyl cyanoacrylate) Nanoparticles by Means of Click Chemistry**, Macromol. 41: 8418-8428.

[27] Lu J, Shi M, Shoichet MS (2009) **Click Chemistry Functionalized Polymeric Nanoparticles Target Corneal Epithelial Cells through RGD-Cell Surface Receptors**, Bioconj. Chem. 20: 87-94.

[28] Jalil RA, Zhang Y (2008) **Biocompatibility of Silica Coated NaYF$_4$ Upconversion Fluorescent Nanocrystals**, Biomaterials 29: 4122-4128.

[29] Sivakumar S, Diamente PR, van Veggel FCJM (2006) **Silica-Coated Ln$^{3+}$-Doped LaF$_3$ Nanoparticles as Robust Down- and Upconverting Biolabels**, Chem. Eur. J 12: 5878-5884.

[30] Kong D, Quan Z, Yang J, Yang P, Li C, Lin J (2009) **Avidin Conjugation to Up-conversion Phosphor NaYF$_4$:Yb$^{3+}$, Er$^{3+}$ by the Oxidation of the Oligosaccharide Chains** *J. Nanopart. Res.* 11, 821-829.

[31] Lu H, Yi G, Zhao S, Chen D, Guo LH, Cheng J (2004) **Synthesis and Characterization of Multi-functional Nanoparticles Possessing Magnetic, Up-conversion Fluorescence and Bio-affinity Properties**, J. Mater. Chem. 14, 1336 – 1341.

[32] Wang M, Mi CC, Wang WX, Liu CH, Wu YF, Xu ZR, Mao CB, Xu SK **Immunolabeling and NIR-Excited Fluorescent Imaging of HeLa Cells by Using NaYF$_4$:Yb,Er Upconversion Nanoparticles**, ACS Nano, 2009, 3, 1580-1586

[33] Wang Y, Cai J, Rauscher H, Behm RJ, Goedel WA (2005) **Maleimido-Terminated Self-Assembled Monolayers**, Chem. Eur. J. 11, 3968-3978.

[34] Lin P-C, Ueng S-H, Yu S-C, Jan M-D, Adak AK, Yu C-C, Lin C-C (2007) **Surface Modification of Magnetic Nanoparticle via Cu(I)-Catalyzed Alkyne-Azide [2+3] Cycloaddition**, Org. Lett. 9: 2131-2134.

# 5 Analytical Applications for UCNPs

## 5.1 UCNPs as Labels for Proteins and Oligonucleotides

It was envisioned to use upconverting nanoparticles (UCNPs) functionalized with either biotin or maleinimide (see table 4.3) as labels in protein or gene assays. First experiments were performed based on the well known interaction between the biotin group and (strept)avidin. For this purpose, UCNPs of type **NP-1-C-6** (azido modified UCNPs clicked to alkyne-biotin) were incubated with avidin, which had been fluorescently labeled with Cy-3. A schematic representation of the interaction between the biotinylated UCNPs and the protein is shown in figure 5.1.
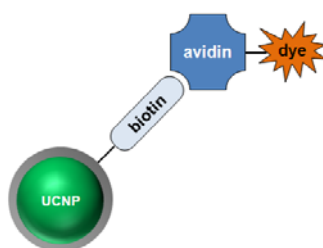


**Figure 5.1** Schematic representation of biotinylated UCNPs bound to a fluorescently labeled avidin.

The fluorescence of the avidin label (Cy-3) could be detected on the surface of the particles after repeated washing steps to remove excess protein. However, reference experiments using UCNPs without the biotin functionality (type **NP-1-C**) together with the labeled avidin also gave high signals for Cy-3 on the particle surface caused by electrostatically bound protein. This electrostatical adsorption could not be reduced by addition of a surface blocking protein, such as bovine serum albumin (BSA). Therefore, it could not be proven that the avidin is indeed bound to the particle surface via the biotin-avidin interaction and not only via adsorption and this approach was not further investigated.

In a second approach, maleinimide functionalized UCNPs were used to label thiolated oligonucleotides (SH-oligos) for the development of a heterogeneous oligonucleotide assay. UCNPs of type **NP-1-C-7** (azido modified UCNPs clicked to

alkyne-maleinimide) were incubated with the thiolated oligos to covalently attach the oligos via the maleinimide group as shown in figure 5.2, left. An oligonucleotide strand with a sequence complementary to the SH-oligo was immobilized in microtiter plate (MTP) wells. It was investigated whether the SH-oligo had bound to the UCNP surface in a hybridization assay with the surface bound counter strand. The concentration of the counter strand was varied whereas the amount of the UCNPs incubated with the SH-oligos was kept constant. The presence of bound UCNPs was detected by measuring the upconversion luminescence intensity at 550 nm and 660 nm following laser (980 nm) excitation, respectively.
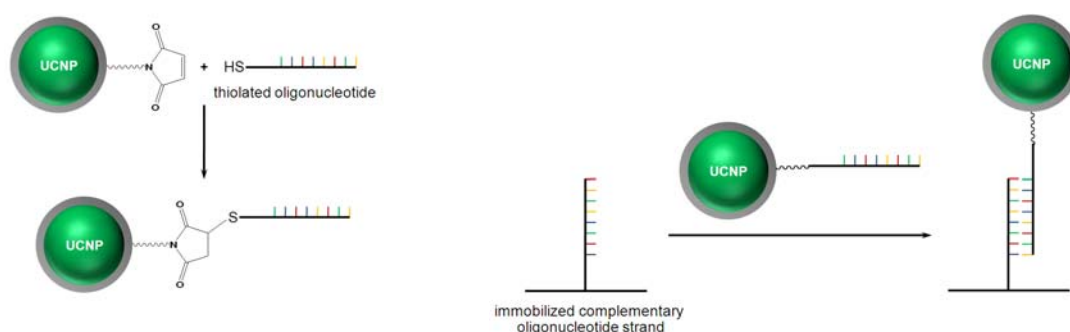


**Figure 5.2** Schematic representation of the oligonucleotide MTP assay. *(Left)* Thiolated oligonucleotides are covalently linked to UCNPs of type **NP-1-C-7**. *(Right)* The thiolated oligos attached to the UCNPs are bound to a complementary strand that is immobilized on the surface of an MTP well.

Unfortunately, the cubic UCNPs of type **NP-1** used for this assay gave fairly low signals in general which is why a relatively high concentration of the UCNPs had to be applied. Therefore, the background luminescence in wells where the concentration of the counter strand was zero and only the UCNPs were added was too high in comparison to determine a distinct difference from the signals in the wells where the hybridization should have occurred. It could not be verified whether the SH-oligos had covalently bound to the particle surface and whether hybridization had occurred. A variety of different labeling and hybridization protocols was applied but with no improvement in results. Finally, the SH-oligos were labeled with the alkyne-modified maleinimide (**7**) prior to the click reaction with the azido-particles. The formation of the oligo-maleinimide could be confirmed via separation with HPLC but the yield was only 30 % with a 50 fold excess of the maleinimide. Therefore, the

concentrations of the oligo-maleinimide applied to the click reaction with the azido modified particles of type **NP-1-C** were rather low. The product of this click reaction was applied to the hybridization assay. Yet again, no distinct signal could be obtained in the wells where the hybridization should have taken place. The principal feasibility of this oligonucleotide assay was ensured by labeling amino modified oligos (with the same sequence as the SH-oligos) with carboxy modified UCNPs. When adding these particle-labeled oligos to an increasing concentration of the immobilized counter strand a notable enhancement in the UCNP emission could be detected with relatively high standard deviations of the intensity signals, though. This indicates that the principal configuration of the oligo assay is operational.

Maleinimide functionalized UCNPs were also considered as labels for proteins such as human serum albumin (HSA). For that purpose, particles of type **NP-1-C-7** were incubated with HSA in aqueous solution to give UCNPs with covalently bound HSA (see figure 5.3a). These particles with HSA on their surface were applied to a heterogeneous competitive binding assay. HSA antibodies were immobilized on the surface of MTP wells. Varying concentrations of free HSA and particle-bound HSA were added to the wells to investigate competitive binding of the UCNPs (see figure 5.3 for a schematic representation).
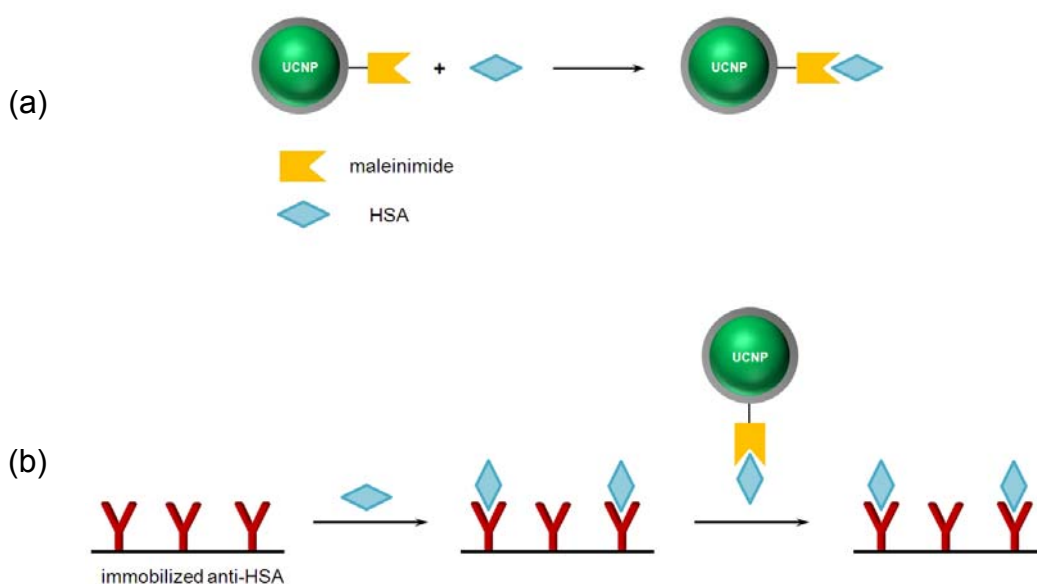


**Figure 5.3** Schematic representation of the envisioned HSA microplate assay. (a) Covalent attachment of HSA using particles of type **NP-1-C-7** with maleinimide functionality. (b) Competitive binding of free HSA and UCNP labeled HSA to anti-HSA.

The concentration of the particle-labeled HSA was kept constant and the amount of the free HSA was varied. The assay buffer contained BSA in excess to minimize electrostatical interactions. With increasing concentration of free HSA (3 ng/mL to 25 µg/mL) a decrease in the UCNP signal measured at 550 nm was obtained (see figure 5.4). A broad linear range from 6 ng/mL to 1.55 µg/mL could be determined in a doubly-logarithmic plot.
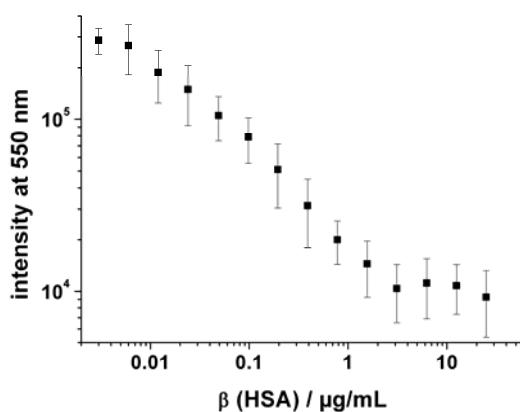


**Figure 5.4** Signal of the UCNPs at 550 nm with increasing concentration of free HSA, doubly-logarithmic plot.

Unfortunately, the standard deviation of the signals is fairly high which is due to the overall low signal intensities of the cubic UCNPs. A reference experiment using azido-modified UCNPs without the maleinimide functionality incubated with HSA was also performed and considerable adsorption of the protein to the particles surface was observed. For that reason, it could not be proven with certainty that the HSA is covalently bound to the maleinimide particles.

## 5.2 pH Sensing using UCNPs

It was shown in chapter 4 that the luminescence intensity of the UCNPs is independent of pH in the range from 3 to 10. Moreover, it is possible to quench the UCNP emission via the inner filter effect of dyes absorbing in the range of the particle emission. Therefore, these particles can be used for the development of a pH sensing system using suitable pH indicators to create a pH-dependent inner filter effect. This concept has already been shown with upconversion nanorods along with

bromothymol blue as the pH probe.[1] In this work, three different pH-indicators were chosen all of which have a pH dependent absorbance overlapping with the green peak of the UCNPs only. The red emission of the particles in turn remains unaffected by any pH changes. This allows for ratiometric measurements using the red peak as an internal standard.

The first pH probe investigated in this work (phenol red, PR) undergoes a large spectral shift (from 435 nm to 560 nm) and a distinct color change (from yellow to pink) with increasing pH. Absorption spectra at three typical pH values, and the overlap with the green emission of the nanoparticles are shown in figure 5.5, left. The pK$_a$ value of PR in water at 25 °C has been reported[2] to be 7.9. PR is not fluorescent by itself. Depending on whether PR is present in its (pink) base form or in its (yellow) acidic form, the dye was expected to either exert or not to exert an inner filter effect on the green emission of the nanoparticles. Experiments were performed with a mixture of PR (40 µM) and UCNPs (50 µg/mL) in buffered solution. This dye to particle ratio empirically was found to give the best results.



**Figure 5.5** *(Left)* Absorption spectra of phenol red in aqueous solutions of pH 5, 7 and 9, respectively. Luminescence emission of **NP-3**. *(Right)* Luminescence spectra of **NP-3** in a solution of phenol red at different pH values, spectra are normalized to the peak at 655 nm.

On changing their pH, the solutions undergo the color changes shown in figure 5.6. The intensity of the green emissions of the nanoparticles varies with pH even though the nanoparticles by themselves have an emission that is independent of pH. The red emission of the UCNPs, in contrast, is not affected by the filter effect of the pH indicator. Therefore, this peak can serve as internal standard to allow for ratiometric measurements. By determining the ratio of the green to the red peak

($I_{541}/I_{655}$) the measurement becomes independent of fluctuations of the intensity of the laser, the particle concentration and inhomogenities of the solution.



**Figure 5.6** Ratio of the green to the red emission of **NP-3** in a PR solution at different pH values after 980 nm excitation. Inset: Photograph of the PR and **NP-3** system in solution at pH values between 4 and 10.

The ratio of the intensities ($I_{541}/I_{655}$) of the green and red UCNP emissions changes from 2.5 (at acidic pH) to 1.3 (at basic pH) as can be seen from figure 5.6. With this system, the neutral range is well covered.

Other pH ranges can be covered by choosing different pH indicators with lower or higher $pK_a$ values, respectively. For the weakly acidic range, methyl red (MR) is an adequate pH indicator with a $pK_a$ value of 5.1. MR changes its color from pink to yellow with increasing pH, with the absorbance maximum shifting from 525 nm to 430 nm. Absorption spectra at three typical pH values, and the overlap with the green emission of the nanoparticles are shown in figure 5.7, left. The dye to particle was the same as for the phenol red system.
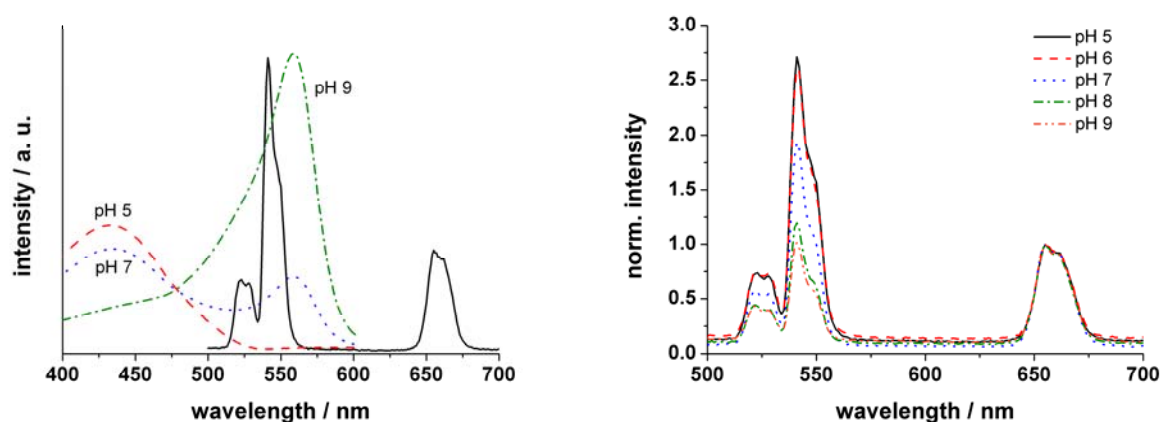
**Figure 5.7** *(Left)* Absorption spectra of methyl red in aqueous solutions of pH 3, 5 and 7, respectively. Luminescence emission of **NP-3**. *(Right)* Luminescence spectra of **NP-3** in a solution of methyl red at different pH values, spectra are normalized to the peak at 655 nm.

In a solution of MR, the green emission of the UCNPs is screened away at pH values below 5 and remains unaffected at high pH values (see figure 5.7, right). The intensity of the red emission remains unchanged and again serves as internal standard. The solutions undergo a color change with increasing pH shown in figure 5.8. The ratio of the intensities of the green and red UCNP emissions ($I_{541}/I_{655}$) changes from 1.4 (at acidic pH) to 2.7 (at basic pH) as can be observed from figure 5.8. With this system, the weakly acidic range is well covered.
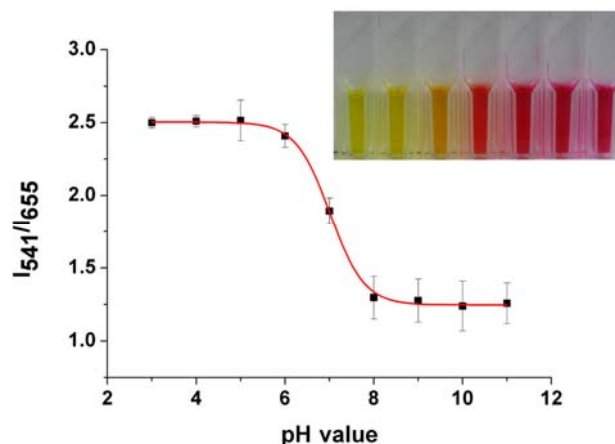


**Figure 5.8** Ratio of the green to the red emission of **NP-3** in a MR solution at different pH values after 980 nm excitation. Inset: Photograph of the MR and **NP-3** system in solution at pH values between 3 and 8.

Phenolphthalein (PT) is an indicator for the weakly basic range. Its $pK_a$ is reported to be 9.7. PT is colorless at acidic and neutral pH and pink at basic pH values. Its absorbance is peaking at 560 nm in the basic range. Absorption spectra at three typical pH values, and the overlap with the green emission of the nanoparticles are shown in figure 5.9, left. In a solution of PT, the green emission of the UCNPs is unaffected at pH values below 8 and filtered at high pH values (see figure 5.9, right). The intensity of the red emission remains unchanged and again serves as internal standard. The dye to particle ratio was chosen as 66.7 µM of PT to 50 µg/mL of the UCNPs.
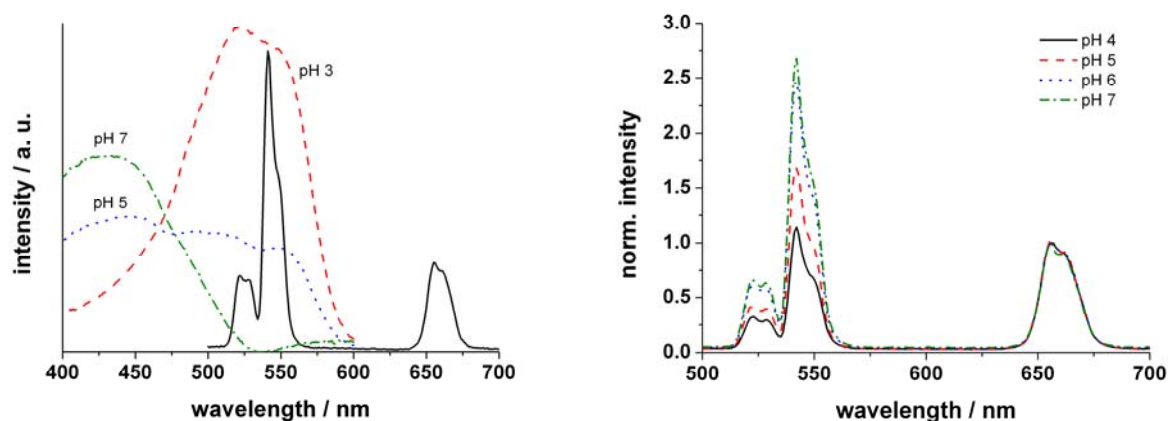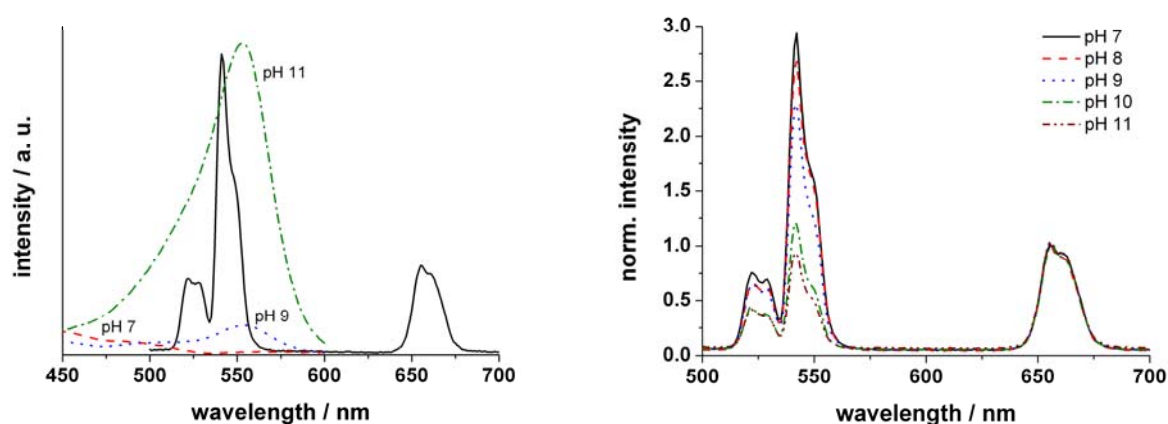


**Figure 5.9** *(Left)* Absorption spectra of phenolphthalein in aqueous solutions of pH 7, 9 and 11, respectively. Luminescence emission of **NP-3**. *(Right)* Luminescence spectra of **NP-3** in a solution of phenolphthalein at different pH values, spectra are normalized to the peak at 655 nm.

The solutions undergo a color change with increasing pH shown in figure 5.10. The ratio of the intensities of the green and the red emission of the UCNPs ($I_{541}/I_{655}$) changes from 2.5 (in the acidic and neutral range) to 0.7 (in the basic range) (figure 5.10). The inner filter effect of PT is very strong, the intensity of the green peak is almost completely screened away.
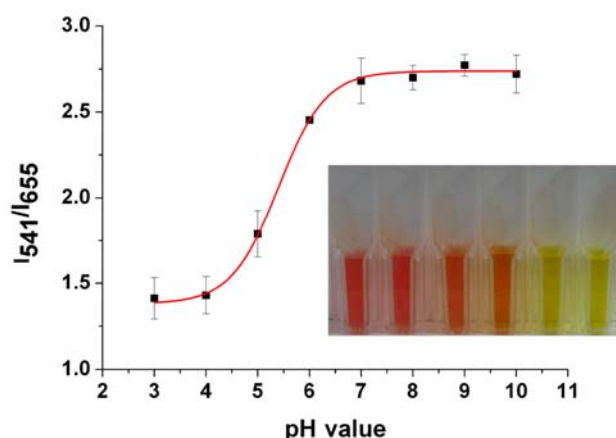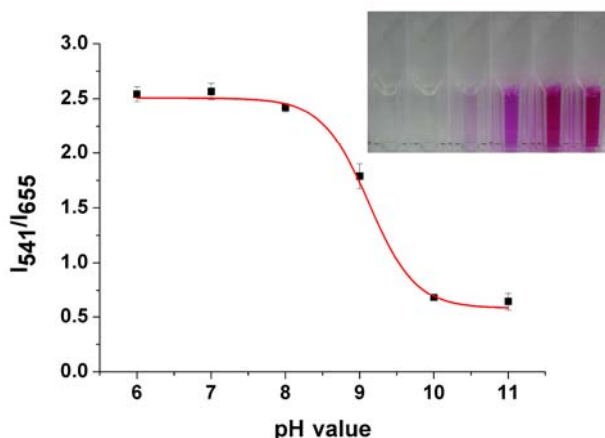
**Figure 5.10** Ratio of the green to the red emission of **NP-3** in a PT solution at different pH values after 980 nm excitation. Inset: Photograph of the PT and **NP-3** system in solution at pH values between 6 and 11.

This concept for determining the pH via the inner filter effect on pH sensitive probes on the UCNP emission can be expanded to the detection of acidic or basic gases. This is demonstrated in the following for the basic gas ammonia.

## 5.3 Ammonia Sensing using UCNPs

There is an increasing demand for robust ammonia sensing systems. Particularly, detection systems for continuous monitoring[3] are needed as ammonia is toxic to many aquatic organisms even in very low concentrations. Furthermore, large quantities of ammonia are released in the farming industries, and produced and used in the chemical industry, e. g. in fertilizers or refrigeration systems. Leakage of ammonia can lead to life-threatening situations. Therefore, there is also a need for alarm systems warning of dangerous ammonium concentrations.[4] Ammonia sensors also are being used as transducers in biosensors where ammonia is released as a result of enzymatic activity.[5,6]

Various kinds of optical sensors have been described for ammonia.[7] It may be sensed in the gas phase via its NIR absorption.[8] In being a weak base it also may be detected via the pH changes it can induce in immobilized pH indicators.[9] The latter approach is more sensitive and can be applied to aqueous solutions. In fact, most optical sensing approaches for ammonia are based on transduction via pH, often

along with fiber optics.[10,11] Usually, a pH indicator dissolved in a buffer solution[12] is entrapped in a gas-permeable polymer. Ammonia, on penetrating the polymer, causes the pH to change, this resulting in a change in color or fluorescence of the indicator dye.[4,13]

Therefore, the effect observed for the **NP-3** and PR system was exploited to build an ammonia sensing system. A sensor film was designed composed of (a) **NP-3** (b) the pH indicator probe PR; and (c) a proton impermeable polystyrene matrix that hosts the NPs and retains the pH indicator. The resulting "cocktail" (a solution of all components in chloroform) was spread onto an inert and optically transparent polyester support made from poly(ethylene terephthalate) to form a film with a thickness of ~12 µm after evaporation of the solvents. This film, a cross section of which is shown in figure 5.11, is insensitive to pH changes in surrounding solutions because the polystyrene matrix is impermeable to protons. Ammonia, on the other hand, is capable of penetrating polystyrene and inducing an increase in the pH and thus induce the (expected) color change of the sensor foil from yellow to pink.
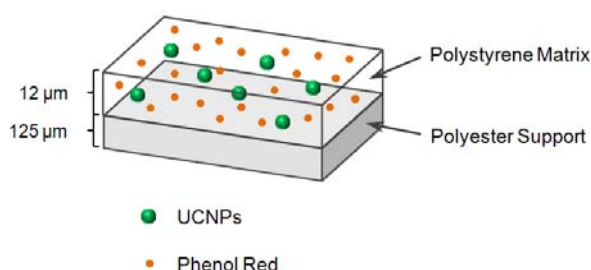


**Figure 5.11** Cross-section of the sensor membrane

At low pH, the upconversion emission of **NP-3** is not affected as the sensor film does not show any absorbance between 500 and 700 nm. With increasing concentrations of ammonia and an associated rise of the pH, the absorbance of the film between 500 and 600 nm (with its peak at 560 nm) increases substantially, thus screening off the green emission of the UCNPs. The red emission of the UCNPs, in contrast, is not affected by the filter effect of the pH indicator. Therefore, this peak can serve as internal standard to allow for ratiometric measurements. By determining the intensity ratio of green to red peak

($I_{541}/I_{655}$) the sensor becomes independent from inhomogenities in the sensor membrane, particle concentration and fluctuations of the intensity of the laser.
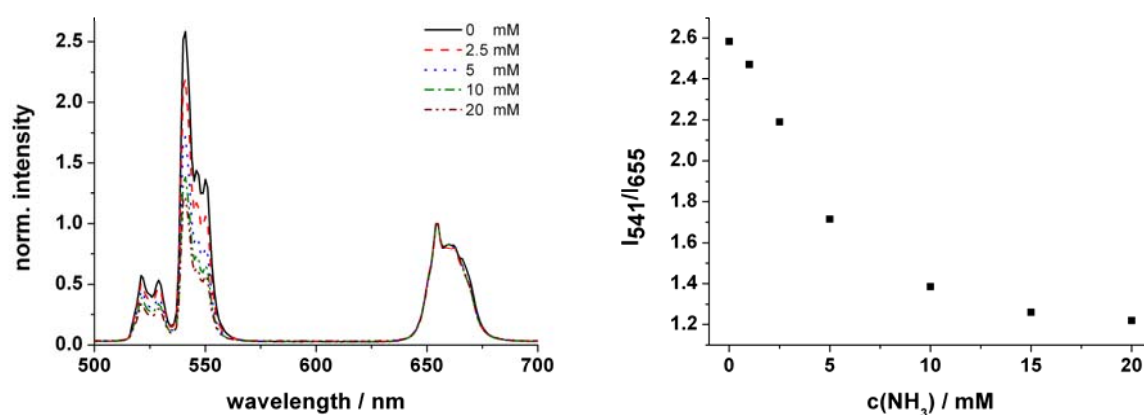


**Figure 5.12** *(Left)* Representative luminescence spectra of the sensor film at ammonia concentrations between 0 and 20 mM following photo-excitation at 980 nm. Spectra are normalized to the peak at 655 nm whose intensity is not affected by ammonia. *(Right)* Ratio of the green to the red emission of **NP-3** in the sensor film as a function of ammonia concentration.

Figure 5.12 shows the decrease in the intensity of the green emission in presence of different concentrations of $NH_3$. The ratio of the intensities of green and red emission of the UCNPs changes from 2.6 (in absence of ammonia) to 1.2 (saturation with ammonia) as can be seen from figure 5.12, right. This effect is not due to any absorption of light of the 980-nm laser because neither PR nor the polystyrene has measurable absorbance at this wavelength.
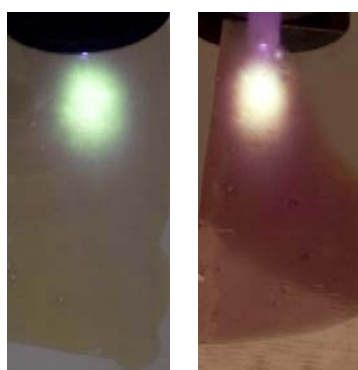


**Figure 5.13** Photographs of the sensor foil under 980 nm excitation. *(Left)* In absence of dissolved ammonia. *(Right)* After exposure to a 20 mM aqueous solution of ammonia.

The color of the UCNP emission detected by the naked eye changes from bright green to yellow (mixture of green and red), see figure 5.13. The sensor membrane responds to aqueous solutions of ammonia in concentrations between 1 mM and 20 mM, corresponding to 40 to 800 ppm. A response curve of the sensor is shown in figure 5.14. Repetitive cycling between a 10 mM $NH_3$ solution and water was performed with a sensor membrane. For that purpose, the membrane was placed in a cuvette filled with either 3 mL of distilled water or 3 mL of a 10 mM ammonia solution and the ratio of the intensities of green and red peak were constantly measured. The water in the cuvette was changed once during the regeneration step. Good reversibility, with vitually no leaching of the indicator, is observed. The long response times (which are typical for ammonia sensors[14,15]) are due to the slow diffusion of ammonia through the membrane and may be shortened (at the expense of signal intensity) by using thinner sensor layers. The dynamic range may be lowered by choosing an indicator with a lower $pk_a$.
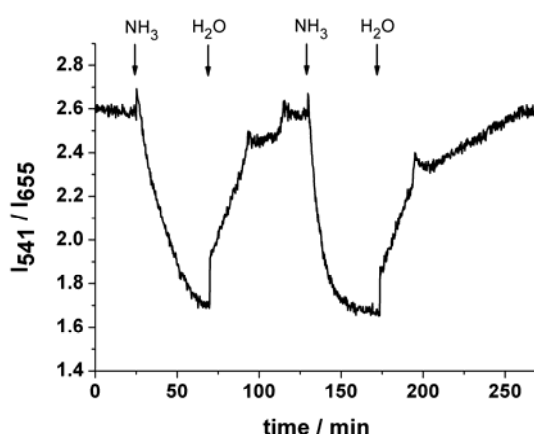


**Figure 5.14** Response curve of the sensor film on exposure to 10 mM $NH_3$ and reversibility in water by monitoring the ratio of the green to the red upconversion emission.

## 5.4 Cell Imaging Using UCNPs

It was investigated whether the UCNPs described in this work are suitable for bioimaging. Normal rat kidney (NRK) cells were treated with unmodified UCNPs of type **NP-3** overnight. Unbound UCNPs were washed away and the cells were fixed using glutaraldehyde and subsequently imaged using a confocal fluorescence microscope equipped with a 1 W 980 nm laser diode.

**Figure 5.15** NRK cells treated with ~250 µg UCNPs of type **NP-3**, overlay of a bright field image of the cells and a dark field image of the UCNP emission under 980 nm excitation. *(Left)* Green channel. *(Right)* Red channel.

Figure 5.15 illustrates an overlay of a bright field image of the NRK cells and the upconversion emission of the particles under NIR excitation. The left picture shows the green emission, the right picture the red emission of the particles collected from the respective color channels of the CCD camera. The luminescence of the partially hexagonal $NaYF_4$: Yb, Er nanoparticles (**NP-3**) is very bright and clearly visible. It can be observed that the UCNPs are taken up by the cells. Single cells exhibit a very high uptake of particles which seems to be harmful to the cells.
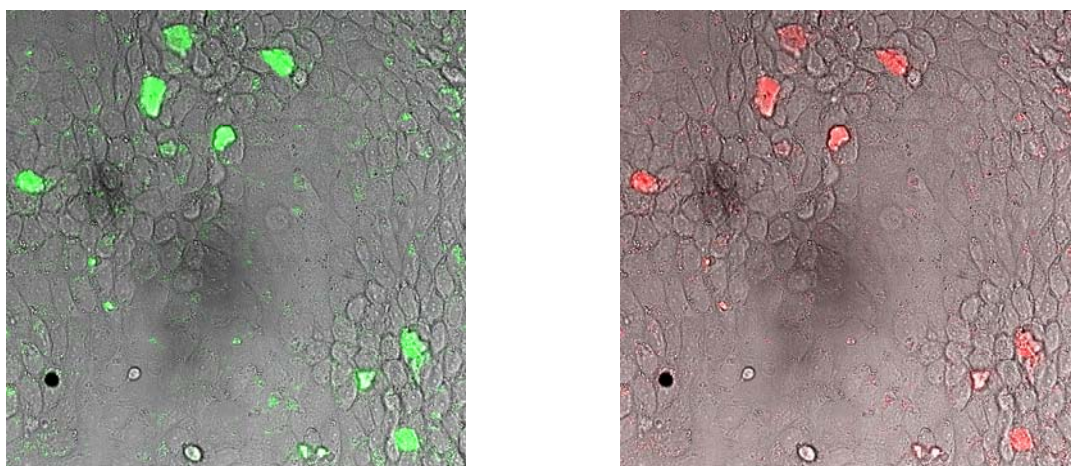


**Figure 5.16** NRK cells treated with ~250 µg UCNPs of type **NP-3-C**, overlay of a bright field image of the cells and a dark field image of the UCNP emission under 980 nm excitation. *(Left)* Green channel. *(Right)* Red channel.

The experiment was repeated using silica coated, azido modified UCNPs of type **NP-3-C**. As can be observed from figure 5.16, these particles are also taken up by the cells. The silica coated particles appear to be more benign for the cells and the distribution seems to be more homogeneous

Figure 5.17 shows a detail from figure 5.16. The luminescence of single particles is clearly visible. Therefore, it can be stated that the UCNPs presented in this work are suitable for further use in bioimaging experiments. It is assumed that the cell-uptake of the UCNPs takes place via clathrin-mediated endocytosis. This is the major route for endocytosis in most cells. The large protein clathrin assists in the formation of a coated pit on the inner surface of the plasma membrane of the cell. This pit then invaginates into the cell to form a coated vesicle around the intruding particle. Finally, the Clathrin-coated vesicle separates from the plasma membrane carrying the particle. Following detachment from the plasma membrane, the clathrin is quickly uncoated from the vesicle surface. However, the exact cell-uptake mechanism is not known as this topic has not been discussed in literature so far.
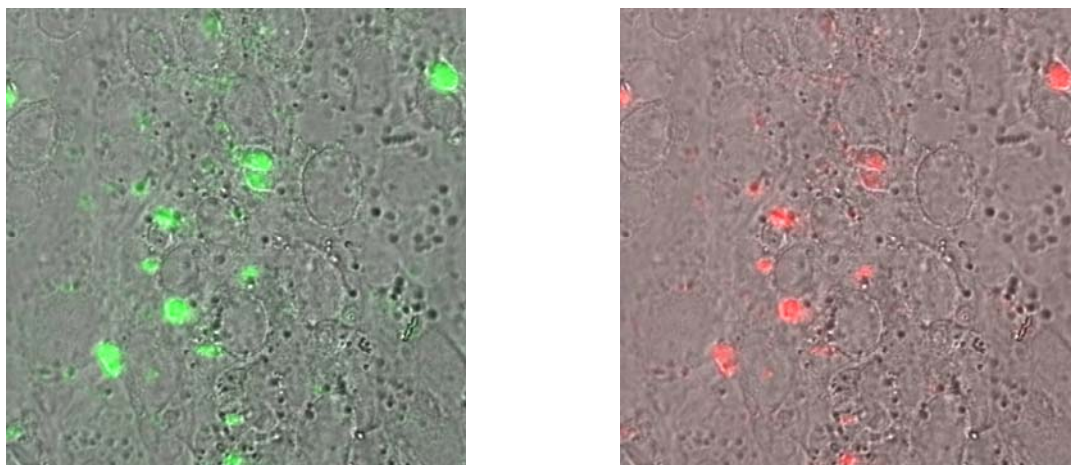


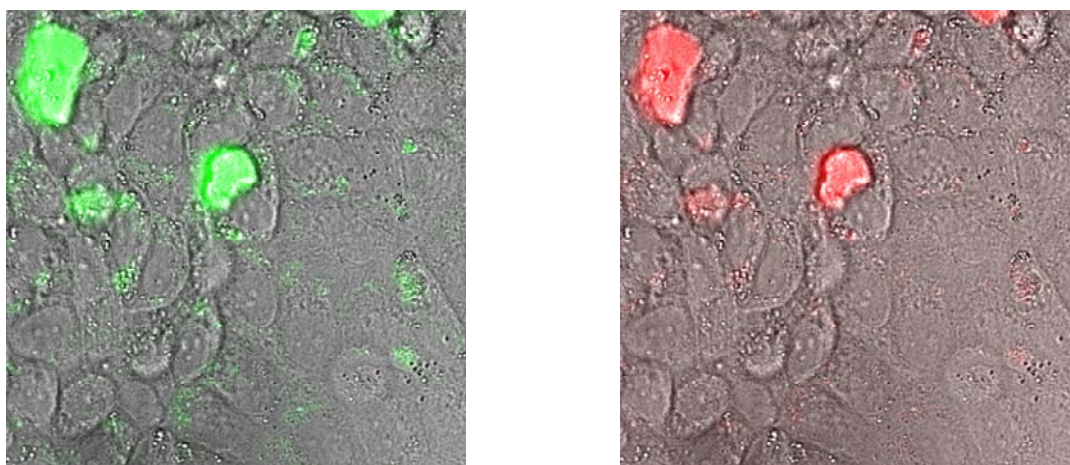**Figure 5.17** NRK cells treated with ~250 µg UCNPs of type **NP-3-C**, detail of the overlay of a bright field image of the cells and a dark field image of the UCNP emission under 980 nm excitation. *(Left)* Green channel. *(Right)* Red channel.

## 5.5 Discussion

There are several reports in the literature[16,17] where surface modified UCNPs have been used as labels for proteins and oligonucleotides. However, all attempts to

develop a selective assay for proteins or thiolated oligonucleotides with the UCNPs described in this work failed in that the selective recognition of the target molecules could not be ensured. In case of the oligonucleotide assay, it could be proven that the alkyne maleinimide (**7**) selectively binds to the thiolated oligonucleotides. However, oligos bound to the particles could be detected. It is assumed that the amount of both, the maleinimide bound to the particle surface and the concentration of the oligos used, need to be controlled very carefully. Another possible reason for the failure of this assay might be the insufficient brightness of the upconverting particles used in these experiments. Substitution of the used particles of type **NP-1** by the brighter particles of type **NP-3** might substantially increase the sensitivity of the assay and enable the detection of very low amounts of bound oligonucleotide. This could not be tested as all MTP assay measurements were performed at the Department of Biotechnology in Turku (Finland) during a 3 month visit and **NP-3** was not developed until after this stay. It is also conceivable that the linker used to attach the maleinimide group to the particles surface is too short to enable a selective and specific binding of the target protein or oligonucleotide. This might also be true for the biotin moiety. The biotin-(strept)avidin interaction possibly is sterically hindered as the biotin is located very close to the particle surface. Introduction of a longer spacer between the biotin and the click site could solve this problem. The unselective electrostatical binding of proteins to the silica surface of the particles proved to be another problem. Avidin (pI 10) is a highly basic protein with an overall positive charge at neutral pH this giving rise to nonspecific binding to the negatively charged silica surface. By introduction of charge compensating groups to the silica surface this kind of electrostatical binding is likely to be substantially reduced. The competitive binding of HSA coated UCNPs to an immobilized anti-HSA antibody could be shown. Nevertheless, the covalent attachment of the protein to the maleinimido group on the particle surface could not be definitely proven. Furthermore, the standard deviation of the intensity readings for this assay was very high, again due to the use of the particles of type **NP-1** with only moderate brightness. Concluding it has to be stated that the objective to develop a click based immuno or gene assay was not achieved.

On the other hand, it was shown that UCNPs have large potential for sensing applications. Using different pH indicators with a pH dependent absorbance overlapping with the green emission of the UCNPs of type **NP-3** allows for the

development of upconversion based pH sensors covering a broad pH range. Compared to the literature example[1] with bromothymol blue as the pH probe the systems presented here are advantageous as the red emission of the UCNPs is not affected by the pH dependent color change of the indicators thereby allowing ratiometric sensing.

Moreover, this effect can be exploited for the sensing of acidic and basic gases by incorporating the UCNP indicator system into a proton impermeable polymer matrix. Thus, the first ammonia sensor known in literature based on upconversion luminescence was presented. The ratiometric readout using the red peak of the UCNPs as reference peak renders the system independent of excitation intensity and particle concentration. This allows for measurements in turbid or inhomogeneous samples. The detection range attained for the sensor membrane of 40 to 800 ppm of dissolved ammonia admittedly is too high for use as a trace ammonia detection system. However, this robust and simple sensing scheme can be enhanced by choosing a pH indicator with a lower $pK_a$, e. g. methyl red. In comparison to ammonia sensing systems based on the use of conventional organic fluorophores[7,9] the NIR excitation of this sensor system minimizes negative effects from background luminescence.

In addition, initial experiments have shown that the upconverting nanoparticles presented in this work are suitable for bioimaging applications. Cells of the NRK type displayed a considerable uptake of the UCNPs. The silica coated particles in particular appeared to be benign for the cells especially when applied in low concentrations. Separate images of the green and the red particle emission were acquired. This paves the way for ratiometric measurements within cells. This concept has not been described in the literature so far. Consequently, the functionalization of the UCNPs with clickable DNA,[18,19] peptides[20] or antibodies could lead to the development of sensitive new tumor markers[21] or release systems for siRNA.[22]

# 5.6 References

[1] Sun L, Peng H, Stich MIJ, Achatz D, Wolfbeis OS (2009) **pH Sensor Based on Upconverting Luminescent Lanthanide Nanorods**, Chem. Comm. 5000-5002.

[2] Berthois Y, Katzenellenbogen JA, Katzenellenbogen BS (1986) **Phenol Red in Tissue Culture Media is a Weak Estrogen: Implications Concerning the Study of Estrogen-Responsive Cells in Culture,** Proc. Natl. Acad. Sci. USA 83: 2496-2500.

[3] Masserini RT, Fanning KA (2000) **A Sensor Package for the Simultaneous Determination of Nanomolar Concentrations of Nitrite, Nitrate, and Ammonia in Seawater by Fluorescence Detectio**n, Mar. Chem. 68: 323-333.

[4] Timmer B, Olthuis W, van der Berg A (2005) **Ammonia Sensors and Their Applications—a Review,** Sens. Actuators B 107: 666-677.

[5] Kar S, Arnold MA (1992) **Fiber-optic Ammonia Sensor for Measuring Synaptic Glutamate and Extracellular Ammonia,** Anal. Chem. 94: 2438-2443.

[6] Elamari A, Gisin N, Munoz JL, Poitry S, Tsacopoulos M, Zbinden H (1997) **Photon-counting Optical-fiber Sensor for the Detection of Ammonia in Neurochemical Applications**, Sens. Actuators B, 38-39, 183-188.

[7] Waich K, Borisov S, Mayr T, Klimant I (2009) **Dual Lifetime Referenced Trace Ammonia Sensors**, Sens. Actuators. B 139: 132-138.

[8] Totschnig G, Lackner M, Shau R, Ortsiefer M, Rosskopf J, Amann MC, Winter F (2003) **High-speed Vertical-cavity Surface-emitting Laser (VCSEL) Absorption Spectroscopy of Ammonia ($NH_3$) near 1.54 µm**, Appl. Phys. B 76: 603-608.

[9] Mills A, Wild L, Chang Q (1995) **Plastic Colorimetric Film Sensors for Gaseous Ammonia** Microchim. Acta 121: 225-236.

[10] Wolfbeis OS (2008) **Fiber-Optic Chemical Sensors and Biosensors,** Anal. Chem. 80: 4269-4283.

[11] Rhines TD, Arnold MA (1988) **Simplex Optimization of a Fiber-optic Ammonia Sensor Based on Multiple Indicators,** Anal. Chem. 60: 76-81.

[12] Lobnik A, Wolfbeis OS (1998) **Sol-gel Based Optical Sensor for Dissolved Ammonia**, Sens. Actuators B 51: 203-207.

[13] Preininger C, Mohr GJ, Klimant I, Wolfbeis OS (1996) **Ammonia Fluorosensors Based on Reversible Lactonisation of Polymer-entrapped Rhodamine Dyes and the Effects of Plasticizers,** Anal. Chim. Acta. 334: 113-123.

[14] Werner T, Klimant I, Wolfbeis OS (1995) **Ammonia-sensitive Polymer Matrix Employing Immobilized Indicator Ion Pairs**, Analyst 120: 1627-1631.

[15] McDonagh C, Burke CS, MacCraith BD (2008) **Optical Chemical Sensors,** Chem. Rev. 108: 400-422.

[16] Sivakumar S, Diamente PR, van Veggel FCJM (2006) **Silica-Coated $Ln^{3+}$-Doped $LaF_3$ Nanoparticles as Robust Down- and Upconverting Biolabels**, Chem. Eur. J 12: 5878-5884.

[17] Zhang P, Rogelj S, Nguyen K, Wheeler D (2006) **Design of a Highly Sensitive and Specific Nucleotide Sensor Based on Photon Upconverting Particles**, J. Am. Chem. Soc. 128: 12410-12411.

[18] Berndl S, Herzig N, Kele P, Lachmann D, Li X, Wolfbeis OS, Wagenknecht H-A (2009) **Comparison of a Nucleosidic vs Non-Nucleosidic Postsynthetic "Click" Modification of DNA with Base-Labile Fluorescent Probes**, Bioconjugate Chem. 20: 558-564.

[19] Gierlich J, Gutsmiedl K, Gramlich PME, Schmidt A, Burley GA, Carell T (2007) **Synthesis of Highly Modified DNA by a Combination of PCR with Alkyne-Bearing Triphosphates and Click Chemistry**, Chem. Eur. J. 13: 9486 – 9494.

[20]   Kele P, Mezö G, Achatz D, Wolfbeis OS (2009) **Dual Labeling of Biomolecules by Using Click Chemisty: A Sequential Approach**, Angew. Chem. Int. Ed. 48: 344-347, Angew. Chem. 121: 350-353.

[21]   Hu H, Xiong L, Zhou J, Li F, Cao T, Huang C (2009) **Multimodal-Luminescence Core-Shell Nanocomposites for Targeted Imaging of Tumor Cells**, Chem. Eur. J. 15: 3577-3584.

[22]   Jiang S, Zhang Y (2010) **Upconversion Nanoparticles-Based FRET System for Study of siRNA in Live Cells**, Langmuir published online DOI: 10.1021/la904011q

# 6 Experimental Section

## 6.1 Particle Synthesis

### 6.1.1 Silica Nanoparticles

10 nm silica nanoparticles (referred to as SiNP) were obtained from Nanostructured & Amorphous Materials, Inc. (www.nanoamor.com) and directly used for surface modification.

### 6.1.2 Upconverting Microparticles (UCµPs)

Two types of commercially available UCµPs, referred to as µP-1 and µP-2 (see Table 1) were used. Microparticles of type µP-1 are composed of $La_2O_2S$ and doped with ytterbium and erbium ions, those of type µP-2 consist of $Y_2O_2S$ and are doped with ytterbium and thulium ions. Both were obtained from MolTech GmbH Berlin (www.mt-berlin.com).

### 6.1.3 Upconverting Nanoparticles (UCNPs)

The UCNPs were synthesized using the established[1,2] co-precipitation method. 0.2 M lanthanide stock solutions were prepared by dissolving the respective lanthanide trichlorides in water. The solutions were adjusted to pH 2 with 1 M hydrochloric acid to avoid hydrolysis. Subsequently, a cocktail of the lanthanides was prepared by mixing the appropriate volumes of the stock solutions according to the desired composition of the NPs (see table 6.1). 20 mL of a 0.2 M ethylenediaminetetraacetic acid (EDTA) solution were added to from Ln-EDTA complexes. Then, this complex solution was injected into 60 mL of a 0.83 M sodium fluoride solution. Instantaneously, the precipitation of nanoparticles can be observed. The reaction mixture was stirred for 1h at room temperature. The colorless precipitate was separated by centrifugation at 4000 rpm for 30 min, washed 3 times with water and then once with ethanol. The precipitate was dried in a drying furnace and under vacuum. Afterwards, the colorless powder was tempered at 400°C for 4.5 h under

argon atmosphere in either a tube furnace or a muffle furnace distributed by Nabertherm (www.nabertherm.de).

**Table 6.1** Volumes of lanthanide chlorides for NP preparation

| Code | Composition | V(YCl$_3$) | V(YbCl$_3$) | V(ErCl$_3$) | V(TmCl$_3$) | V(HoCl$_3$) |
|------|-------------|------------|-------------|-------------|-------------|-------------|
| | | | | in mL | | |
| NP-1 | 17 % Yb, 3 % Er | 16 | 3.4 | 0.6 | | |
| NP-2 | 20 % Yb, 2 % Er | 15.6 | 4 | 0.4 | | |
| NP-3 | 25 % Yb, 2 % Er | 14.6 | 5 | 0.4 | | |
| NP-4 | 17 % Yb, 1.5 % Tm | 16 | 3.4 | | 0.3 | |
| NP-6 | 25 % Yb, 2 % Ho | 14.6 | 5 | | | 0.4 |
| NP-7 | 25 % Yb, 0.5 % Ho | 14.9 | 5 | | | 0.1 |

**NP-5** with 24.5% Yb and 0.5 % Tm was synthesized by Daniela Achatz.[3] **NP-8** was prepared in an ethylammonium nitrate (EAN) ionic liquid solution.[4] 97.1 mg of YCl$_3$, 26.3 mg of YbCl$_3$ and 4.6 mg of ErCl$_3$ were dissolved in 5 mL of EAN and the solution was heated to 160°C. Subsequently, the lanthanide mixture was injected into a solution of 0.21 g (5 mmol) of NaF in 5 mL of EAN also heated to 160°C. The resulting mixture was stirred for 1h and the colorless precipitate was separated by centrifugation at 4000 rpm for 30 min, washed 3 times with water and then once with ethanol. The precipitate was dried in a drying furnace and under vacuum. **NP-9** was synthesized in a microemulsion of EAN in dodecane with 1-hexadecyl-3-methylimidazolium chloride as the surfactant.[4,5] 10 mL of a microemulsion solution containing 50 w% dodecane, 40 w% surfactant and 10 w% EAN were prepared. 97.1 mg of YCl$_3$, 26.3 mg of YbCl$_3$ and 4.6 mg of ErCl$_3$ were dissolved in 5 mL of this solution. Then, 0.21 g of NaF were dissolved in the remaining microemulsion solution. Both solutions were heated to 160°C and combined. The resulting mixture was stirred for 1h. The nanoparticles were was separated by centrifugation at 4000 rpm for 30 min, washed 6 times with water and then once with ethanol.

## 6.2 Coating and Surface Modification

### 6.2.1 Reagents

*2-Azidoethyl trimethyl orthosilicate* (**1**) was synthesized in a two step procedure. 2-Azidoethanol was prepared from 2-bromoethanol according to literature procedures.[6] 1.2 g (9.6 mmol) of bromoethanol were dissolved in 10 mL of water in a 25 mL round bottom flask. 2.43 g (40 mmol) of sodium azide were added and the reaction mixture was stirred under reflux for 16h. The solution was allowed to cool to room temperature and extracted three times with 6 mL of dichloromethane. The organic phases were combined and dried over $NaSO_4$. The solvent was evaporated to give the product 2-azidoethanol as a yellow, oily substance. Yield: 0.29 g (35 %). 2-Azidoethanol was directly used for reaction with tetraethoxysilane (TMOS) without further purification.



**Figure 6.1** Synthesis of 2-azidoethyl trimethyl orthosilicate (**1**)

0.5 mL (3.4 mmol) of TMOS were dissolved in 10 mL of dry toluene in a 25 mL round bottom flask. 0.29 g (3.3 mmol) of 2-azidoethanol were added and the mixture was stirred at 80°C for 6h. The reaction mixture was directly used for particles functionalization without further purification. $^1$H-NMR (300 MHz, $CDCl_3$): δ = 3.94 (t, 2H), 3.55 (s, 6H), 3.32 (t, 2H). IR (neat) $\nu$ = 2113, 2846, 2922, 2964 cm$^{-1}$. MS (m/z): M$^+$ calculated: 207.3, found 207.1, 208.1.

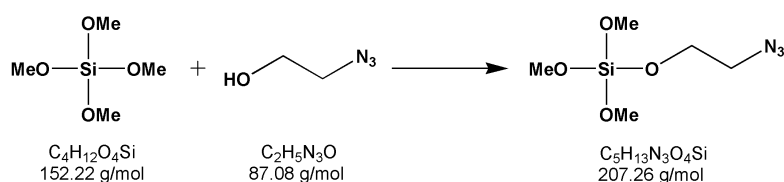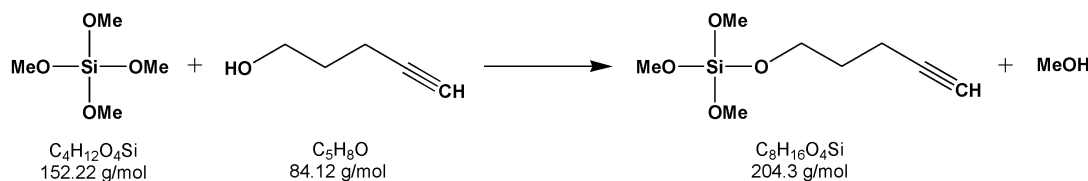*Trimethyl pent-4-ynyl orthosilicate* (**2**):



**Figure 6.2** Synthesis of trimethyl pent-4-ynyl orthosilicate (**2**)

1.6 mL (10.8 mmol) of TMOS were dissolved in 15 mL of dry toluene in a 50 mL round bottom flask. 1 mL of 4-pentin-1-ol were added and the mixture was stirred at 80°C for 6h. The reaction mixture was directly used for particles functionalization without further purification. $^1$H-NMR (300 MHz, CDCl$_3$): δ = 3.77 (t, 2H), 3.59 (s, 6H), 2.36 (dt, 2H,), 1.97 (t, 1H,), 1.79 (quint, 2H), MS (m/z): M$^+$ calculated: 204.3, found 204.1.

*(3-Azidopropyl)triethoxysilane* (**3**) was synthesized from (3-chloropropyl)triethoxysilane by Daniela Achatz.[7]

*O-(Propargyloxy)-N-(triethoxysilylpropyl)urethane* (**4**) was purchased from ABCR (www.abcr.de) and used without further purification.

*Azido-biotin* (**5**) was synthesized by a modification of the method described in the literature[8] using 2-azidoethylamine[9] as the amino linker. 50 mg (0.15 mmol) of commercially available biotin NHS ester were dissolved in dry dimethylformamide (DMF), and 23 mg (0.25 mmol) of 2-azidoethylamine was added. 45 µL (0.32 mmol) of triethylamine were added and the solution was stirred overnight at room temperature. The solvent was evaporated to give the crude product as a yellow, oily substance. It was crystallized from ethanol to give the product (**5**) as a colorless solid. Yield: 26.2 mg (56 %). $^1$H NMR (300 MHz, MeOD): δ = 4.49 (dd, 1H,) 4.30 (dd, 1H), 3.21 (t, 2H), 2.95 (t, 2H), 2.71 (dd, 1H), 2.26 (dd, 1H), 2.38 (t, 2H), 1.8-1.4 (m, 6H). MS (m/z): M$^+$ calculated: 312.1, found 311.9, 312.9.

*Propargyl-biotin*[10] (**6**) was synthesized by dissolving 16 mg (0.04 mmol) of NHS-biotin in dry DMF. After stirring for 10 min, 6 µL (0.08 mmol) of propargylamine was added dropwise and the mixture stirred for another 4 h at room temperature. The solvent was removed under reduced pressure to give a yellow oily substance. The

crude product was then purified by column chromatography using a gradient of methylene chloride and methanol as eluents to yield propargylbiotin (**6**) as a colorless solid. Yield: 7 mg (62 %). $^1$H-NMR (300 MHz, D$_6$-DMSO): δ = 8.22 (bs, 1H), 6.41 (s, 1H), 6.35 (s, 1H), 4.29 (t, 1H), 4.10 (m, 1H), 3.83 (dd, 2H), 3.08 (m, 2H), 2.81 (dd, 1H), 2.57 (d, 1H), 2.08 (t, 2H), 1.60-1.40 (m, 4H), 1.60-1.40 (m, 2H). MS (m/z): M$^+$ calculated: 281.1, found 280.9.

*Propargyl-maleimide* (**7**) was synthesized from maleic acid anhydride and propargylamine by Martin Link and Jana Kleim.[11]

## 6.2.2 Surface Modification of SiNPs

100 mg of SiNPs were suspended in 20 mL of dry toluene in a 100 mL Schlenk flask and flushed with dry nitrogen. 150 µL of the respective silane (**1** or **2**) were added and the mixture was stirred for 48 h at 90°C. The mixture was allowed to cool and the particles were separated by centrifugation for 20 min at 4000 rpm. The particles were washed several times with ethanol and acetone, and finally dried in a drying furnace at 60 °C.

## 6.2.3 Surface Modification of UCµPs

200 mg of UCµPs of type µP-1 were rinsed 3 times with 2 mL of 0.1 M acetic acid and washed several times with doubly distilled water. The particles were filtered using a suction filter and then dried overnight in a drying furnace. The activated UCµPs were then suspended in 20 mL of dry toluene in a 100 mL Schlenk flask and flushed with dry nitrogen. 200 µL of the respective silane (**3** or **4**) were added and the mixture stirred for 48 h at 90 °C. The mixture was allowed to cool and the particles were separated by centrifugation for 15 min at 4000 rpm. After removal of the supernatant, the particles were washed several times with ethanol and acetone, and finally dried in a drying furnace at 60 °C.

## 6.2.4 Coating and Surface Modification of UCNPs

The particles were coated with a silica shell via a modified Stöber process.[12] Two different procedures were used. In the first method, 75 mg of the UCNPs were dispersed in 80 mL of ethanol by ultrasonication for 10 min. Subsequently, the mixture was heated to 40 °C, and 500 µL of water and 500 µL of 25 w% ammonia were added, followed by 400 µL of tetraethoxysilane (TEOS). The solution was stirred for 30 min. The respective functionalized silane (**3** or **4**; 25 µL) was added and the mixture stirred for another 2.5 h. After cooling to room temperature, the particles were purified by size exclusion chromatography (on Sephadex LH-60) using ethanol as the eluent to remove unreacted TEOS and ammonia. The proper fraction was recognized by its slight turbidity and by illuminating it with a 980-nm laser which results in visible luminescence. The resulting silica-coated UCNPs were stored in ethanol solution to avoid aggregation. To transfer the particles into aqueous solution, the reaction mixture from the Stöber coating process was diluted with water and purified again by size exclusion chromatography using Sephadex G-75 (which is better water-compatible than LH-60) with distilled water as the eluent. The resulting suspensions in either ethanol or water are stable for several months.

In the second procedure, 30 mg of the UCNPs were dispersed in 80 mL of ethanol via ultrasonication for 10 min. The mixture was heated to 40 °C, and 7.5 mL of $H_2O$, and 8.5 mL of 25 w% ammonia were added, followed by 100 µL of TEOS. The solution was stirred for 2h. Subsequently, 25 µL of the respective silane (**3** or **4**) were added and the mixture was stirred for another hour. The work up was performed analog to the first method.

For the microemulsion process, 16 mg of the UCNPs were dispersed in 1160 µL of distilled $H_2O$ via ultrasonication. The microemulsion was prepared from cyclohexane (30 mL), Triton X-100 (1.77 mL), and n-hexanol (1.8 mL). The dispersed UCNPs were added to 20 mL of the microemulsion together with 240 µL of ammonia (33 w%) and the mixture was ultrasonicated for 10 min. 932 µL of $H_2O$, 100 µL of TEOS, and 60 µL of azidosilane **3** were added to the remaining microemulsion and then, both mixtures were combined. The resulting reaction mixture was ultrasonicated for 10 min and then vortexed for 2h. After 1h the mixture was ultrasonicated again for 10 min. The microemulsion was broken by addition of 6 mL

of acetone. The particles were separated via centrifugation at 2860 rpm for 5 min and washed 2 times with ethanol and 2 times with water. The particles were stored in aqueous dispersion.

## 6.3 Click Reaction

Click reactions were generally performed in water/ethanol mixtures (1:10 to 10:1; v/v) by adding a mixture of copper(II) sulfate and ascorbic acid. Catalytic quantities of triethylamine accelerate the cycloaddition. In a standard procedure, 0.5 – 1 mg of one of the clickable reagents (**5** - **15**) is added to 2 mL of a 1 mg/mL dispersion of the respective UCP or SiNP in a water/ethanol mixture. Thereafter, 10 µL of a 20 mM aqueous solution of copper sulfate, 10 µL of a 0.1 M solution of sodium ascorbate, and 10 µL of triethylamine were added. The mixture was stirred at room temperature for 1 to 14 h. Experiments without the copper catalyst were performed in parallel at all stages. In case of UCµPs and silica nanoparticles, the solutions were centrifuged and washed several times with water and ethanol. In case of UCNPs, work up was accomplished by size exclusion chromatography (Sephadex LH-60) to remove unreacted dyes, any biomolecules, and catalyst.

## 6.4 UCNPs as Protein and Oligonucleotide Labels

### 6.4.1 Oligonucleotide Assay

All experiments regarding the oligonucleotide and the protein assay were carried out at the Department of Biotechnology, University of Turku, Turku, Finland.

Sequence of the thiol-oligonucleotide (SH-oligos): 5'- cat tgc cga cag ga -3'.

Sequence of the biotinylated-oligonucleotide (bio-oligo): 5'- tcc tgt cgg caa tg -3'.

SH-oligos were labeled with UCNPs of type **NP-1-C-7**. 5 nmol of the SH-oligos were dissolved in 400 µL of phosphate-buffered silane (PBS) buffer. 4 µL of a 15 mM *tris* (2-carboxyethyl) phosphine (TCEP)-solution were added as reducing agent. After stirring at 30 min at room temperature, the SH-oligos were added to 1.5 mg of **NP-1-**

**C-7** in 100 µL of PBS. The mixture was stirred overnight and the particles were separated by centrifugation at 12000 rpm for 7 min and washed 3 times with PBS buffer.

In the assay, three replicates of appropriate dilutions of the bio-oligos in 50 µL assay buffer were first incubated in streptavidin wells (streptavidin MTPs, 8x12 wells regular, obtained from Kaivogen Oy, www.kaivogen.com,) for 30 min at room temperature with slow shaking. The wells were washed once with wash solution (Delfia Platewash, Perkin Elmer Life and Analytical Sciences, www.perkinelmer.com), and 75 µL of **NP-1-C-7-Oligo** (5 µg/mL) were added. Wells were incubated for 1.5 h with slow shaking, washed four times and the luminescence of the UCNPs was measured in a 3x3 raster per well.

## 6.4.2 Protein Assay

Special, white, low-fluorescence MaxiSorp microtitration wells (Nunc A/S Denmark, www.nuncbrand.com) were coated with anti-human serum albumin (anti-HSA produced in rabbit, obtained from Sigma Aldrich, www.sigma-aldrich.com) by physical adsorption to prepare low-capacity, anti-HSA-coated microtitration wells. In the coating, the wells were first incubated at 35 °C for 2 h with 375 ng of anti-HSA in 50 µL of 200 mM phosphate buffer (pH 7.8). The coated wells were washed twice and saturated for 1h at room temperature with 150 µL of 50 mM Tris-HCl buffer, pH 7.2, containing 0.1 % BSA, 0.1 % Germall II, and 3% trehalose. The wells were aspirated, dried in a laminar hood overnight, and stored at 4 °C in a sealed package with desiccant.

HSA coated UCNPs were prepared by dispersing 5 mg of **NP-1-C-7** in 400 µL of PBS via ultrasonication and addition of 100 µL of a 10 mg/mL solution of HSA in PBS. The mixture was stirred overnight. The particles were collected via centrifugation at 12000 rpm for 7 min and washed 3 times with PBS.

In the assay, three replicates of appropriate dilutions of free HSA in 25 µL assay buffer were pipetted into the anti-HSA coated wells, followed by 75 µL of **NP-1-C-7-HSA** (7.5 µg/mL) in assay buffer. The solution was incubated for 1h at room temperature with slow shaking. The wells were washed four times with wash solution.

The luminescence of the UCNPs was measured in a 3x3 raster per well.

## 6.5 pH Sensing

All measurements were performed in 40 mM Britton-Robinson buffer. Silica coated UCNPs of type **NP-3-C** (50 µg/mL) were dispersed in buffered solutions of the respective pH-indicator. Concentrations of the indicators were 66.7 µM for phenolphthalein, and 40 µM for both phenol red and methyl red.

## 6.6 Ammonia Sensor

In order to minimize leaching of the dye and improving its solubility in the hydrophobic polymer, the sodium ion of the indicator phenol red was replaced by the tetrabutyl ammonium ion.[13] Phenol Red (10 mg) was dissolved in 30 mL of water and extracted with 30 mL of chloroform containing 9 mg of tetrabutyl ammonium chloride. The organic phase containing the tetrabutyl ammonium salt of phenol red (TBA-PR) was collected and dried using a rotary evaporator. The probe TBA-PR (3 mg) was then dissolved in 2 mL of a 10 % solution of polystyrene in chloroform. Then, 5 mg of the $NaYF_4$: Yb, Er were added and the mixture stirred for 5 h. The sensor "cocktail" was spread onto the polyester support (Mylar™, obtained from Goodfellow, www.goodfellow.com) using a home-made device. The resulting layer was dried at air at room temperature. From the quantities of materials and solvents employed, the thickness of the dried membrane was calculated to be 12 µm.

## 6.7 Instrumental Techniques

Scanning electron microscopy (SEM) images were acquired on a Jeol (www.jeolusa.com) instrument (JSM 800). Transmission electron microcopy (TEM) images were acquired using a 120 kV Zeiss (www.smt.zeiss.com) instrument of type Leo 912AB equipped with a Proscan CCD (www.proscan.de) camera (UCNPs) or a

120 kV FEI instrument of type TEMCM12 (www-fei.com) equipped with a Gatan CCD-camera (www.gatan.com) (SiNPs). ^{1}H-NMR spectra were recorded on an Avance 300 NMR-spectrometer from Bruker Bio Spin (www.bruker-biospin.com). Tetramethylsilane (TMS) was used as the internal standard. Elemental analysis and mass spectrometry was performed by the Central Analytics Department at the University of Regensburg. DR-FTIR spectra were acquired on a FT/IR – 6100 IR spectrometer distributed by Jasco (www.jascoinc.com). A diffuse reflectance accessory (EasiDiff) provided by Pike Technologies (www.piketech.com) was used for sample preparation. UV-spectra were recorded with a Cary 50 Bio UV-visible Spectrophotometer from Varian (www.varian.com). Fluorescence microscopy images were acquired on a Leica DMRE microscope (www.leica.de). A mercury lamp acted as the light source, and the excitation band (515 to 560 nm) was adjusted by using a bandpass filter. Fluorescence was collected after it had passed a longpass filter with a cut-off wavelength of 590 nm. Luminescence spectra of particles and fluorescence spectra of dyes were recorded on a Cary Eclipse fluorometer (from Varian; www.varianinc.com). A 980-nm fiber-optic diode laser (5 mW cw; from Roithner Lasertechnik; www.roithner-laser.com) was used as the light source for upconversion photoexcitation. Spectra are not corrected. All microplate measurements were acquired on a HIDEX Plate Chameleon Multilabel Detection Platform (www.hidex.com) using a 980-nm laser diode as the excitation source and a 550 nm or 660 nm bandpass filter for collecting the signal of the green and red peaks respectively.[14] Upconversion microscopy images were taken on a Leica SP5 Confocal Microscope (www.leica-microsystems.com) with Acousto-Optical Beam Splitter and a resonant scanner using a 980 nm laser diode (1 W) as the excitation source.

## 6.8 References

[1]     Yi G, Lu H, Zhao S, Ge Y, Yang W, Chen D, Guo L-H (2004) **Synthesis, Characterization, and Biological Application of Size-Controlled Nanocrystalline NaYF$_4$: Yb, Er Infrared-to-Visible Up-Conversion Phosphors**, Nano Lett. 4: 2191-9196.

[2]     Mader HS, Link M, Achatz DE, Uhlmann K, Li X, Wolfbeis OS (2010) **Surface-Modified Upconverting Microparticles and Nanoparticles for Use in Click Chemistries**, *Chem.-Eur. J., accepted.*

3   Achatz DE, Meier RJ, Fischer LH, Wolfbeis OS (2010) **Oxygen Sensor based on NaYF$_4$:Yb, Tm Upconverting Nanoparticles**, submitted

4   Zech O (2010) **Ionic Liquids in Microemulsions – a Concept to Extend the Conventional Thermal Stability Range of Microemulsions**, Dissertation, University of Regensburg

5   Zech O, Thomaier S, Bauduin P, Rück T, Touraud D, Kunz W (2009) **Microemulsions with an Ionic Liquid Surfactant and Room Temperature Ionic Liquids As Polar Pseudo-Phase**, J. Phys. Chem. B 113: 465-473.

6   Demko ZP, Sharpless KB (2001) **An Intramolecular [2+3] Cycloaddition Route to Fused 5-Heterosubstituted Tetrazoles**, Org. Lett. 3, 4091-4094.

7   Achatz DE (2008) **Fluorescent Silica Nanoparticles for Click Labeling of Proteins**, Diplomarbeit, University of Regensburg,

8   Lin P-C, Ueng S-H, Zseng M-C, Ko J-L, Hunag K-T, Yu S-C, Adak AK, Chen Y-J, Lin C-C (2006) **Site-Specific Protein Modification trough Cu$^I$-Catalyzed 1,2,3-Triazole Formation and its Implementation in Protein Microarray Fabrication.** Angew. Chem. Int. Ed. 45: 4286-4290.

9   Mayer T, Maier ME (2007) **Design and Synthesis of a Tag-Free Chemical Probe for Photoaffinity Labeling**, Eur. J. Org. Chem. 4711-4720.

10  Meier JL, Mercer AC, Rivera H, Burkart MD (2006) **Synthesis and Evaluation of Bioorthogonal Pantetheine Analogues for in Vivo Protein Modification**, J. Am. Chem. Soc. 128: 12474-12184.

11  Link M, Li X, Kleim J, Wolfbeis OS, (2010) **Novel Method for Introducing Maleinimido Groups into Thiol-Reactive Labels**, Eur. J. Org. Chem. submitted.

12  Stöber W, Fink A (1968) **Controlled Growth of Monodisperse Silica Spheres in the Micron Size Range**, J. Colloid. Interf. Sci. 26: 62-69.

13  Mohr GJ, Werner T, Oehme I, Preininger C, Klimant I, Kovacs B, Wolfbeis OS (1997) **Novel Optical Sensor Materials Based on Solubilization of Polar Dyes in Apolar Polymers,** Adv. Mater. 9: 1108-1113.

14  Soukka T, Kuningas K, Rantanen T, Haaslahti V, Lövgren T (2005) **Photochemical Characterization of Up-Converting Inorganic Lanthanide Phosphors as Potential Labels**, J. Fluorescence 15: 513-528.

# 7 Summary

## 7.1 In English

Upconverting nanoparticles (UCNPs) of the NaYF$_4$ type with narrow size distribution from 60 to 90 nm, were prepared using the established co-precipitation method. The particles were codoped using Yb$^{3+}$ as the sensitizer ion, Er$^{3+}$, Tm$^{3+}$ or Ho$^{3+}$, respectively as the emitting activator ions. Erbium doped particles displayed the brightest luminescence (green and red). A dopant ratio of 25% Yb$^{3+}$ and 2% Er$^{3+}$ proved to be the best composition to enable a partial phase transfer from the cubic α-NaYF$_4$ with moderate luminescence to the hexagonal β-NaYF$_4$ with much higher upconversion emission intensities. Effects of fluctuations of the oven temperature on the resulting luminescence intensity during the annealing step of the particle preparation could not be completely eliminated. The ionic liquid ethylammonium nitrate (EAN) proved to be a suitable solvent for the preparation of small UCNPs with diameters around 30 nm. However, the direct synthesis of hexagonal NaYF$_4$ failed and the annealing step could not be circumvented.

Commercially available silica nanoparticles (SiNPs) and upconverting microparticles (UCμP) as well as the synthesized UCNPs were successfully functionalized with azido and alkyne groups, respectively. Thereby the particle surfaces become compatible with click chemistry which is highly versatile, particularly with respect to bioconjugation as it is bioorthogonal and thus not troubled by functional groups often present in biological samples. It was shown that SiNPs and UCμPs can be directly functionalized using the appropriate silanes. The UCNPs were coated with a layer of SiO$_2$ (silica) and click functionalized in a one step Stöber procedure. Purification of the coated UCNPs via size exclusion chromatography minimized aggregation of the particles and guaranteed good dispersibility in aqueous solutions.

Fluorescently labeled SiNPs covering emission wavelengths from green to red were prepared by covalent attachment of click functionalized dyes. Color and intensity of the particles are easily fine-tuned via strict control of dye load and reaction times. UCμPs and UCNPs click labeled with fluorescent dyes have attractive spectral features in giving dual emissions depending on the wavelength of excitation

which can be exploited for encoding applications. The photoexcitation of an organic dye by the UCNPs emission was shown for the green emitting UCNPs of type **NP-3** and a click derivative of rhodamine B. The energy transfer from the UCNP to the dye did not occur in a non-radiative FRET mechanism but most likely by the actual emission and reabsorption of photons, with the UCNPs acting as "nano-lamps".

Bioreactive particles, functionalized with either maleinimide or biotin were also prepared via the click reaction. Unfortunately, the reactivity of maleinimide functionalized UCNPs to thiol groups and the affinity of UCNPs modified with the biotin group to (strept)avidin could not successfully be exploited for the labeling of proteins and oligonucleotides.

On the other hand, it was demonstrated that UCNPs have high potential in sensing applications. Sensing schemes for the determination of pH were presented based on the inner filter effect of selected pH indicators on the emission of the UCNPs. This concept was extended to the development of an ammonia sensor membrane doped with UCNPs of type **NP-3** and the pH indicator phenol red. Using this fully reversible sensor membrane, ammonia concentrations ranging from 1 to 20 mM (40 – 800 ppm) could be determined in a ratiometric setup. Moreover, it was shown that unmodified as well as silica coated UCNPs are taken up by normal rat kidney cells and therefore are suitable tools for bioimaging applications.

## 7.2 In German

Upconvertierende Nanopartikel (UCNPs) vom $NaYF_4$ Typ mit einer engen Größenverteilung von 60 bis 90 nm wurden mittels der etablierten Co-Präzipitationsmethode hergestellt. Die Partikel wurden mit $Yb^{3+}$ als Sensitizer Ion und $Er^{3+}$, $Tm^{3+}$ beziehungsweise $Ho^{3+}$ als emittierendes Aktivator Ion co-dotiert. Die hellste Lumineszenz (grün und rot) wurde für Erbium dotierte Partikel gemessen. Ein Dotierungsverhältnis von 25% $Yb^{3+}$ und 2% $Er^{3+}$ erwies sich als die beste Zusammensetzung, um einen teilweisen Phasenübergang vom nur mäßig lumineszenten kubischen $\alpha$-$NaYF_4$ zum hexagonalen $\beta$-$NaYF_4$ zu erreichen. Dieses weist wesentlich höhere Upconversions-Emissionsintensitäten auf. Ein Einfluss von Schwankungen der Ofentemperatur während des Sinterns der Partikel auf die

resultierende Lumineszenzintensität konnte nicht völlig eliminiert werden. Die ionische Flüssigkeit Ethylammoniumnitrat (EAN) erwies sich als geeignetes Lösungsmittel für die Herstellung von kleinen UCNPs mit Durchmessern von ungefähr 30 nm. Die direkte Synthese von hexagonalem $NaYF_4$ scheiterte jedoch und das Sintern der Partikel konnte nicht umgangen werden.

Kommerziell erhältliche Silicananopartikel (SiNPs) und upconvertierende Mikropartikel (UCµPs) sowie die synthetisierten UCNPs wurden erfolgreich mit Azido- beziehungsweise Alkingruppen funktionalisiert. Dadurch wurden die Partikel zugänglich für die Click Chemie. Diese ist auf Grund ihrer Bioorthogonalität sehr vielseitig, vor allem in Hinblick auf Biokonjugation, da sie durch in biologischen Proben häufig vorkommende funktionelle Gruppen nicht beeinträchtigt wird. Es wurde gezeigt, dass SiNPs und UCµPs mit geeigneten Silanen direkt funktionalisiert werden können. Die UCNPs wurden mittels eines Stöber Prozesses mit einer Schicht $SiO_2$ (Silica) überzogen und gleichzeitig click funktionalisiert. Die Aufreinigung der gecoated UCNPs erfolge mittels Größenausschlusschromatographie wodurch die Partikelaggregation minimiert und eine gute Dispersibilität der Partikel in wässrigen Lösungen erreicht wurde.

Fluoreszenzmarkierte SiNPs mit Emissionswellenlängen von grün bis rot wurden durch kovalente Bindung von click-funktionalisierten Farbstoffen hergestellt. Durch strikte Kontrolle der Farbstoffmenge und der Reaktionszeiten lassen sich Farbe und Fluoreszenzintensität der Partikel leicht abstimmen. Mittels Click Reaktion fluoreszenzmarkierte UCµPs and UCNPs zeigen attraktive spektrale Eigenschaften, da sie eine von der Anregungswellenlänge abhängige duale Emission aufweisen. Dies kann für Encoding Anwendungen genutzt werden. Die Photoanregung eines organischen Farbstoffes durch die UCNP Emission wurde für die grün emittierenden UCNPs vom Typ **NP-3** und ein click-Derivat von Rhodamin B gezeigt. Die Energieübertragung vom UCNP zum Farbstoff fand nicht durch einen strahlungslosen FRET Mechanismus statt, sondern vermutlich durch die tatsächliche Emission und Reabsorption von Photonen, wobei die UCNPs als „Nano-Lampen" agieren.

Des Weiteren wurden bioreaktive Partikel, die entweder mit Maleinimide oder Biotin funktionalisiert sind, durch Click Reaktion hergestellt. Leider konnte die Reaktivität von Maleinimide funktionalisierten UCNPs gegenüber Thiolgruppen und

die Affinität von UCNPs, die mit Biotin modifiziert sind, zu (Strept)avidin nicht erfolgreich für die Markierung von Proteinen und Oligonukleotiden genutzt werden.

Allerdings wurde dargelegt, dass UCNPs hohes Potenzial für sensorische Applikationen aufweisen. Sensorische Strategien für die Bestimmung des pH-Wertes, die auf dem inneren Filter Effekt von ausgewählten pH-Indikatoren auf die Emission der UCNPs basieren, wurden vorgestellt. Dieses Konzept wurde auf die Entwicklung einer Ammoniaksensormembran, die mit UCNPs des Typs **NP-3** und dem pH-Indikator Phenolrot dotiert wurde, ausgeweitet. Mittels dieser vollständig reversiblen Sensormembran konnte Ammoniak in einem Konzentrationsbereich von 1 bis 20 mM (40 – 800 ppm) in einem ratiometrischen Aufbau bestimmt werden. Außerdem wurde gezeigt, dass sowohl unmodifizierte als auch silica gecoatede UCNPs von „normal rat kidney" Zellen aufgenommen werden und daher fürs Bioimaging geeignet sind.

# 8 Curriculum Vitae

**Heike Sabine Mader**

born on May 22, 1982 in Munich

## Education

| | |
|---|---|
| 09/1988 – 06/2001 | **Primary and Secondary School in Bietigheim-Bissingen**<br>**General qualification for university entrance** |
| 10/2001 – 11/2006 | **Chemistry Studies, Diploma, Regensburg University**<br><br>**Diploma Thesis at the Institute of Analytical Chemistry, Chemo- and Biosensors, Prof. Otto S. Wolfbeis:**<br>"Fluorescent Labels for Glycoproteins Based on Boronic Acids" |
| 11/2006 | **Diploma degree in Chemistry (equivalent to M. Sc.)** |
| 12/2006 - present | **PhD Thesis at the Institute of Analytical Chemistry, Chemo- and Biosensors, Prof. Otto S. Wolfbeis:**<br>"Surface Modification of Silica and Upconverting Particles based on Click Chemistry" |

## Work Experience

| | |
|---|---|
| 09/2000 – 08/2005 | **Regular Summer Jobs at Elbe Schleiftechnik, Bietigheim-Bissingen (Manufacturer of Grinding Tools)** |
| 10/2004 - present | **Regular Tasks as Student and Graduate Assistant:**<br>Supervision of laboratory courses for medical, dentistry and chemistry students, tutorials in inorganic and organic chemistry for medical and dentistry students |
| 10/2006 - present | **Private Lessons in Inorganic, Physical and Organic Chemistry for Medical and Dentistry Students** |
| 06/2007 – 12/2007 | **Assistance in the Organization of the Conference „Methods and Applications of Fluorescence - MAF10", Salzburg** |
| 06/2009 – 08/2009 | **Visiting Scientist at the Institute of Biotechnology, Turku University, Finland** |

**Language Skills**

German (native), English (fluent), Spanish (good, Unicert II), French (moderate), Swedish (basic), Finnish (basic)

**Publications**

H. S. Mader, O. S. Wolfbeis, **Boronic Acid Based Probes for Microdetermination of Saccharides and Glycosylated Biomolecules**, *Microchim. Acta* 2008, 162, 1-34.

H. Mader, X. Li, S. Saleh, M. Link, P. Kele, O. S. Wolfbeis, **Fluorescent Silica Nanoparticles**, *Ann. N. Y. Acad. Sci.* 2008, 1130, 213-223.

H. S. Mader, M. Link, D. E. Achatz, K. Uhlmann, X. Li, O. S. Wolfbeis, **Surface-Modified Upconverting Microparticles and Nanoparticles for Use in Click Chemistries**, *Chem.-Eur. J.* 2010, published online, doi: 10.1002/chem.201000117.

S. M. Saleh, R. Müller, H. S. Mader, A. Duerkop, O. S. Wolfbeis, **Novel Multicolor Fluorescently Labeled Silica Nanoparticles for Interface Fluorescence Resonance Energy Transfer to and from Labeled Avidin**, *Anal. Bioanal. Chem.* 2010, accepted.

H. S. Mader, O. S. Wolfbeis, **Optical Ammonia Sensor based on Upconverting Luminescent Nanoparticles**, *submitted for publication.*

H. S. Mader, P. Kele, S. M. Saleh, L. H. Fischer, O. S. Wolfbeis, **Upconverting Nanoparticles for Bioconjugation**, *Curr. Opin. Chem. Biol. in preparation.*

**Posters**

Summerschool of the Graduate College "Sensory Photoreceptors in Natural and Artificial Systems" 2008, Kostenz, Germany.
**"Functionalization of Upconverting Microparticles Using Click Chemistry"**

Conference Methods and Applications of Fluorescence (MAF-11) 2009, Budapest:
**"Surface-Modified Upconverting Nanoparticles for Use in Click Chemistries"**